Genetic control of differentiation of anther wall cells surrounding male meiocytes in rice

Seijiro ONO

Doctor of Philosophy

Department of Genetics
School of Life Science
The Graduate University for Advanced Studies (SOKENDAI)

Experimental Farm
National Institute of Genetics

2015

CONTENTS

ABSTRACT

The anther, the male reproductive organ of angiosperm species, is composed of multiple and radial cell layers in a cross section; the innermost germline cells and their surrounding somatic cells, called inner-anther wall cells or companion cells, in addition to the outermost epidermal cells. All companion cells are produced from parietal cells, differentiated from primordial germ cells concurrently with the germ cell. Primary parietal cells with a stem cell-like ability divide periclinally and produce an undifferentiated cell layer inward, called secondary parietal cells, in addition to endothecium outward. Secondary parietal cells further divide periclinally and differentiate into middle layer and tapetal cells. Such a highly organized cellular patterning implies that in addition to the importance of germ cell development themselves, successful development of nursery companion cells adjacent to germ cells is indispensable to achieve sexual reproduction events in plants. Compared to the knowledge about earlier cell differentiation events of these anther wall cells and characteristic functions of tapetum cells at later post-meiotic stages, little is known about the function of anther wall cells during meiotic stages. Therefore, in this study, I tried to find and figure out characteristic and novel functions of anther wall cells at early-meiotic stages. To accomplish these tasks, I identified that a paralogous pair of bHLH transcription factor-encoding genes, *bHLH141* and *bHLH142*, play important functions in development of layered structure of inner-anther walls in rice.

bhlh142, a loss-of-function mutant of *bHLH142* gene, exhibited undifferentiated tapetal and middle layer cells at meiotic stages, suggesting bHLH142 functioned in cell differentiation of inner anther wall layers just after division of secondary parietal cells into two layers. On the other hand, *bhlh141* showed differentiated tapetum and middle layer at meiotic stages, however, at later post-meiotic stages, tapetal cells developed abnormally and therefore mutant lines exhibited male sterility, suggesting that unlike bHLH142, bHLH141 functions in development after differentiation of tapetum. Realtime PCR and fluorescent cytological analyses revealed that mRNA and protein expressions of bHLH142 were found in early-meiotic tapetum and middle layer and those of bHLH141 were found in tapetum at early- and post-meiotic stages, showing differential expression patterns with each other. Furthermore, expressions of bHLH141 were dependent on bHLH142, also supporting the result that bHLH142 and bHLH141 are required for differentiation of tapetum and subsequent development, respectively. Previous reports about bHLH141/EAT1 and bHLH142/TIP2 suggested that bHLH141 plays important roles in programmed cell death event in post-meiotic tapetum and acts under the control of bHLH142 signaling. In addition to previous results, I got several new findings in this study. First, I cleared the nuclear localization of both bHLHs in tapetal cells, while bHLH142 was expressed also in middle layer-cell nuclei, by cytological observations of transgenic rice plants expressing GFP- or YFP-fused proteins. Second, I found that bHLH141 expression peaked twice; the first peak was prominent during the early-meiotic stage, where no bHLH141 expression had been

reported, and the second peak in post-meiosis, as previously reported. Furthermore, I newly confirmed by ChIP-PCR that the firstly peaked bHLH141 directly bound to the upstream cis-regulatory region of the *DCL3b* gene, encoding an Dicer-like endoribonuclease required for biogenesis of 24-nt phased small interfering RNAs (phasiRNAs) abundant in rice floral organs and anthers. In addition to *DCL3b* gene, from the results of realtime PCR analysis using *bhlh* mutants, phasiRNA precursor transcripts were also predicted under the control of bHLH142 and bHLH141 cascades, and consequently, the amounts of mature 24-nt phasiRNA molecules were hardly detected both in *bhlh142* and *bhlh141* mutant anthers. Based on these findings, I concluded that bHLH141, firstly peaked during early-meiosis, activated the transcription of *DCL3b* gene and 24-nt phasiRNA precursors as substrates of the DCL3b enzyme, and bHLH142 was located in upstream of this bHLH141 cascade.

The function of reproductive 24-nt phasiRNAs in tapetum and/or germline development is still remained enigmatic. However, an Argonaute protein, MEL1, essential for pre-meiotic and meiotic development of rice meiocytes, is recently revealed to preferentially bind 21-nt phasiRNAs in pre-meiotic germ cells. Collectively with previous reports, the findings of this study will not be limited only in events in anther-wall cells, but also provide new insights to the mechanisms that promote anther development, including small RNA-mediated gene regulatory systems and cell-to-cell communication between germ cells and their companion somatic cells.

INTRODUCTION

The life cycle of sexual organisms is dependent on fertilization and meiosis. In most animals, meiosis directly produces haploid gametes. In contrast, in land plants, spores are meiotic products, and germinate multicellular haploid gametophyte, within which haploid gametes are produced. For example, ferns produce spores by meiosis on their sporophytic diploid body, and the spore produces prothallus, a gametophytic haploid body. Antheridium formed on prothallus produces swarm male gametes, which are fertilized with female gametes on archegonium to reproduce sporophytic zygotes. These facts obviously indicate that a mode of sexual reproduction is tremendously diversified among land plant species.

In angiosperm species, sexual reproduction is achieved by highly organized multicellular but ultimately simplified gametophytes, pollen and embryo sac. Mature pollen, the male gametophyte, is composed of three cells; a vegetative cell retaining two sperm cells in the cytoplasm (Bhojwani and Bhatnagar, 2008). Pollen is produced in the anther, a male reproductive organ. Primordial germ cells (PGCs) of angiosperms are initiated at the subepidermal layer (L2) in stamen, which differentiates into the anther and the filament in future (Goldberg et al. 1993). In anther, PGCs produce microsporangia, composed of the innermost sporogenous cells, which mature into male meiocytes, and surrounding somatic cells, called parietal cells. The sporogenous cells undergo several rounds of mitotic divisions, and multiple meiocytes within an anther locule to prepare for meiosis (Armstrong et al. 2003;

Nonomura et al. 2006; 2011). On the other hand, parietal cells undergo anticlinal divisions to be proliferated, and also divide periclinally to make layered structure of inner-anther walls. The mature anther wall is eventually composed of four layers in each anther lobe; epidermis, endothecium, middle layer and tapetum, from outward to inward. Except for epidermis, the inner three layers and male meiocytes are originated from PGCs (Fig. 1). The innermost tapetal layer adhering to meiocytes provides nutrients and materials for meiocytes to successfully pass through meiosis and early gametogenesis (Chapman 1987; Caubal et al. 2000). That is, besides the importance of germ cell development, successful development of somatic companion cells adjacent to germ cells is indispensable to achieve sexual reproduction events in plants.

In rice (*Oryza sativa* L.), a lot of genetic factors are known to control specification of meiocytes and parietal cells. A Leucine-Rich Repeat Receptor Like Kinase (LRR-RLK) gene, *MULTIPLE SPOROCYTE1* (*MSP1*, Nonomura et al., 2003) plays important roles for the specification of parietal cells and meiocytes interplaying with its ligand molecule, *MICROSPORELESS2/TPD1-likeA* gene (*MIL2/TDL1A*, Hong et al., 2012; Zhao et al., 2008). During anther wall speciation, *MSP1* is strongly expressed in innermost cell layers of anther wall overlapping with *MIL2/TDL1A* expression. Phenotypes of loss-of-function mutant *msp1* and *mil2-1* are almost identical showing disrupted layered structures in anther wall that mostly lack inner tapetum and/or middle layer cells, and ectopic appearance of meiocyte-like cells instead of inner anther wall cells. It is believed that signal transduction pathways

involving MSP1 and MIL2/TDL1A is important to establish the cellular identities of parietal cells. Glutaredoxin is proposed as another key for anther wall cell specification. *MICROSPORELESS1* (*MIL1,* Hong et al., 2010) encoding plant specific CC-type glutaredoxin is expressed in early sporogenous cells and inner anther wall cells. In *mil1* mutants, disordered anther wall layers are frequently observed. Functions of MIL1 protein are supposed to activate TGA1, a basic Leucine-Zipper (bZIP) transcription factor, in response to redox changes. In Arabidopsis, *TGA9* and *TGA10*, homologous genes of rice *TGA1*, are also expressed in sporogenous cells and inner anther wall cells, and *tga9 tga10* double mutant exhibits abnormal tapetum development (Murmu et al., 2010). In addition, *GAMYB* (Kaneko et al., 2004, Tsuji et al., 2006 and Liu et al., 2010), a gibberelin activated MYB transcription factor gene, is highly expressed throughout the anther development. A loss-of-function mutant of *GAMYB*, *gamyb-4* (Liu et al., 2010), exhibits abnormal development of anther wall cells, suggesting that gibberellin signaling also contributes development of anther wall cells. *Undeveloped Tapetum 1* (*UDT1,* Jung et al., 2005), encodes basic Helix-Loop-Helix (bHLH) transcription factor, is known as transcriptional regulator for early anther development. Although detailed function is still largely unknown, an ER membrane associated protein gene, *DEFECTIVE TAPETUM AND MEIOCYTES 1* (*DTM1*, Yi et al., 2011) is also involved in anther wall development. As described above, significance of anther wall formation and specification has been well discussed, because defects in early anther-wall development frequently result in severe male sterility (reviewed in Zhang and Yang, 2014 and Kelliher and

Walbot, 2014).

Besides knowledge about earlier development of anther wall cells, post-meiotic development of tapetum cells is also well studied because of their crucial roles for post-meiotic anther developmental events. When meiocytes finish their meiotic divisions and produce microspores, tapetum cells begin to degenerate by themselves through activating programmed cell death (PCD) pathway. The finding of *Tapetum Degeneration Retadation* (*TDR*, Li et al., 2006), a bHLH transcription factor gene, is one of key hallmarks on the studies about post-meiotic tapetum functions in rice. *TDR* is strongly expressed in tapetum cells at post-meiotic stages. In *tdr* mutant, no PCD activation is observed in tapetum and finally anther wall cells enlarge abnormally and crush inner developing microspores. As downstream targets of TDR, *CP1*, *CYP704B2* and *C6* have been demonstrated about their functions in post-meiotic anther wall (Lee et al., 2004, Li et al., 2010, Zhang et al., 2010). *CP1* encodes cysteine protease and is supposed to function to facilitate PCD and degeneration of tapetum cells (Lee et al., 2004). CYP704B2 catalyzes fatty acid metabolism in tapetum (Li et al., 2010), and *C6* encodes small secretary lipid transfer protein and is also expressed in post-meiotic tapetum (Zhang et al., 2010). *cyp704B2* mutants and *C6* RNAi knockdown lines exhibit severe defects in microspore development, implying that an important contribution of tapetum cells in male reproductive events is biosynthesis and delivery of the nutrients and pollen coat materials to developing microspores. Furthermore, it was reported that another transcriptional regulator *PERSITENT TAPETAL CELL1* (*PTC1*, Li et al., 2011), encodeing a

PHD-finger homeodomain protein, also activates tapetum PCD and specific metabolisms independent of the *TDR* regulatory cascade. The activated PCD pathway in post-meiotic stage seems to be coupled with and probably facilitates the secretion abilities of tapetum cells (Bhojwani and Bhatnagar, 2008).

On the contrary, little is known about the cellular function and its significances on tapetum and/or other anther wall cells during meiotic stages. Several reports suggest a possibility of intercellular communications between meiocytes and anther wall cells, which likely to be important to accomplish and progress the meiotic events properly (Heslop-Harison, 1966; Nonomura et al. 2003; Hord et al. 2006).

Recently, it was reported that small interfering RNA (siRNA) molecules have important roles in male reproductive events as well as other developmental events in rice. Ding et al., (2011) and Zhou et al., (2011) reported that causal mutation of photoperiod- and thermo-sensitive male sterility in rice occurred in 21-nt siRNA generating locus as a point mutation, and this mutation leads to premature developmental defects on the microspore and anther wall cells under the long-day and high-temperature conditions. Although the detailed mechanisms on how such mutated siRNAs contribute to the sterile phenotypes remains largely unknown, the production of some sort of siRNAs and subsequent biological regulations seem to be important for promoting rice reproductive events. It was also reported that 21-nt and 24-nt siRNAs were abundantly expressed in reproductive organs including anthers in rice (Johnson et al. 2009; Song et al. 2012a; Komiya et al. 2014). The reproductive

24-nt siRNAs are derived from 4,822 precursor loci distributed through all rice chromosomes (Johnson et al. 2009). In 35 of these loci, the reproductive siRNAs aligned regularly in a 24-mer phased interval, and so they are called phased siRNAs or phasiRNAs. The phasiRNA precursor loci are transcribed by RNA polymerase II to produce long non-coding single-stranded RNAs (ssRNAs) (Song et al. 2012b). The ssRNAs are cleaved within 22-mer miR2775 target sites conserved in 5'-termini of most precursor ssRNAs, and subsequently, double-stranded by a RNA-dependent RNA polymerase, RDR6 (Song et al. 2012b). These double-stranded RNAs are cleaved in regular 24-nt phased interval by a Dicer-like potein, DCL3b, and then, huge amounts of 24-nt reproductive phasiRNA are produced in floral organs including anthers in rice (Song et al. 2012a: 2012b). However, the functions of reproductive phasiRNAs abundantly expressed in reproductive organs have been remained elusive.

At the beginning of this study, I tried to find and figure out characteristic and novel functions of anther wall cells at early-meiotic stages. To accomplish this task, I identified and characterized two mutants of bHLH transcription factor genes, *bHLH142* and *bHLH141*, which preferentially expressed in early-meiotic anther wall cells. Recently, both genes were reported as essential genes for anther wall development and post-meiotic tapetum development (Niu et al. 2013; Fu et al. 2014; Ko et al. 2014). Besides these roles, I found the novel functions of these transcription factors at early-meiotic stages of anther wall cells. That is, these two bHLH genes are involved in induction of 24-nt phasiRNA biogenesis specific for

rice reproduction, specifically by activating and transcribing *DCL3b* gene and precursors of phasiRNAs in tapetum cells. Because of small sizes and expected high mobility of siRNAs, generated phasiRNAs might move into and have function in adjacent meiocytes. This study might be helpful findings to understand possible interactions between meiocytes and anther wall cells at meiotic stages.

MATERIALS AND METHODS

Plant materials

Among the rice *Tos17* insertion mutant, *msp1* mutant (ND0018) was originally isolated and maintained in our laboratory (Nonomura et al., 2003). *bhlh141* mutant (NF9876) was obtained from Rice Genome Resource Center on the National Institute of Agrobiological Sciences, Japan. A T-DNA insertion line on *bHLH142* locus (1B-24309) was obtained from seed stock center in Pohang University of Science and Technology (POSTECH), Republic of Korea.

PCR genotyping of each mutant line was performed using gene specific primers, ND0018F1 and ND0018R1 for *msp1*, NF9876F1 and NF9876R1 for *bhlh141* and 1B24309F1 and 1B24309R1 for *bhlh142*. In addition, *Tos17* specific primer T17LTR2MF for *msp1* and *bhlh141* and T-DNA specific primer LB1R for *bhlh142* was also employed.

msp1, *bhlh141* and their wild-type (WT) cultivar cv. Nipponbare were grown in the experimental field of National Institute of Genetics (NIG) in the city of Mishima, Shizuoka, Japan. *bhlh142* and some other transgenic lines were grown in the isolated green house in NIG and/or in the growth chamber, Biotoron (NK system).

Anther morphology observation

Plastic sections of rice anthers were made using Technovit7100 resin (Kulzer). Before

infiltration, young panicles of rice plant were fixed with 4% paraformaldehyde in 1xPMEG buffer (50 mM PIPES, 10 mM EGTA, 5 mM $MgSO_4$ and 4% Glycerol, pH6.8) and washed by 1xPMEG buffer 6 times. Then, anthers were dissected, dehydrated with ethanol series, infiltrated and solidificated by Technovit7100 resin according to manufacture's instruction.

Plastic blocks were sliced at 2 μm thick using a microtome (Leica RM2255). Sections were stained with 0.1% Toluidine blue O (Wako pure chemicals) for light microscopy observation. For cellulosic cell wall staining, sections were stained with a drop of Runaissence2200 (Runaissence chemicals) reagent diluted in 2% with VECTASHIELD (Vector) containing 10 μg/ml of Propidium Iodide (PI). Fluorescent signals were captured using Fluoview FV300 CLSM system (Olympus).

RNA in situ hybridization

To make *bHLH142* antisense and sense RNA probes, a fragment of transcribed regions of *bHLH142* was amplified from rice flower cDNA sample and cloned into pCRII vector (Invitrogen) using primers bHLH142F1 and bHLH142R1. For *bhLH141* probes, two fragments were amplified and cloned into pCRII using primers, bHLH141F1 paired with bHLH141R1 and bHLH141F2 paired with bHLH141R2. After PCR amplification of cloned fragments using primers M13-20 and M13-Rev, in vitro transcription was conducted using T7 and SP6 RNA polymerases (Roche) and DIG RNA labeling kit (Roche) according to

manufacture's instruction.

WT rice flowers were fixed with FAA fixative (1.8% formaldehyde, 5% acetic acid and 45% ethanol), dehydrated with ethanol series, infiltrated and solidificated with ParaplastPlus (McCormick Scientific). The paraffin section was sliced with microtome (Micron HM315) at 10 μm thick. After removal of paraffins, sections were treated with Proteinase K and hybridized with RNA probes at 200 ng/mL concentration in hybridization buffer (50% formamide, 1% dextran sulfate, 0.3 M NaCl, 10 mM Tris-Cl pH7.5, 1 mM EDTA pH7.5 and 60 mM DTT in 1x Denhardt's solution containing 150 μg/mL tRNA and 500 μg/mL poly(A)). Hybridized RNA probes were labeled and detected using anti-DIG-AP (Roche) and NBT/BCIP solution (Roche) according to manufacture's instruction.

Construction of p*bHLH142*::*N-YFP-bHLH142* and p*bHLH141*::*bHLH141-C-GFP* and transformation into mutant plants

A *Spe*I-*Spe*I 6.6 kbp genomic fragment including entire bHLH142 gene, 4 kbp upstream and 0.5 kbp downstream was digested from rice BAC clone OSJNBa0001E17 and cloned into pBS-SK(-) vector. Then, a 1.8 kbp *Hin*dIII-*Sal*I fragment including *bHLH142* translational initiation site was subcloned into new pBS-SK(-). From this plasmid, a 1.5 kbp 5' upstream region and a 300 bp 3' downstream region of bHLH142 translational initiation site were amplified using primers bHLH142start-NcoI-link paired with M13-Rev and bHLH142start-BsrGI-link paired with T7EcoRI-link. These fragments were cloned into

pEYFP (a cloning vector having EYFP sequence in pUC18 backbone) using *Hin*dIII, *Nco*I, *Bsr*GI and *Eco*RI site. Resultant plasmid having EYFP sequence in *bHLH142* translational initiation site in frame was digested using *Hin*dIII and *Sal*I. Other *Spe*I-*Hin*dIII and *Sal*I-*Spe*I fragments were also digested from previously subcloned 6.6 kbp fragment, and these three fragments were reconstructed in new pBS vector again. Finally, resultant 7.4 kbp *Spe*I-*Spe*I fragment was digested, blunt-ended and cloned into pGWB601 binary vector (Nakamura et al., 2010).

A 5.8 kbp *Hin*dIII-*Xho*I fragment including upper part of *bHLH141* gene and its promoter region were cloned into pBS-SK(-) vector from BAC clone OSJNBa0010K21. A 1.2 kbp *Xho*I-*Eco*RV fragment including latter part of *bHLH141* gene was also subcloned into another pBS vector. 200 bp upstream and 1 kbp downstream of bHLH141 stop codon were amplified using primers bHLH141-stop-BamHI paired with bHLH141-XhoI-BamHI and bHLH141stop-NotI-link paired with M13-Rev. These fragments were cloned into psGFP (a cloning vector having sGFP sequence in pUC18 backbone) using *Bam*HI, *Not*I and *Eco*RI. Resultant plasmid having sGFP sequence in *bHLH141* C-terminus region was digested with *Xho*I and *Eco*RV and reconstructed in pPZP2H-lac binary vector combined with previously subcloned *Hin*dIII-*Xho*I fragment.

Each construct was introduced into *bhlh142* and *bhlh141* calli using *Agrobacterium* mediated rice transformation method as described previously (Toki et al., 2006).

GFP and YFP signal observation in rice anther tissues.

YFP (or GFP) observations of anther samples were conducted using agarose section. Anthers were dissected from young flowers and poured into pre-warmed 6% Seakem GTG agarose (Lonzo) gel. After the gelation, agarose blocks were sliced at 50 μm thick using a microslicer (MicroSlicer, ZERO1, D.S.K.), and mounted with a drop of VECTASHIELD with DAPI (Vector). Fluorescent signals of YFP (or GFP) and DAPI were captured using Fluoview FV300 CLSM system (Olympus).

RNA extraction and quantitative reverse transcription (qRT)-PCR

Anther samples from *bhlh142*, *bhlh141* and their WT plants were carefully collected from young panicles and divide them according to their developmental stages (Table 1). Total RNAs were extracted using TRIzol reagent (Life technologies) according to manufacture's instruction.

About 1 μg of total RNA in each samples were reverse transcribed using oligo$(dT)_{12-18}$ primer (Invitrogen) and SuperscriptIII (Invitrogen) reverse transcriptase. After reverse transcription, samples were 20 fold diluted and assayed for raeltime PCR quantification using KAPA SYBR FAST universal qPCR Kit (KAPA biosystems). Realtime amplification was detected with Thermal Cycler Dice Real Time System (TAKARA). For internal standard, expression levels of *Ubiquitine* gene were quantified using further 5 fold diluted samples and with primers UbqF1 and UbqR1.

For the quantifications of small RNA experiments, about 2 μg of total RNA samples were reverse transcribed using a mixture of eight stem-loop RT primers. After reverse transcription, samples were 5 fold diluted and assayed for realtime PCR quantification. As internal standard, another 100 ng of total RNA samples were reverse transcribed using U6 snoRNA specific primer. After reverse transcription, samples were 100 fold diluted and assayed for realtime PCR using U6 specific primers.

Chromatin immunoprecipitation-quantitative PCR (ChIP-qPCR)

Flowers at early meiotic stages (around 2.0 mm lemma length) were collected from plants carrying p*bHLH142*::*N-YFP-bHLH142* or p*bHLH141*::*bHLH141-C-GFP* and fixed in the fixative (1% formaldehyde, 0.4 M sucrose, 0.1M Tris-Cl and 50 mM EDTA pH8.0). Flowers also collected and fixed from siblings having no transgene as negative control for each experiment. Nuclear fractions were extracted, sonicated and immunoprecipitated with anti-GFP antibody (MBL, No.598) and Dynabeas Protein A (Life Technologies). For antibody-negative control, half of nuclear fractions were also immunoprecipitated without anti-GFP antibody. IP fractions were washed, extracted and treated with ProteinaseK to digest plant proteins and antibodies. After phenol-chloroform extraction and ethanol precipitation, DNA samples were assayed realtime PCR quantification.

RESULTS

bHLH142 and *bHLH141* are candidate genes which are preferentially expressed in anther wall cells

For exploitation of the genes preferentially expressed in anther wall cells, first I analyzed the expression profile of genes in anthers of WT and the rice mutant, *multiple sporocyte1 (msp1)* (Nonomura et al., 2003) using the microarray data previously examined in our laboratory (Ueda et al., unpublished data), The *MSP1* gene is specifically expressed in inner-anther walls during anther wall specification, and its loss-of-function mutant produces anthers mostly lacking inner-walls, including the innermost tapetum layer. Thus, it was expected that the genes preferentially expressed in inner wall cells might be down-regulated in *msp1* anthers.

From the comparison of microarray results between the WT and *msp1* mutant, I found that two bHLH family transcription factor genes, *bHLH141* (Os04g0599300) and *bHLH142* (Os01g0293100) (Fig. 2A), were 15.6-fold and 9.58-fold down-regulated in the *msp1* mutant anther, respectively (Fig. 2B). This result was further confirmed by qRT-PCR (Fig. 2C), In addition, according to the results of the gene expression profile database, RiceXPro (http://ricexpro.dna.affrc.go.jp/), high and specific expression of both *bHLH141* and *bHLH142* was only detected in young anthers at meiotic stages.

Sequence similarity and phylogenetics of bHLH142 and bHLH141

Both bHLH142 and bHLH141 belonged to plant bHLH subfamily 9 (Carretero-Paulet et al., 2010), which contains no rice bHLH gene other than these genes. Deduced amino acid sequences of bHLH141 and bHLH142 shared 86.7% similarity (48.3% identity) in the bHLH domain (IPR001092, http://www.ebi.ac.uk/interpro/), and 81.8% similarity (41.6% identity) in the C-terminus (Fig. 2D). The C-terminal sequence was also conserved in all subfamily-9 bHLHs of other species. In contrast, no obvious sequence similarity was found in the N-termini of two rice bHLHs.

Though two other bHLH genes, *Tapetum Degeneration Retadation* (*TDR*) and *Undeveloped Tapetum1* (*UDT1*), were reported previously as essential genes for anther development and male reproduction in rice (Li et al., 2006, Jung et al., 2005), both of them belonged to the subfamily 1, different from *bHLH141* and *142* (Carretero-Paulet et al., 2010). Therefore, *bHLH142* and *bHLH141* were phylogenetically distinct from *TDR* and *UDT1*, and supposed novel bHLH members acting in rice anthers.

Both *bhlh142* and *bhlh141* mutations cause male sterile phenotypes

Next, putative loss-of-function mutants were identified to characterize the function of *bHLH141* and *bHLH142* genes in rice anther development. For the *bHLH142* gene, a T-DNA tag line (Jeong et al., 2006), in which the T-DNA is inserted into the third intron of *bHLH142* gene, was selected (Fig. 2A). For the *bHLH141* gene, the line with an insertion of the

endogenous retrotransposon *Tos17* (Hirochika et al., 1996) into the second exon of *bHLH141* gene was selected (Fig. 2A).

As expected, both mutant lines segregated male sterile individuals (see below for details). Both *bhlh141* and *bhlh142* homozygous plants showed normal vegetative growth compared to their heterozygous and WT plants. At flowering stage, both *bhlh141* and *bhlh142* mutants exhibited immature, short and whitish anthers, in contrast to well-developed and yellowish anthers of WT plants (Figs. 3A and 4A). I performed the iodine-potassium iodide staining to visualize mature and fertile pollen grains whose vegetative cells are filled with starch granules. This revealed that no mature pollen was observed inside both mutant anthers, while a number of viable pollen grains were inside the anthers of each WT line (Figs. 3B, C and 4B, C). In outcrossing with WT pollen grains, flowers of both *bhlh142* and *bhlh141* homozygous mutants set seeds comparable to WT siblings; 54.5 % (6/11) in the *bhlh142* and 78.3% (65/83) in the *bhlh141* while no seeds were yielded by self-pollination in both mutant. These results indicate that both of *bhlh142* and *bhlh141* homozygous mutants are male sterile due to defects in anther development but show normal fertility in female side.

In the progeny of plants heterozygous for the T-DNA insertion into the *bHLH142* gene, fertile and male-sterile plants were segregated likely in a Mendelian fashion (19:9, $\chi 2 = 1.92$ for 3:1, $P>0.38$, $N=27$), though the population size was too small because of limited space to grow transgenic plants. This was the case also for the progeny of heterozygous plants in the *bHLH141* line (137:41, $\chi 2 = 1.21$ for 3:1, $P>0.54$, $N=178$). In both cases, I confirmed that

T-DNA or *Tos17* was inserted homozygously in all male-sterile plants. These results revealed that the male sterile phenotype segregated in *bHLH142* and *bHLH141* lines was genetically linked with the insertion of T-DNA and *Tos17* sequences, respectively.

To further confirm that either T-DNA or *Tos17* insertion caused male sterility in *bHLH142* and *bHLH141* lines, I performed the complementation tests of the mutation phenotype by the genomic fragment harboring one of WT *bHLH* genes. A genomic fragment containing the *bHLH142* putative promoter sequence and bHLH142 protein coding region, in which the YFP protein was fused at the N-terminus of hHLH142 in frame (p*bHLH142*::*N-YFP-bHLH142*), was transformed into *bhlh142* homozygous plants (Fig. 3D). Two independent transgenic lines were obtained and both recovered fertility in T_0 generation (Fig. 3E, F), while transgenic lines introducing the empty vector, as a negative control, did not recover the fertility (Fig. 3G). Of 22 plants in selfed T_1 progenies, 13 plants carrying the p*bHLH142*::*N-YFP-bHLH142* transgene recovered the fertility, and 9 plants without the transgene did not (r=1, P<0.001). In the case of *bHLH141*, GFP-tagged genomic sequence at the 3'-terminus of *bHLH141* gene in frame, whose expression was driven by a putative endogenous promoter (p*bHLH141*::*bHLH141-C-GFP*), were introduced into *bhlh141* homozygous plants (Fig. 4D). Two independent plants, carrying p*bHLH141*::*bHLH141-C-GFP* recovered fertility at T_0 generation, and furthermore, 15 fertile and 9 sterile T_1 progenies were segregated again in complete correlation to presence or absence of the transgene (r=1, P<0.001, Fig. 4E-G). Thus, I concluded that the T-DNA and

Tos17 insertions into *bHLH142* and *141* genes were the causal mutation of the male sterility in both lines selected in this study.

Aberrant mRNAs are transcribed in both *bhlh142* and *bhlh141* mutants

Next, to confirm whether the expressions of *bHLH141* and *142* genes were affected in respective mutant lines or not, RNAs extracted from flowers containing meiotic-stage anthers were supplied for the RT reaction and the quantitative realtime PCR. In the case of the *bhlh142* mutant, when PCR primer sets to amplify the upstream sequences of the T-DNA insertion were used, relative transcript amounts were reduced compared to the WT amounts. On the other hand, using primers for the sequence downstream of the insertion, no amplification was detected in the *bhlh142* mutant (Fig. 5A, B). This result suggests that *bhlh142* anthers expressed the aberrant mRNA in which the exons on the fourth were truncated somehow, probably because of a large T-DNA insertion. Thus, resultant transcripts were predicted to produce, if any, aberrant bHLH142 proteins lacking the C-terminal 23 amino acids. As described above, the C-terminal regions of both bHLH142 and bHLH141 carries a characteristic amino acid sequence conserved among all subfamily-9 bHLHs, although the function of this conserved sequence is unclear yet. From the result that the truncation of C-terminal 23 amino acids of bHLH protein caused male sterility, it is supposed that the C-terminal conserved domain of bHLH has some important functions. In the case of the *bhlh141* mutant, when the primer sets designed within the downstream region of the

Tos17 insertion were used, the amplification was hardly detected. On the other hand, the expression level of the N-terminal coding region upstream of the *Tos17* insertion was higher than that of WT (Fig. 5C, D). The 3'-terminal *bHLH141* transcript downstream of the *Tos17* insertion encoded the bHLH domain, in addition to the C-terminal conserved domain. Thus, it was concluded that the resultant transcript of *bhlh141* produced dysfunctional bHLH141 protein.

bhlh142 and _bhlh141_ mutations have compromised anther development at different levels

To characterize the male sterility of *bhlh142* and *bhlh141* in detail, the morphology of anther cells were observed using plastic sections from pre-meiotic to post-meiotic stages. These observations turned out that two *bhlh* mutants showed differential levels of defect on anther development. In anthers at pre-meiotic or early-meiotic stages, the anther wall became four-layered in WT (Figs. 6A-C and 7A-C), *bhlh142* mutants (Fig. 6H-I) and *bhlh141* mutants (Fig. 7H-I). Prior to this stage, parietal cells generate the endothecium outward, and the inward secondary parietal cells still retain an undifferentiated state to further develop middle layer and tapetum (Fig. 1). At early four-layered stage, corresponding to early-meiotic stage, characteristics of middle-layer cells were almost similar to those of tapetal cells, and no remarkable differences ware observed between WT and both mutant anthers (Figs. 6A, B, H, I and 7A, B, H, I).

The morphological defects emerged in the *bhlh142* mutant at subsequent middle and late of four-layered stages, corresponding to meiotic-prophase I pachytene and later stages. In WT anthers at this stage, the outward middle layers and the inward tapetum, both derived from secondary parietal cells, began to differentiate with showing clear morphological differences; the cytoplasm components of tapetal cells became densely stained, and middle layer cells was extremely thinned to radial direction (Fig. 6C, D, G). However, in *bhlh142* mutant anthers, the innermost tapetum-like layer cells had no densely stained cytoplasm, and in addition, no thinning down of the second innermost layer occurred (Fig. 6J, K, N), resulting in both layers hardly distinct with each other in their cellular characteristics. In subsequent stages, tapetum-like cells in *bhlh142* anthers underwent excess periclinal divisions and partially made five or more wall layers, resulting in inward meiosytes squashed and collapsed (Fig. 6L-N). In contrast to the *bhlh142* mutant, the *bhlh141* mutant anthers seemed to differentiate tapetum and middle layer normally (Fig. 7C-E, G, J-L, N). However, in subsequent stages, *bhlh141* anther displayed morphological defects in anther loculi. In WT anthers in this stage, developing pollen grains adhered to tapetal cells going to PCD, and cellular components from degenerated tapetum seemed to be kept at intercellular space between wall layer and pollen grains, resulting in a vacant space at the longitudinal axis of each anther locule (Fig. 7F). In contrast, in the *bhlh141* anthers, intercellular space in the anther locule was fully filled with tapetal cell components, and the circular shape in the cross section of loculi was frequently distorted (Fig. 7M), suggesting somewhat unusual degeneration of tapetum. These results

suggest that bHLH142 acts in differentiation of middle-layer and tapetal cells in anthers at early four-layered stage, and bHLH141 acts in maturation of tapetal cells at mid four-layered stage, after differentiation of middle-layer and tapetal cells.

Next, I observed rapid replacement of cell-wall components, which generally occurs in anther loculi at transition stage from mitosis to meiosis. In *Arabidopsis thaliana*, rapid loss of cellulosic cell wall components of anther locule cells, around tapetal cells and meiocytes, is one of key characteristic events in meiotic anthers (Matsuo et al., 2013). In this study, Renaissence2200, a specific fluorescent reagent, which stains beta 1-4 glucan chain of cellulose, was used for evaluation of the rapid cellulose loss in anther loculi in rice, and I confirmed that the degradation of cellulosic signals occurred around WT tapetal cells and meiocytes in rice (Figs. 8A-D and 9A-D), as well as in *Arabidopsis*.

Renaissence2200 staining revealed a remarkable difference between WT and *hhlh142* mutant anthers. At the middle of four-layered stage, cellulosic signals in cell walls around tapetum and meiocytes disappeared in WT anthers, and in contrast, both anther loculi in the *bhlh142* mutant still retained cellulosic signals at the same stage (Fig. 8F). Furthermore, in subsequent stages, innermost tapetum-like cells aberrantly continued periclinal divisions, and partially generated extra cell layers, exhibiting bright cellulosic cell wall signals (Fig. 8G, H). This result corresponded to the observation of cellular morphology in plastic sections (Fig. 6L-N). On the other hand, a staining pattern of *hhlh141* anthers seemed almost comparable to WT anthers (Fig. 9E-H). This result suggests that degradation of cellulosic components of

anther loculi occurred in *hhlh141* mutant just as following differentiation of middle layer and tapetum in wild type anthers, and that degradation of cellulose and subsequent differentiation of two inner-most layers did not occur in *bhlh142* mutant anthers.

In a short summary, the *bhlh142* mutant shows obvious defects in differentiation of tapetum and middle layer, which occurs at middle-meiotic stage in WT anthers. The *bhlh141* anther seemed to differentiate middle layer and tapetum normally, while tapetal PCD and microspore development were likely impaired at post-meiotic stages. Though the developmental defect of *bhlh141* anthers seemed milder than that of *bhlh142*, both defects gave a critical impact to anther development and male gametogenesis.

bHLH142 and _bHLH141_ expression in anther wall cells showing distinct patterns with each other

To further understand when and where these bHLHs function during anther development, it is necessary to examine detailed expression of the *bHLH* genes. To know expression profiles of *bHLH* transcripts, total RNAs were extracted from anthers at various developmental stages, ranging from pre-meiotic to post-meiotic stages. The detailed description of sample criteria and typical anther morphologies in each category are summarized in Table 1. After the reverse transcription, gene expression levels were evaluated using quantitative PCR. Primer pairs in the 3' UTR region (Fig. 5A, C) were used for the evaluation of expression levels in both cases of *bHLH142* and *bHLH141*, and expression of

Ubiquitin gene was employed as internal standard for normalization of gene expressions.

The *bHLH142* expression was detected and peaked during the developmental stage 2 of WT anthers (ST.2) and ST.3 (Fig. 10A, B), in which male meiocytes were doing leptotene and pachytene, respectively, and middle layer and tapetum began to differentiate (Table 1), and gradually downed at and after ST.4 (Fig. 10A, B), when tapetum and middle layer differentiation and male meiotic division were completed. The expression of *bHLH141* was also elevated and peaked at ST.2 and/or ST.3 (Fig. 10C, D). However, after once downed at ST.4, the expression was elevated again at ST.5 (Fig. 10C, D), when tapetum cells started PCD. A characteristic pattern of the expression of each *bHLH* gene was reproducible in two independent sample sets in each line; three sample sets from *bHLH141* WT anthers (the *japonica* rice cultivar Nipponbare) and three sample sets from *bHLH142* WT anthers (*japonica* cv. Dongjing). *bhlh142* and *bhlh141* mutant anthers hardly expressed *bHLH142* and *bHLH141*, respectively, throughout all developmental stages (Fig. 10A, C). Altogether, it was concluded that the expression of *bHLH142* was peaked at the onset of differentiation of tapetum and middle layer, and that the *bHLH141* had two distinct peaks in its mRNA expression, once at early-meiotic stage and the other at post-meiotic microspore developmental stages.

The spatio-temporal expressions of both *bHLH* genes were further investigated by RNA in situ hybridization. At the stage in which meiocytes underwent early-meiosis, the positive hybridization signals were concentrated at anther wall cells, especially in innermost tapetum

cells in both cases of *bHLH142* and *bHLH141*, while sense-strand probes as negative controls gave signals only at a background level (Fig. 11A-D). In addition, the *bHLH141* probe gave signals also in tapetum at post-meiotic microspore stage (Fig. 11E, F), This result is consistent with that of the realtime PCR, in which dual peaks of *bHLH141* expression during early- (STs.2 and 3) and post-meiosis (ST.5), whereas the *bHLH142* expression showed one peak concurrent with the first of two *bHLH141* peaks.

The expression pattern of both bHLHs described above was also confirmed at a protein level. Here, transgenic lines expressing GFP-tagged bHLH141 and YFP-tagged bHLH142, that were used for the complementation test as described above (Figs. 3D and 4D), were employed for fluorescent microscopy observations. Since transgenic lines having p*bHLH142*::*N-YFP-bHLH142* and p*bHLH141*::*bHLH141-C-GFP* recovered sterile phenotypes of *bhlh142* and *bhlh141*, respectively, I concluded that recombinant YFP-tagged bHLH142 and GFP-tagged bHLH141 proteins were functional in rice plants, and these transgenic plants were used for the following experiments.

The observations of fluorescent signals were conducted in various anther stages, from the pre-meiotic three-layered to the post-meiotic microspore stages. In three-layered anthers, just before secondary parietal cells differentiating tapetum and middle layer, fluorescent signals were hardly observed (Fig 12A). In the subsequent stage, in which tapetum and middle layer were differentiated, strong expression of the YFP-tagged bHLH142 protein was prominent in tapetal cell nuclei, and in addition, weaker signals were observed in nuclei of

middle layer cells (Fig. 12B). The signals were recognizable until middle-meiotic anther stages, but disappeared after the late-meiotic stages (Fig. 12C-F). In the case of bHLH141-GFP, fluorescent signals also began to appear in anthers at the early-meiotic stage (Fig. 13A, B), and however, different from the case in bHLH142-YFP, the bHLH141 signal was restricted only in tapetal cell nuclei (Fig. 13C). The fluorescent signal disappeared once in the anther at the middle-meiotic stage (Fig. 13D, E), but reappeared at the post-meiotic microspore stage (Fig. 13F). These observations revealed that bHLH142 protein accumulation in tapetal cell nuclei was in one peak in early four-layered stage anthers, but bHLH141 accumulation showed dual peaks at both the onset of four-layered stage and post-meiotic microspore stage, consistent with realtime PCR results (Fig. 10).

bHLH142 **is upstream to** ***bHLH141***

Severe developmental defects observed in *bhlh142* mutant in comparison to that of *bhlh141* implicated the genetic epistasis of *bHLH142* to *bHLH141*. To validate this possibility, I measured the expression levels of *bHLH141* gene in the *bhlh142* mutant and vise versa. As a result, the *bHLH142* expression level was not significantly different between the WT and *bhlh141* mutants in early-meiotic stage anther (Fig. 10C). In contrast, the *bHLH141* transcript was completely absent in the *bhlh142* mutant throughout anther development (Fig. 10D). These results clearly showed that *bHLH141* expression depended on the presence of functional *bHLH142*, but it was not applicable in the opposite case.

Such a *bHLH142* dependent *bHLH141* expression was also confirmed at the protein level. In transgenic plants carrying the p*bHLH141*::*bHLH141-C*-GFP construct, the fluorescent signals were clearly detected in tapetal cell nuclei in genetic backgrounds homozygous and heterozygous for the WT *bHLH142* allele (Fig. 14A, B), while no signal was detected in the *bhlh142* mutant homozygous background (Fig. 14C), indicating that the accumulation of bHLH141 protein depended on the *bHLH142* gene function. In contrast, in transgenic plants carrying the p*bHLH142*::*bHLH142-C*-YFP, the fluorescent signals were detected in tapetal cell nuclei in genetic backgrounds of all three *bHLH141* genotypes, including the *bhlh141* homozygous mutant (Fig. 15), suggesting that *bhlh141* mutation did not affect the bHLH142 protein expression.

It should be noted that before use in this assay, the p*bHLH141*::*bHLH141-C*-GFP transgene was confirmed to restore seed fertility when introduced into the *bhlh141* mutant background by crossing, implicating that the construct produces a functional protein (Fig. 4). In contrast, the p*bHLH142*::*bHLH142-C*-YFP was directly introduced into the *bhlh141* mutant and used in this assay, leaving a possibility that the bHLH142-C-YFP protein in this assay may exhibit a different nature from the endogenous bHLH142 protein. However, I confirmed that spatiotemporal expression of the bHLH142-C-YFP (Fig. 15) was almost comparable to the N-YFP-bHLH142 expression (Fig. 12). In addition, the bHLH142-C-YFP expression was examined in three independent T_0 lines (Fig. 15B-F). So, I thought that the bHLH142-C-YFP was compatible with the endogenous bHLH142 in their protein functions,

and that data obtained in this assay was reliable.

Genetic networks involve bHLH142 and bHLH141

From their amino acid sequences, the protein functions of both bHLH141 and bHLH142 were supposed as transcription factors (Fig. 2C). This idea was also supported by subcellular localization of both proteins exclusively localized in the nuclei of somatic cells surrounding male meiocytes (Figs. 12 and 13). Thus, it is expected that these bHLHs regulate the expression of some sort of genes as downstream targets. To figure out the gene regulatory networks governed by bHLH142 and bHLH141, expression levels of several reported and functionally-unknown genes, preferentially expressed in tapetal and/or middle layer cells, were examined and compared between WT and either of *bhlh142* or *bhlh141* anthers by qRT-PCR. To pick up rice genes expressed in anther wall cells, I employed the microarray screening by using *msp1* mutant (*msp1* microarray), same to the strategy when I identified *bHLH142* and *bHLH141*, as described above (Fig. 2B). In addition, several genes were picked up according to the information from previous reports. At the end, total 15 genes (9 reported and 6 unreported) were examined in their expression patterns in this study. Up- or down-regulation of each of 16 genes in the *msp1* mutant was estimated in anthers at ST.2, at which male meiocytes undergo early meiotic prophase I (leptotene or zygotene; Table 1), and the results were shown at the right-most bar graph in each panel of Figures 16 to 22.

Among reported genes, first I picked up and used four genes for the qRT-PCR; *MSP1*

(Nonomura et al., 2003), *GAMYB* (Kaneko et al., 2004, Tsuji et al., 2006 and Liu et al., 2010), *UDT1* (Jung et al., 2005) and *DTM1* (Yi et al., 2012). All four genes were reported to function in anthers during earlier developmental stages (see Discussion), and actually, each showed an expressional peak in anthers at ST.2 or earlier (Fig. 16). Interestingly, compared to WT anthers, in *bhlh142* mutant anthers, the expression of the four genes was not declined, rather increased at ST.3 or later, as outstripping the WT level (Fig. 16). On the other hand, the expression was not affected by the *bhlh141* mutation (Fig. 16). This category of genes may be expressed in anthers concurrently with or earlier than the *bHLH142* expression; because undifferentiated cells were aberrantly continued in replacement of middle-layer and tapetal cells in the *bhlh142* mutant (Figs. 6L-N and 8), resulting in continuous expression of genes for earlier anther development in late developing stages.

Next, the expression of genes reported as key players for tapetum degradation and PCD at post-meiotic stages was examined; such as *TDR* (Li et al., 2006), *PTC1* (Li et al., 2011) and *CYP704B2* (Li et al., 2010). The expression of all three genes was peaked at ST.5 (Fig. 17A-C), corresponding to their previously reported roles in tapetal cells. Interestingly, the *TDR* expression showed dual peaks in its expression (Fig. 17A), similar to the *bHLH141* expression (Fig. 10C, D), whereas the first *TDR* peak was detected at ST.3, just as following the first *bHLH141* peak at ST.2. In *bhlh142* mutant anthers, the expression of these three was almost absent, and in contrast, unaffected or rather increased in *bhlh141* anthers (Fig. 17A-C). This category of genes is suggested to function in the tapetum PCD independently of the

bHLH141 gene function.

Both *AP25* and *AP37* are also known to function in taptum PCD, but their transcription is directly promoted by bHLH141 transcription factor (Liu et al., 2012), different from *TDR*, *PTC1* and *CYP704B2* genes. In this study, the expression of *AP25* was completely absent in both *bhlh142* and *bhlh141* mutants (Fig. 17D), consistent with the previous result (Niu et al. 2013). On the other hand, the *AP37* expression was lost in the *bhh142* mutant, but kept at the WT level in the *bhlh141* anthers (Fig. 17D, E). The *AP37* expression pattern in *bhlh141* in this study seemed inconsistent with the previous results in which *AP37* gene is a direct target of the bHLH141 transcription factor (Niu et al. 2013). However, the authors also described a possibility that in addition to bHLH141, other unknown factors also act in *AP37* transcription (Niu et al. 2013). The inconsistent results between previous and this study may be attributable to unsettled contribution of bHLH141 in different growth conditions. In either way, at least in this study, the *AP25* expression was reconfirmed to completely depend on bHLH141 function in anthers at ST.5.

Next, by means of the *msp1* microarray, I selected six genes functionally unknown and highly expressed in ST.3 and/or ST.4 anthers, including meiocytes in almost any meiotic stages; *MS8 homolog a* (*MS8a*), *MS8 homolog b* (*MS8b*), *HEXO3-Like*, *NDST-a*, *XTH19* and *MYB35-like*. Their reduced expression in the *msp1* mutant anthers at ST.2 (Fig. 18) implicates these genes preferentially expressed in pre-meiotic, developing inner-wall layers. The expression of all six was lost completely in *bhlh142* anthers, while not significantly affected

by the *bhlh141* mutation (Fig. 18). The *MYB35-like* expression was peaked in WT anthers at meiotic ST.2 or ST.3, and interestingly, the peak seemed shifted to post-meiotic ST.5 in *bhlh141* anthers (Fig. 18F). This result may suggest that *MYB35-like* gene expression is fully dependent on bHLH142 function during meiosis, and in turn, repressed by bHLH141 at post-meiotic stages. Altogether, this category of genes, preferentially expressed in developing inner wall cells within meiotic anthers, requires bHLH142 for their expression.

In a short summary, the *msp1* microarray, incorporated with previous knowledge, enabled to categorize 15 genes, whose expression was specified to inner-anther walls, into three classes. The class-I genes (*MSP1*, *GAMYB*, *UDT1*, *DTM1*) are expressed highly in pre-meiotic or early-meiotic anthers (ST.1 and/or ST.2). The class-II genes (*MS8a*, *MS8b*, *HEXO3-Like*, *NDST-a*, *XTH19*, *MYB35-like*) are expressed through almost any meiotic stages (ST.2 to ST.4). The expression of the class-III genes (*TDR*, *PTC1*, *CYP704B2, AP25, AP37*) is peaked in post-meiotic anthers with tapetel cells going to PCD (ST.5).

The class-I gene expression is unlikely involved in the gene-regulatory cascade of either bHLH142 or 141, because it seems somewhat retained in both *bhlh142* and *bhlh141* mutants (Fig. 16). The class-II genes are likely regulated directly or indirectly by bHLH142, but independently of bHLH141 regulatory cascade. That is because their expression is largely inhibited by the *bhlh142* mutation, but unaffected by the *bhlh141* mutation (Fig. 18). The class-III genes can be divided in at least two subclasses. *AP25* gene is likely regulated under bHLH141 cascade, but the remaining genes are regulated independently of bHLH141.

***DCL3b* is a candidate gene regulated by first of dual peaks of bHLH141 expression**

A new finding of this study is that the bHLH141 expression exhibits dual peaks, earlier of which is detected in meiotic ST.2 or ST.3 anthers (Fig. 10C, D). Though the later bHLH141 peak at ST.5 is implicated in induction of tapetum PCD as described by Niu et al. (2013), roles of the earlier peak are unknown yet. The gene directly regulated by the earlier bHLH141 peak is expected to display an expression pattern meeting the following conditions; (1) the expression is exclusive at ST.2 or ST.3, at which the bHLH141 expression is firstly peaked, and (2) the expression is down-regulated or lost in both *bhlh142* and *bhlh141* mutant anthers. Of 16 genes examined above, only the *XTH19* expression fulfilled the two conditions.

I further sought other genes meet with the above two conditions, and then, focused on rice *DCL3b* gene, encoding a Dicer-like endoribonuclease required for biogenesis of 24-nucleotides trans-acting small interfering RNAs (24-nt tasiRNAs) (Song et al. 2012a). Recent studies have revealed the importance of small RNA-mediated gene silencing in reproductive organ development in rice (Johnson et al. 2009; Toriba et al. 2010; Song et al. 2012a; 2012b; Komiya et al. 2014), and the maize *DCL4,* a *DCL* paralog, is reported to be preferentially expressed in anther wall somatic cells (Kelliher and Walbot; 2014). In addition, the *msp1* microarray suggested that rice *DCL3b* is expressed in inner walls of developing anthers (Fig. 19A), and the result was reconfirmed by qRT-PCR (Fig. 19B). The expression

of *DCL3b* was exclusive in anthers at early meiotic ST.2, and almost absent in the *bhlh142* and 2.5-fold down-regulated in *bhlh141* mutant anthers at ST.2 (Fig. 19B). This pattern fullfilled the two conditions expected above for genes regulated by the first peak of bHLH expression. This result let me conceive a possibility of a direct interaction of bHLH141 transcription factor with the *DCL3b* expression.

The rice genome encodes eight paralogs of *Dicer-like* (*DCLs*) genes (Kapoor et al. 2008), function of which is supposed in small RNA biogenesis. Here, the expression of the other three *DCL* paralogs. *DCL1*, *DCL3a* and *DCL4,* was also examined by the qRT-PCR, but no remarkable difference was detected between WT and either *bhlh142* or *bhlh141* mutant anthers at meiotic ST.2 (Fig. 19C-E). The expression of *DCL3a* and *DCL1* was almost comparable between WT and *msp1* mutant anthers at ST.2 (Fig. 19B, E), suggesting the expression of these three paralogs was unlikely to be specific for the inner anther wall cells. Interestingly, the *DCL4* expression was peaked at early post-meiotic ST.5 anthers, and in addition, up-regulation of the expression in *msp1* mutant anthers at early meiotic ST.2 suggests that *DCL4* gene is preferentially expressed in meiocytes (Fig. 19D), different from *DCL3b* expression supposed in the anther wall. Generally, DCL4 is involved in 21-nt small interfering RNA (siRNA), and numerous 21-nt siRNA species are abundantly expressed in reproductive organs in rice (Komiya et al. 2014). Regardless of the interaction with bHLH regulatory cascades, *DCL4* expression in early post-meiotic germline cells will be worthy for deeper considerations in future.

The expression of three paralogs of RNA-dependent RNA polymerase genes (*RDR*s), *RDR2*, *RDR3* and *RDR6*, was also examined. RDRs are also involved in small RNA biogenesis and double-strandize ssRNA precursors for further processing by DCLs (Song et al. 2012b). As a result, no remarkable difference was observed in all three *RDR* paralogs between WT and either *bhlh142* or *bhlh141* anthers (Fig. 20). Thus, of genes encoding enzymes for small RNA biogenesis, *DCL3b* gene is a preferred candidate regulated by the first bHLH141 peak.

The expression of 24-nt phasiRNA precursor transcripts and their processing DCL3b enzyme is orchestrated by bHLH141 transcription factor

The gene expression analysis in rice anthers in this study suggested a possibility that the *DCL3b* gene expression is under the control of the earlier peaks of the bHLH141 expression (Fig. 19A). To further confirm this possibility, I performed ChIP-qPCR in flowers of transgenic plants expressing the bHLH141-C-GFP fusion protein by using anti-GFP antibody. The 1-kbp sequence upstream from the DCL3b translation initiation site (TIS) contained five consensus sequences, called E-box (Fig. 21A). PCR primer sets were designed to enclose three DCL3b-Ebox unit sites. This assay clearly indicated that bHLH141 transcription factor directly bound to the DCL3b-Ebox2, at the position -761 to -841 from DCL3b TIS (Fig. 21B, t=2.93, P<0.05). Significant binding of bHLH141 to DCL3b-Eboxe 3 was also detected (Fig. 21B, t=6.68, P<0.01) but not detected in DCL3b-Ebox 1 (Fig. 21B, t=2.26, P>0.05). In

addition, ChIP-qPCR experiments in flowers of transgenic plants expressing the N-YFP-bHLH142 revealed that, bHLH142 could not bind to all three DCL3b-Eboxes 1, 2 and 3 (Fig. 21B, t=0.90, 0.90 and 2.67, respectively, P>0.05). Two *DCL* paralogous genes, *DCL3a* and *DCL4*, also have conserved consensus E-box sequences within the upstream sequences of their TISs (Fig. 21C). However, in contrast to *DCL3b* upstream sequences, both bHLH141 and bHLH142 showed no significant binding to the sequences upstream of both *DCL3a* and *DCL4* genes (Fig. 21D, t=0.88 and 1.60 in bHLH141 and t=1.13 and 0.80 in bHLH142, respectively, P>0.05). These results clearly indicated that DCL3b expression is directed promoted by bHLH141 transcription factor specifically expressed in middle-layer and tapetal cells in early-meiotic ST.2 anthers.

As described in the INTRODUCTION part, DCL3b was reported to be involved in reproductive 24-nt phasiRNA biogenesis pathway. Thus, I investigated the expression of the genes involved in 24-nt phasiRNA biogenesis in anthers of WT and three mutants (*bhlh142*, *bhlh141* and *msp1*). The following five independent loci encoding 24-nt phasiRNA precursors were examined; *chr5-8*, *chr6-11*, *chr10-56*, *chr10-57* and *chr12-29*. In addition, three kinds of *pri-miR2275* precursor transcripts were also examined; *pri-miR2275a*, *pri-miR2275b* and *pri-miR2275f*. Interestingly, the expression patterns of the 24-nt phasiRNA and miR2275 precursor transcripts, other than *pri-miR2275f*, showed specifically elevated expressions only in early-meiotic stages (ST.2 and/or ST.3), and their expression profiles were similar to that of *DCL3b* gene (Figs. 19A, 22, 23). Moreover, like as *DCL3b*, these transcripts were hardly

detected in *msp1* mutant anthers at early meiotic stages (Fig. 22). However, the *pri-miR2775*s expression was significantly upregulated in early-meiotic ST.2 anthers in the *bhlh141* mutant (Fig. 23) by some unknown reasons, while *DCL3b* was downregulated (Fig. 19A). These results suggest that *DCL3b*-associating precursor transcripts, i.e. substrates of the DCL3b enzyme, were also under the control of *bHLH141* in inner anther wall cells, as well as *DCL3b* itself. In contrast, in the case of miR2275 precursors, these transcripts were under the control of *bHLH142* but not of *bHLH141*.

DCL3b-associated 24nt siRNAs are likely absent in *bhlh142* and *bhlh141* mutant anthers

Next, the amounts of 24-nt phasiRNAs, resultants of processing of phasiRNA precursor transcripts by DCL3b enzyme, were also quantified in early-meiotic anthers. For this purpose, I employed a PCR-based quantification method of small RNA species, described previously (Wan et al. 2010). A schematic diagram for small RNA quantification is shown in Fig. 24. Here, I focused again on the five phasiRNA precursor loci; *chr5-8*, *chr6-11*, *chr10-56*, *chr10-57* and *chr12-29*. These loci encoded 7 species of 24-nt phasiRNAs on either sense or antisense strands (Fig. 25). As a result, relatively higher siRNA expression was found in WT anther samples in the comparison to vegetative WT seedling as negative control samples. On the other hand, both *bhlh142* and *bhlh141* anther samples represented quite lower expression levels, comparable to the values detected in young seedlings (Fig. 26). This result clearly

indicated that siRNAs that arose from phasiRNA precursor loci were almost absent in both *bhlh142* and *bhlh141* anthers.

Finally, the amounts of mature miR2275s were also quantified. Both miR2275a/b and miR2275f showed higher expression in anther sample compared to seedlings, and however, no critical differences were found between WT and *bhlh* anther samples (Fig. 27). This result suggests that the miR2275s are expressed specifically in reproductive phase, and that the expression is unaffected by neither *bhlh142* nor *bhlh141* mutations.

DISCUSSION

bHLH142 functions in cell type differentiation of tapetum and middle layer

The most obvious characteristic of the *bhlh142* mutant is a defect in differentiation of tapetum and middle layer cells observed in late-meiotic anthers. Both middle layer and tapetum arise from secondary parietal cells by periclinical cell division (Fig. 1). In this stage, rapid loss of cellulose from wall cells in anther lobes is a key event representing differentiation of tapetal cells (Matsuo et al. 2013). In the *bhlh142* mutant anthers, tapetum-like cells continued to exhibit the cellulosic signals in meiotic and later stages (Figs. 6 and 8). Actually, expression levels of some glycosyl transferase and glycosyl hydrorase genes, possibly involved in degradation of celluloses in anther lobes, were almost absent in the *bhlh142* mutant (Fig. 18). In addition, excess periclinal divisions made anther-cell walls more than four layers (Figs. 6 and 8). These observations suggested that after secondary parietal cells divided periclinaly, *bhlh142* mutant anthers produced parietal cell-like undifferentiated cells in replacement of tapetal cells, resulting in lacking rapid cellulose degradation and developing extra anther wall layers (Figs. 6 and 8).

Another hallmark of tapetum development is PCD in post-meiotic microspore stage anthers, in which pollen coat materials produced in tapetum are secreted and supplied to developing pollen grains. A lot of genes were reported to be involved in tapetal PCD and pollen coat material metabolisms. In this study, several post-meiotic genes reported to date

were examined in their expression levels in *bhlh142* anthers; *TDR* (Li et al., 2006) as a key transcriptional regulator of post-meiotic tapetum development, *PTC1* (Li et al., 2011) as another regulator of post-meiotic tapetum development, *AP25* and *AP37* (Niu et al., 2013) as tapetum PCD trigger genes like as caspases for apoptosis and *CYP704B2* (Li et al., 2010) as marker gene which catalyzes fatty acid biosynthesis for pollen coat. The expression of all these post-meiotic genes was restricted in tapetum in WT anthers, and was absent or largely downed in *bhlh142* anthers (Fig. 17). This result also supports an idea that *bhlh142* anthers fail to differentiate any wall layers with tapetal cell identify.

In this study, I also examined the expression levels of genes expressed in pre-meiotic, early developmental stage anthers; *UDT1* (Jung et al., 2005) as transcriptional regulator of early anther wall development, *MSP1* (Nonomura et al., 2003) as signal transduction component essential for establishment of anther wall cells, *GAMYB* (Kaneko et al., 2004; Tsuji et al., 2006; Niu et al., 2013) as transcriptional regulator of gibberellin signaling throughout anther development and *DTM1* (Yi et al., 2012) as ER membrane protein essential for early anther development. The qRT-PCR quantification revealed that the expression of these genes was not affected by the *bhlh142* mutation, again leading to allocation of bHLH142 functions before secondary parietal cell division. Rather, the expressions of these genes were getting higher in the *bhlh142* mutant than in the WT (Fig. 16), also implying that undifferentiated cells replacing tapetum in *bhlh142* anthers aberrantly continued to express these pre-meiosis-expressed genes. Taken together this implication, the result that *bhlh142*

anthers develop undifferentiated cells in replacement of tapetum may suggest that bHLH142 directly acts in a switch of cell identity from undifferentiated parietal cells to differentiated tapetal cells.

Differential contributions of *bHLH142* and *bHLH141* on the anther development

The function of bHLH141 was clearly distinct from that of bHLH142 based on histological observations and expression analyses of genes specific to anthers in the mutant. Different from *bhlh142* mutant anthers, differentiated tapetum and middle layer were clearly ovserved in *bhlh141* anthers (Fig. 7). In addition, cell wall composition of *bhlh141* tapetum also exhibited WT like features with rapid degradation of cellulosic signals at meiotic stages (Fig. 9). These results suggest differential contributions of two bHLHs to gene expression networks for anther development. In fact, the expression pattern of *bHLH142* was different from that of the *bHLH141*. *bHLH142* was expressed from early-meiosis to middle-meiosis or late-meiosis stages, while *bHLH141* rapidly downed its expression after early-meiosis stages (Fig. 10). Similarly, in the viewpoint of cellular specificity, bHLH142 protein expression was found in nuclei of both tapetum and middle layer cells, on the other hand, bHLH141 expression was found only in tapetal cell nuclei (Figs. 12 and 13). *bHLH141* expression had two peaks in meiotic and post-meiotic stages (Fig. 10C, D). If restricted in the first peak of bHLH141 expression, *bHLH142* was expressed in wider ranges temporally and spatially compared to that of *bHLH141* expression. Taken together with the genetic relationships of

bHLH142 and *bHLH141* shown in this study (Figs. 10, 14 and 15), bHLH142 is supposed to regulate the expression of bHLH141 expression. Actually, Fu et al. (2014) showed that bHLH142 directly binds to the cis-regulatory upstream sequence of *bHLH141* locus, consistent with the results of this study that bHLH141 expression depended on the *bHLH142* function. bHLH142 also directly targets another bHLH transcription factor TDR (Fu *et al.*, 2014), and in addition, expression of many genes examined were severely down-regulated in *bhlh142* anthers (Figs. 17, 18 and 19). These results may suggest that the bHLH142 transcription factor is involved in other genetic networks for some transcriptional controls independent of the regulatory machineries which are cooperative of both bHLH142 and bHLH141 transcription factors.

Accompanying these observations and previous reports, I proposed that bHLH142 governs tapetal cell differentiation and subsequent meiotic anther development by multiple gene regulatory networks in which a *bHLH141* regulatory cascade is involved. My proposal is consistent with the observation that morphological defects observed in *bhlh141* anthers are milder compared to the phenotypes in *bhlh142* anthers.

A unique feature of bHLH141 having two distinct expression in tapetum development

This study clearly indicated two distinct expressional peaks of *bHLH141* in developing anthers. The earlier peak was found in tapetum cells at early-meiotic stages and the laterone was on post-meiotic tapetum cells (Figs. 10C, D and 13). Though the later peak was already

reported (Niu et al. 2013), the earlier one was newly detected in this study. The earlier bHLH141 peak was sharply detected and comparable to the later peak in a relative expression levels (Fig. 10C, D).

In the later peak, bHLH141 is reported to directly bind to promoter regions of asparatic protease genes, *AP25* and *AP37,* leading to tapetum PCD (Niu et al., 2013), and hence, loss-of-function of *bHLH141* results in delayed tapetum PCD and male sterility. Because no elevated expression of these *AP* genes was found in early-meiotic WT anthers, it is expected that PCD promotion triggered by *AP25* and *AP37* could be absent in early-meiotic anthers. In fact, it is known the timing of tapetal PCD events is strictly regulated and limited only at post-meiotic stages (Li *et al.*, 2006). On the contrary, precocious tapetal PCD triggered by some environmental stresses or genetic mutation causes male sterility as undesirable traits for plant reproduction (Ding et al., 2011). This previous observation suggests that the bHLH141 function other than in tapetal PCD may be attributed to altered expression of former bHLH141 peak newly found in this study.

A fundamental question concerning this unique expression profile of *bHLH141* should be considered. That is, how dual-peaked bHLH141 expressions are regulated during anther development; in other words, whether these two expressions were activated by a common regulatory mechanism or independent mechanisms. In this study, I demonstrated that bHLH142 acted upstream of bHLH141 (Figs. 10D and 14). In addition, from the results of cytological observations, bHLH142 accumulation seemed to overlap with the first peak of

bHLH141 expression in tapetal cell nuclei (Figs. 12 and 13). In contrast, bHLH142 completely disappeared when the secondary peak of bHLH141 was clearly detected in tapetal nuclei (Figs. 10C, D, 12 and 13). These results may suggest that though direct binding of bHLH142 to the cis-regulatory sequences of *bHLH141* locus was reported previously (Fu et al. 2014), it occurs at the early-meiotic stage with high *bHLH142* expression. If so, the later peak of bHLH141 expression may be enhanced by some transcription factors other than bHLH142. As another possibility, both peaks of bHLH141 were promoted by bHLH142 binding to respective promoter regions, but the expression may be interrupted once by some repressive factors or events; such as cell division or differentiation. Actually, during meiotic stages, a tapetal cell carrying a single nucleus becomes binucleared in rice, probably to enforce efficient production of pollen coat materials. In either ways, I propose that differential regulatory mechanisms between early- and post-meiotic stages contribute dual expressions of *bHLH141* distinctly detected during anther development.

The first of dual peaked bHLH141 expression promotes the expression of protein-coding and non-coding transcripts required for 24-nt phasiRNA biogenesis

In Fig. 28A, I summarized a model of genetic regulatory network regulated by bHLH142 and bHLH141 in anther wall cells, especially tapetum cells. As described above, bHLH141 had dual-peaked expression in early- and post-meiotic tapetum. The later, post-meiotic bHLH141 expression is likely involved in tapetum PCD pathway as previously proposed (Niu

et al., 2013). Focusing on early-meiotic stages, two major regulatory cascades could be drawn out. One involves cell type differentiation of tapetum and middle layer that mostly depended on bHLH142, but not on bHLH141. In this cascade, the genes for tapetum cell wall modification could be included (Figs. 8 and 18). In addition, this cell type differentiation seems to be in upstream to any other later events in tapetum development (Fig. 17).

The other cascade involves 24-nt siRNA biogenesis pathway, in which first peak of bHLH141 largely contribute (Figs. 19 to 27 and 28B). As described in the RESULTS section, developing anthers in rice express abundant 24-nt phasiRNAs (Johnson et al. 2009; Song et al. 2012a; 2012b; Komiya et al. 2014). This study clearly revealed that the bHLH transcription factor directly bound to the upstream sequence of the *DCL3b* gene, encoding an endoribonuclease that processes phasiRNA precursor dsRNAs into 24-nt long (Song et al. 2012a). In addition, the result of this study also suggested a possibility that the expression of phasiRNA precursor transcripts, that are substrates of DCL3b enzyme, were also controlled directly by bHLH141 (Figs. 22 and 28B). In *bhlh141* mutant anthers, both *DCL3b* and phasiRNA precursor expression were repressed, and consequently, the amounts of 24-nt phasiRNAs were reduced (Fig. 26).

Interestingly, the expression of miR2275 precursor transcripts was rather up-regulated in *bhlh141* mutant anthers at ST.2 (Fig. 23). In the *bhlh141* mutant, the amount of 24-nt phasiRNAs, the final products of the biogenesis pathway that I focused on this study, were severely reduced (Fig. 26). This result prompt me to propose the existence of some

positive-feedback loop for promoting the production of reduced amounts of phasiRNA, leading aberrantly elevated expression of miR2775 precursors in *bhlh141* mutant anthers. Amounts of mature miR2275 microRNAs were retained at high levels in *bhlh141* and even in *bhlh142* (Fig, 27). The results in *bhlh142* anthers were unexpected and somewhat strange, because the expression levels of *pri-miR2275a*, *pri-miR2275b* and *pri-miR2275f* were almost absent in *bhlh142* mutant. Based on the result that such a reduced expression of *pri-miR2275s*, it was expected that mature miR2275 could be also absent in *bhlh142*. Song et al., (2012) reported that at least eleven miR2275 family loci exist in the genome of *93-11* (an indica rice cultivar). In this study, I examined only three of miR2275 families because it was difficult to identify the counterparts of miR2275 loci in Dongjing genome (a parental rice cultivar of *bhlh142* mutant). As a possibility, other *pri-miR2275* family loci might be transcribed and processed into mature miR2275 even in *bhlh142* anthers, hence high amounts of mature miR2275 were detected even in *bhlh142*. These possible feedback loop and redundancy for *pri-miR2275* expression might assure stable production of mature miR2275s to initiate 24-nt phasiRNA biogenesis in rice anther.

As concluding remarks, this study in both bHLH paralogs of rice revealed an existence of unknown gene regulatory networks governing development of inner-anther wall layers in rice (Fig. 28). It should be noted that this study clarified the direct binding of bHLH141 transcription factor to the upstream promoter sequence of *DCL3b* gene indispensable for small RNA biogenesis. In rice anthers, not only 24-nt, but also 21-nt

phasiRNAs are abundantly expressed (Johnson et al. 2009; Song et al. 2012a; 2012b; Komiya et al. 2014). Recently, it was reported that the 21-nt phasiRNAs are bound by germline-specific Argonaute protein MEL1 in pre-meiotic and meiotic meiocytes, and MEL1 plays essential roles in early meiosis progression in rice (Nonomura et al. 2007; Komiya et al. 2014). Thus, the findings and knowledge obtained in this study should not be restricted in events in anther-wall cells, but propagated for mechanisms to promote anther development, concomitant with small RNA-mediated gene regulatory systems and cell-to-cell communication. The two loss-of-function mutants of bHLH paralogs will open the door to the frontier of plant reproduction studies.

ACKNOWLEDGEMENTS

I greatly acknowledge Dr. Ken-Ichi Nonomura to supervise this study. I also acknowledge the progress report committee members; Drs. Hiroyuki Araki, Hitoshi Sawa, Yumiko Saga and Yoshiaki Tarutani giving me helpful advices and suggestions. I am thankful to all current and past members of Experimental Farm Laboratory giving me helpful discussions and great encouragements.

REFERENCES

Armstrong, S.J., Franklin, F.C.H., and Jones, G.H. (2003). A meiotic time-course for Arabidopsis thaliana. Sex PlantReprod 16, 141-149.

Bhojwani, S.S., and Bhatnagar, S.P. (2008). The embryology of angiosperms, Fifth edition (New Delhi, India: UBS Publishers' Distributors PVT LTD).

Carretero-Paulet, L., Galstyan, A., Roig-Villanova, I., Martinez-Garcia, J.F., Bilbao-Castro, J.R., and Robertson, D.L. (2010). Genome-wide classification and evolutionary analysis of the bHLH family of transcription factors in Arabidopsis, poplar, rice, moss, and algae. Plant physiology 153, 1398-1412.

Chapman, G.P. (1987). The tapetum. International Review Cytology 107: 111-125.

Chaubal, R., Zanella, C., Trimnell, M.R., Fox, T.W., Albertsen, M.C., and Bedinger, P. (2000). Two male-sterile mutants of Zea Mays (Poaceae) with an extra cell division in the anther wall. Am J Bot 87, 1193-1201.

Ding J., Lu Q., Ouyang Y., Mao H., Zhang P., Yao J., Xu C., Li X., Xiao J., and Zhang Q. (2012). A long noncoding RNA regulates photoperiod-sensitive male sterility, an essential component of hybrid rice. Proc Natl Acad Sci U S A. 109, 2654-2659.

Fuse, T., Sasaki, T., and Yano, M. (2001) Ti-plasmid vectors useful for functional analysis of rice genes. Plant Biotechnology 18, 219-222.

Fu Z., Yu J., Cheng X., Zong X., Xu J., Chen M., Li Z., Zhang D., and Liang W. (2014). The Rice basic helix-loop-helix transcription factor TDR INTERACTING PROTEIN2 is a central switch in early anther development. Plant Cell 26, 1512-1524

Goldberg, R.B., Beals, T.P., and Sanders, P.M. (1993). Anther development: basic principles and practical applications. Plant Cell 5, 1217-1229.

Heslop-Harrison, J. (1966). Cytoplasmic connexions between angiosperm meiocytes. Annals Bot 30, 221-230.

Hirochika, H., Sugimoto, K., Otsuki, Y., Tsugawa, H., and Kanda, M. (1996). Retrotransposons of rice involved in mutations induced by tissue culture. Proc Natl Acad Sci U S A 93, 7783-7788.

Hong L., Tang D., Shen Y., Hu Q., Wang K., Li M., Lu T., and Cheng Z. (2012). MIL2 (MICROSPORELESS2) regulates early cell differentiation in the rice anther. New phytologist 196, 402-413.

Hong L., Tang D., Zhu K., Wang K., Li M., and Cheng Z. (2012). Somatic and reproductive cell development in rice anther is regulated by a putative glutaredoxin. Plant Cell 24, 577-588.

Hord, C.L., Chen, C., Deyoung, B.J., Clark, S.E., and Ma, H. (2006). The BAM1/BAM2 receptor-like kinases are important regulators of Arabidopsis early anther development. Plant Cell 18, 1667-1680.

Jeong, D.H., An, S., Park, S., Kang, H.G., Park, G.G., Kim, S.R., Sim, J., Kim, Y.O., Kim, M.K., Kim, S.R., et al. (2006). Generation of a flanking sequence-tag database for activation-tagging lines in japonica rice. The Plant journal : for cell and molecular biology 45, 123-132.

Johnson, C., Kasprzewska, A., Tennessen, K., Fernandes, J., Nan, G.L., Walbot, V.,

Sundaresan, V., Vance, V., and Bowman, L.H. (2009). Clusters and superclusters of phased small RNAs in the developing inflorescence of rice. Genome Res 19, 1429-1440.

Jung, K.H., Han, M.J., Lee, Y.S., Kim, Y.W., Hwang, I., Kim, M.J., Kim, Y.K., Nahm, B.H., and An, G. (2005). Rice Undeveloped Tapetum1 is a major regulator of early tapetum development. Plant Cell 17, 2705-2722.

Kaneko, M., Inukai, Y., Ueguchi-Tanaka, M., Itoh, H., Izawa, T., Kobayashi, Y., Hattori, T., Miyao, A., Hirochika, H., Ashikari, M., et al. (2004). Loss-of-function mutations of the rice GAMYB gene impair alpha-amylase expression in aleurone and flower development. Plant Cell 16, 33-44.

Kelliher, T., and Walbot, V. (2014). Maize germinal cell initials accommodate hypoxia and precociously express meiotic genes. The Plant journal : for cell and molecular biology 77, 639-652.

Komiya, R., Ohyanagi, H., Niihama, M., Watanabe, T., Nakano, M., Kurata, N., and Nonomura, K. (2014). Rice germline-specific Argonaute MEL1 protein binds to phasiRNAs generated from more than 700 lincRNAs. The Plant journal : for cell and molecular biology 78, 385-397.

Ko, S.S., Li, M.J., Sun-Ben, K. M., Ho, Y.C., Lin, Y.J., Chuang, M.H., Hsing, H.X., Lien, Y.C., Yang, H.T., Chang, H.C., Chan, M.T. (2014) The bHLH142 transcription factor coordinates with TDR1 to modulate the expression of EAT1 and regulate pollen development in rice. Plant Cell 26, 2486-2504.

Lee, S., Jung, K.H., An, G., and Chung, Y.Y. (2004). Isolation and characterization of a rice cysteine protease gene, OsCP1, using T-DNA gene-trap system. Plant Mol Biol. 54,

755-765.

Li, H., Pinot, F., Sauveplane, V., Werck-Reichhart, D., Diehl, P., Schreiber, L., Franke, R., Zhang, P., Chen, L., Gao, Y., et al. (2010). Cytochrome P450 family member CYP704B2 catalyzes the {omega}-hydroxylation of fatty acids and is required for anther cutin biosynthesis and pollen exine formation in rice. Plant Cell 22, 173-190.

Li, H., Yuan, Z., Vizcay-Barrena, G., Yang, C., Liang, W., Zong, J., Wilson, Z.A., and Zhang, D. (2011). PERSISTENT TAPETAL CELL1 encodes a PHD-finger protein that is required for tapetal cell death and pollen development in rice. Plant physiology 156, 615-630.

Li, N., Zhang, D.S., Liu, H.S., Yin, C.S., Li, X.X., Liang, W.Q., Yuan, Z., Xu, B., Chu, H.W., Wang, J., et al. (2006). The rice tapetum degeneration retardation gene is required for tapetum degradation and anther development. Plant Cell 18, 2999-3014.

Liu, Z., Bao, W., Liang, W., Yin, J., and Zhang, D. (2010). Identification of gamyb-4 and analysis of the regulatory role of GAMYB in rice anther development. Journal of integrative plant biology 52, 670-678.

Matsuo, Y., Arimura, S., and Tsutsumi, N. (2013). Distribution of cellulosic wall in the anthers of Arabidopsis during microsporogenesis. Plant cell reports 32, 1743-1750.

Murmu J., Bush M.J., DeLong C., Li S., Xu M., Khan M., Malcolmson C., Fobert P.R., Zachgo S., and Hepworth S.R. (2010). Arabidopsis basic leucine-zipper transcription factors TGA9 and TGA10 interact with floral glutaredoxins ROXY1 and ROXY2 and are redundantly required for anther development. Plant physiology 154, 1492-1504.

Nakamura S., Mano S., Tanaka Y., Ohnishi M., Nakamori C., Araki M., Niwa T., Nishimura

M., Kaminaka H., Nakagawa T., Sato Y., and Ishiguro S. (2010). Gateway binary vectors with the bialaphos resistance gene, bar, as a selection marker for plant transformation. Biosci Biotechnol Biochem 74, 1315-1319.

Niu, N., Liang, W., Yang, X., Jin, W., Wilson, Z.A., Hu, J., and Zhang, D. (2013). EAT1 promotes tapetal cell death by regulating aspartic proteases during male reproductive development in rice. Nature communications 4, 1445.

Nonomura, K., Eiguchi, M., Nakano, M., Takashima, K., Komeda, N., Fukuchi, S., Miyazaki, S., Miyao, A., Hirochika, H., and Kurata, N. (2011). A novel RNA-recognition-motif protein is required for premeiotic G1/S-phase transition in rice (Oryza sativa L.). PLoS Genet 7, e1001265.

Nonomura, K., Morohoshi, A., Nakano, M., Eiguchi, M., Miyao, A., Hirochika, H., and Kurata, N. (2007). A germ cell specific gene of the ARGONAUTE family is essential for the progression of premeiotic mitosis and meiosis during sporogenesis in rice. Plant Cell 19, 2583-2594.

Nonomura, K., Nakano, M., Eiguchi, M., Suzuki, T., and Kurata, N. (2006). PAIR2 is essential for homologous chromosome synapsis in rice meiosis I. J Cell Sci 119, 217-225.

Nonomura, K.I., Miyoshi, K., Eiguchi, M., Suzuki, T., Miyao, A., Hirochika, H., and Kurata, N. (2003). The MSP1 geneis necessary to restrict the number of cells entering into male and female sporogenesis and to initiate anther wall formation in rice. Plant Cell 15, 1728-1739.

Song, X., Li, P., Zhai, J., Zhou, M., Ma, L., Liu, B., Jeong, D.H., Nakano, M., Cao, S., Liu, C., et al. (2012a). Roles of DCL4 and DCL3b in rice phased small RNA biogenesis. The

Plant journal : for cell and molecular biology 69, 462-474.

Song, X., Wang, D., Ma, L., Chen, Z., Li, P., Cui, X., Liu, C., Cao, S., Chu, C., Tao, Y., et al. (2012b). Rice RNA-dependent RNA polymerase 6 acts in small RNA biogenesis and spikelet development. The Plant journal : for cell and molecular biology.

Toki, S., Hara, N., Ono, K., Onodera, H., Tagiri, A., Oka, S., and Tanaka, H. (2006). Early infection of scutellum tissue with Agrobacterium allows high-speed transformation of rice. The Plant journal : for cell and molecular biology 47, 969-976.

Toriba, T., Suzaki, T., Yamaguchi, T., Ohmori, Y., Tsukaya, H., and Hirano, H.Y. (2010). Distinct regulation of adaxial-abaxial polarity in anther patterning in rice. Plant Cell 22, 1452-1462.

Tsuji, H., Aya, K., Ueguchi-Tanaka, M., Shimada, Y., Nakazono, M., Watanabe, R., Nishizawa, N.K., Gomi, K., Shimada, A., Kitano, H., et al. (2006). GAMYB controls different sets of genes and is differentially regulated by microRNA in aleurone cells and anthers. The Plant journal : for cell and molecular biology 47, 427-444.

Wan, G., Lim, Q.E., and Too, H.P. (2010). High-performance quantification of mature microRNAs by real-time RT-PCR using deoxyuridine-incorporated oligonucleotides and hemi-nested primers. RNA 16, 1436-1445.

Yi, J., Kim, S.R., Lee, D.Y., Moon, S., Lee, Y.S., Jung, K.H., Hwang, I., and An, G. (2012). The rice gene DEFECTIVE TAPETUM AND MEIOCYTES 1 (DTM1) is required for early tapetum development and meiosis. The Plant journal : for cell and molecular biology 70, 256-270.

Zhang D., Liang W., Yin C., Zong J., Gu F., and Zhang D. (2010). OsC6, encoding a lipid

transfer protein, is required for postmeiotic anther development in rice. Plant physiology 154, 149-162.

Zhang, D., and Yang, L. (2014). Specification of tapetum and microsporocyte cells within the anther. Current opinion in plant biology 17, 49-55.

Zhao X., de Palma J., Oane R., Gamuyao R., Luo M., Chaudhury A., Hervé P., Xue Q., and Bennett J. (2008). OsTDL1A binds to the LRR domain of rice receptor kinase MSP1, and is required to limit sporocyte numbers. Plant journal: for cell and molecular biology 54, 375-387

Zhou H., Liu Q., Li J., Jiang D., Zhou L., Wu P., Lu S., Li F., Zhu L., Liu Z., Chen L., Liu Y.G., and Zhuang C. (2012). Photoperiod- and thermo-sensitive genic male sterility in rice are caused by a point mutation in a novel noncoding RNA that produces a small RNA. Cell Research 22, 549-660.

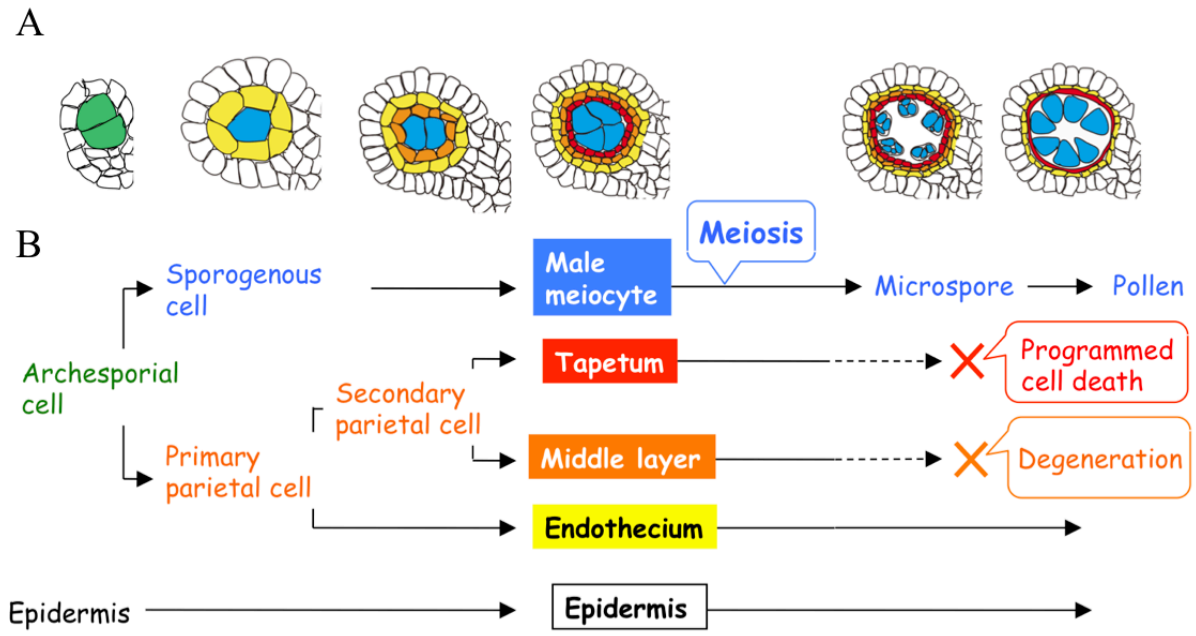

Fig. 1. Schematic representation of anther development in rice.
(A) Illustrations of anther morphology in each developmental stage. **(B)** Cell lineage of developing anther of rice. Cell identities and their positions are corresponding to between (A) and (B) represented in same colors.

A

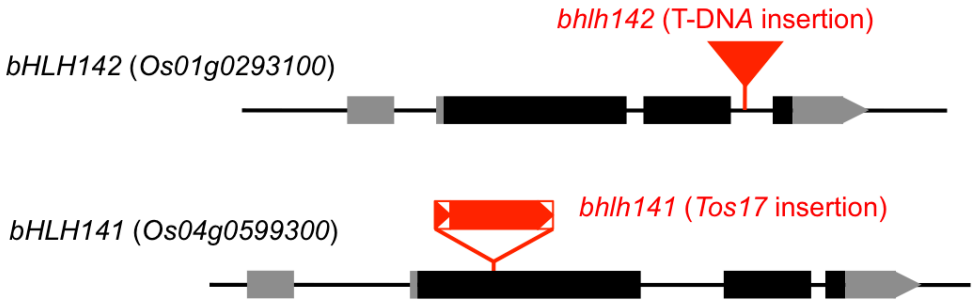

B

Locus (RAD-DB)	Probe set	Normalized signal intensity		Fold change		Gene symbol
		WT	*msp1*	*msp1*/WT	WT/*msp1*	
Os04g0599300	Os.49995.1.S1_at	10.1	0.650	0.0642	15.6	*bHLH141*
Os01g0293100	Os.54828.1.S1_at	11.6	1.21	0.104	9.58	*bHLH142*

C

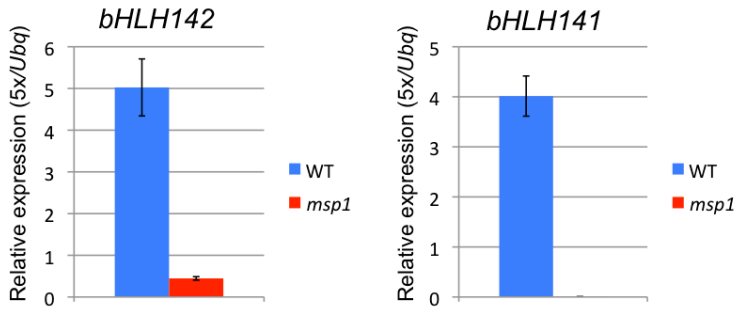

D

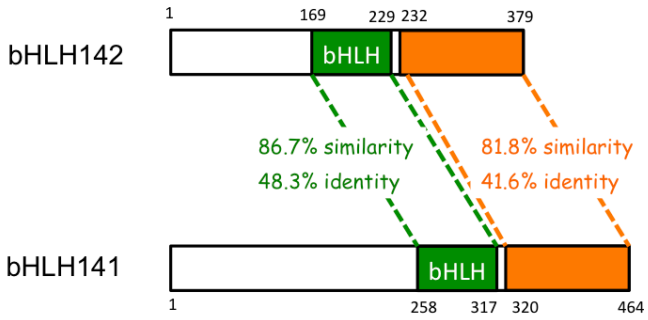

Fig. 2. ***bHLH142*** **and** ***bHLH141*** **as candidate genes which preferentially expressed in anther wall cells**

(A) Genomic structures of *bHLH142* and *bHLH141*. (B) Expression levels of *bHLH142* and *bHLH141* in early-meiotic *msp1* mutant anthers revealed by microarray experiment. (C) Expression levels of *bHLH142* and *bHLH141* in early-meiotic *msp1* mutant anthers reveled by qRT-PCR. Error bars indicate standard errors of three replications in each experiment. (C) Deduced amino acid sequence similarity between bHLH142 and bHLH141 peptide.

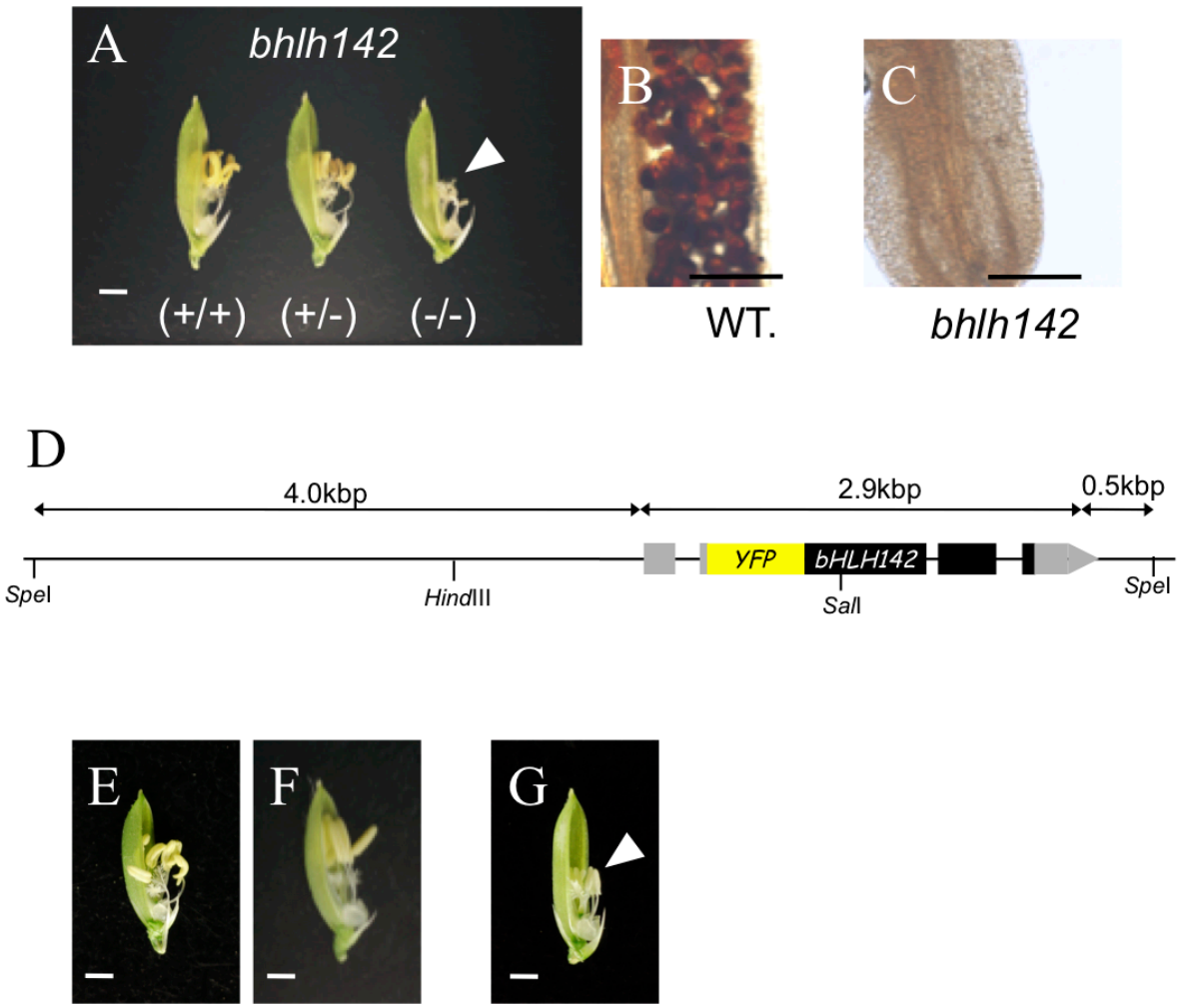

Fig. 3. Male sterility of *bhlh142* and its phenotypic complementation.
(A) Flower morphology of WT homozygous (+/+), WT/*bhlh142* heterozygous (+/-) and *bhlh142* homozygous (-/-) plants. Arrowhead indicates sterile immature anthers. **(B and C)** Iodide-potassium iodide staining of mature anther of WT homozygous (B) and *bhlh142* homozygous (C) plants. Dark brown staining represents fertile pollen grains. **(D)** Schematic representation of structure of transgene p*bhlh142*::*N-YFP-bHLH142* used for phenotypic complementation assay of *bhlh142*. **(E to G)** Flower morphology of transgenic lines carrying p*bhlh142*::*N-YFP-bHLH142* (E and F) and that of a control line carrying vector only (G). Arrowhead indicates immature anthers.
Bars, 1mm in (A), (E), (F) and (G) and 100μm in (B) and (C)

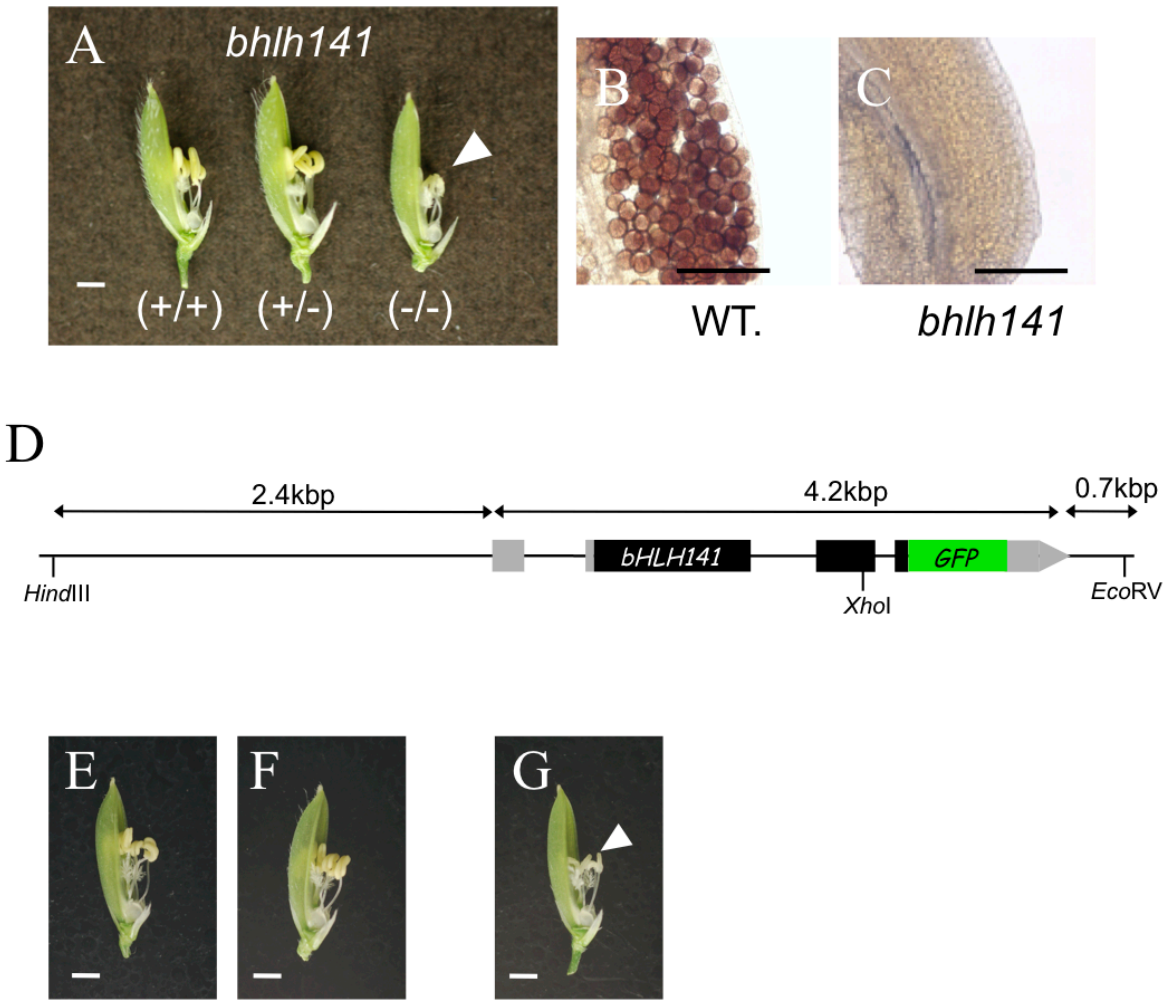

Fig. 4. Male sterility of *bhlh141* and its phenotypic complementation.

(A) Flower morphology of WT homozygous (+/+), WT/*bhlh141* heterozygous (+/-) and *bhlh141* homozygous (-/-) plants. Arrowhead indicates sterile immature anthers. **(B and C)** Iodide-potassium iodide staining of mature anther of WT homozyhous (B) and *bhlh141* homozygous (C) plants. Dark brown staining represents fertile pollen grains. **(D)** Schematic representation of structure of transgene p*bhlh141*::*bHLH141-C-GFP* used for phenotypic complementation assay of *bhlh141*. **(E to G)** Flower morphology of transgenic lines carrying p*bhlh141*::*bHLH141-C-GFP* (E and F) and that of a control line carrying vector only (G). Arrowhead indicates immature anthers.

Bars, 1mm in (A), (E), (F) and (G) and 100µm in (B) and (C)

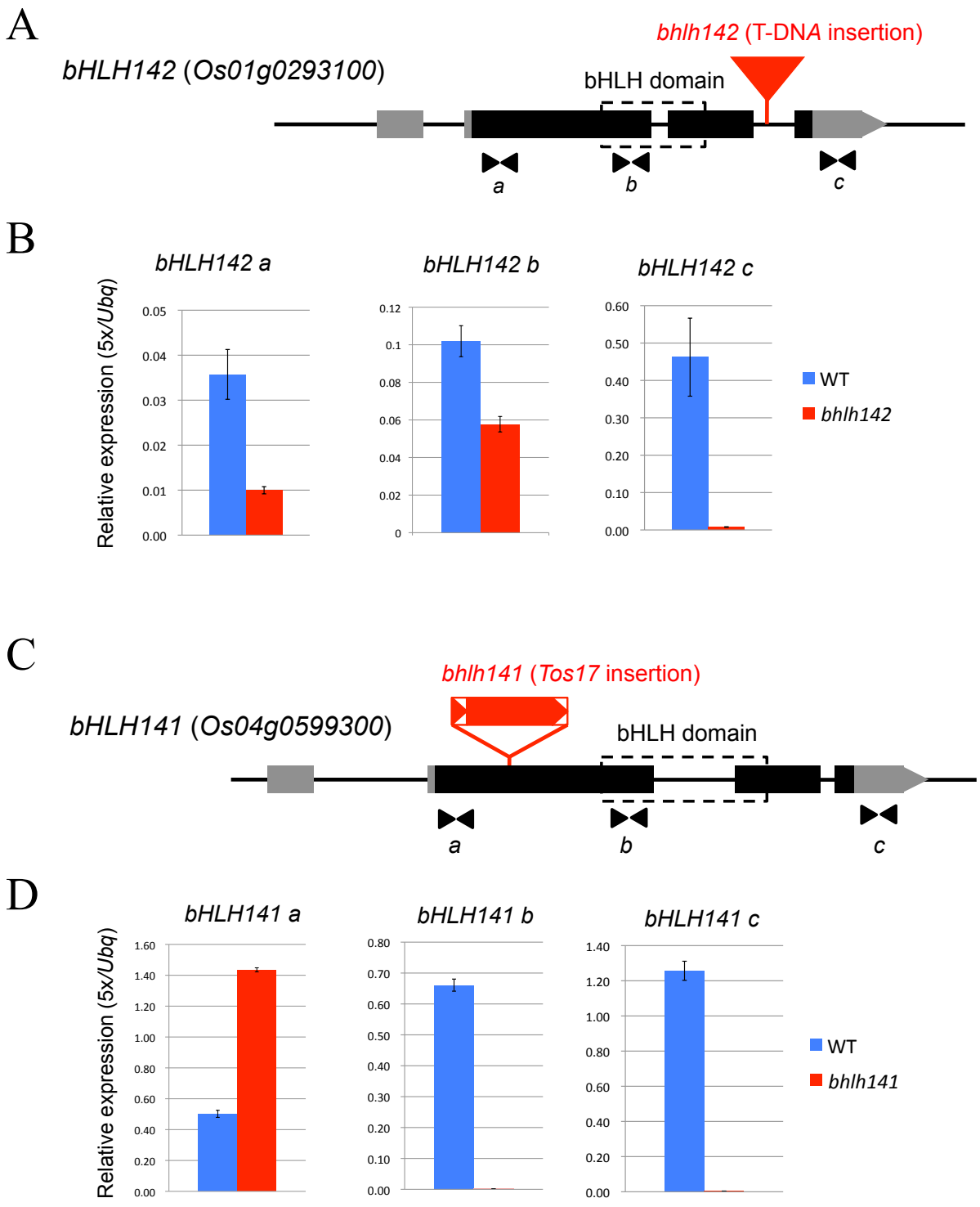

Fig. 5. Characterization of *bHLH142* and *bHLH141* mRNAs in respective mutants.
(A) Gene structure of *bHLH142*. Arrowheads indicate positions of primer pairs examined their transcriptional levels. **(B)** Relative expressions of primer pairs shown in (A) between WT and *bhlh142* flowers. **(C)** Gene structure of *bHLH141*. Arrowheads indicate positions of primer pairs examined their transcriptional levels. **(D)** Relative expressions of primer pairs shown in (C) between WT and *bhlh141* flowers. Error bars represent standard errors of three replications

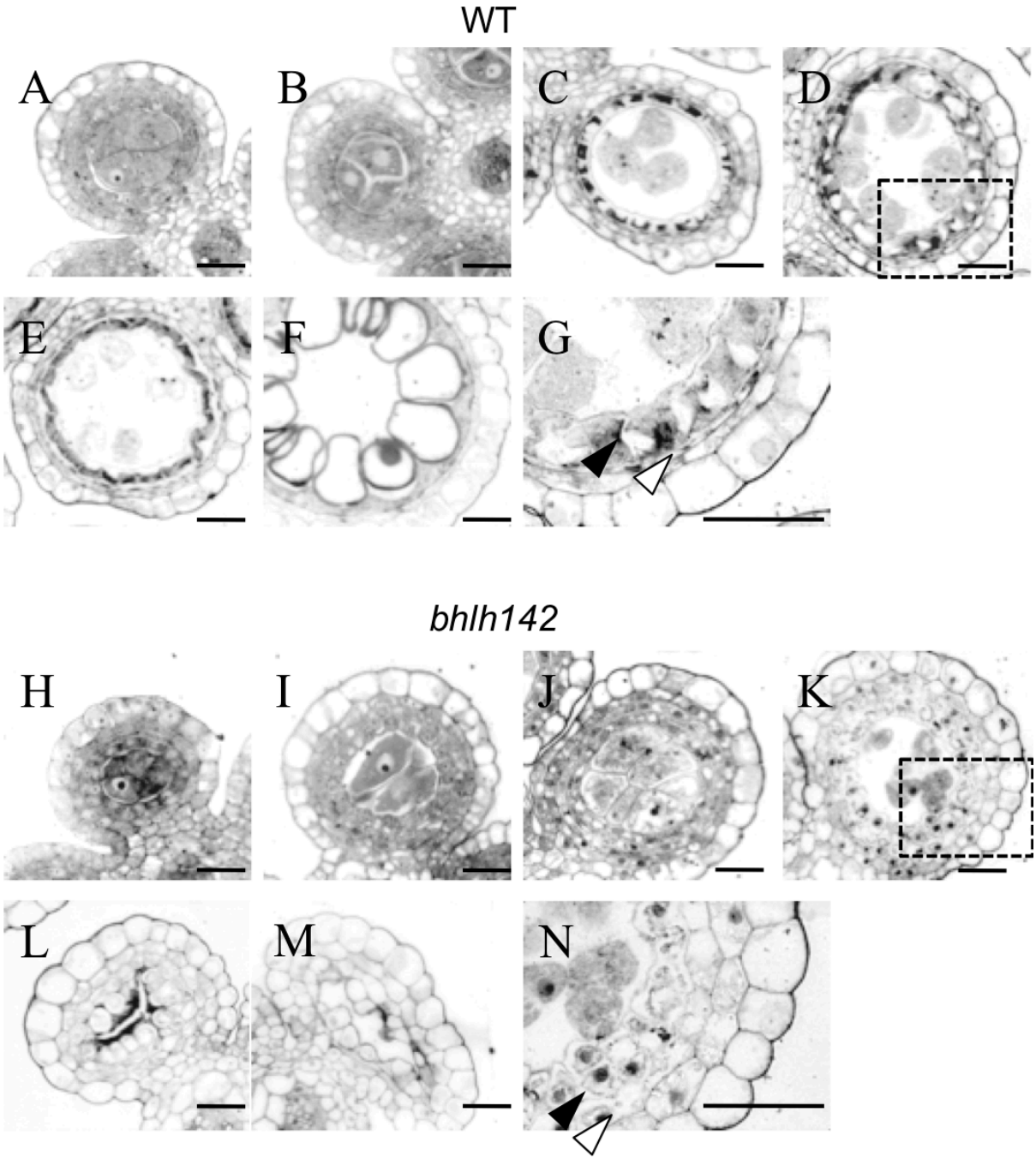

Fig. 6. Anther morphology of *bhlh142*.

(A-G) Cross-sections of anthers from WT homozygous plants. **(H-N)** Cross-sections of anthers from *bhlh142* homozygous plants. **(A and H)** Pre-meiotic stage. **(B and I)** Early-meiotic stage. **(C and J)** Middle-meiotic stage. **(D and K)** Late-meiotic stage. **(E and L)** Microspore stage. **(F and M)** Pollen developmental stage. **(G and N)** Magnified view of enclosed region of dotted lines in D and K, respectively. Solid arrowheads indicate tapetum(-like) cells. Empty Arrowheads indicate middle layer(-like) cells.

Bars, 20μm

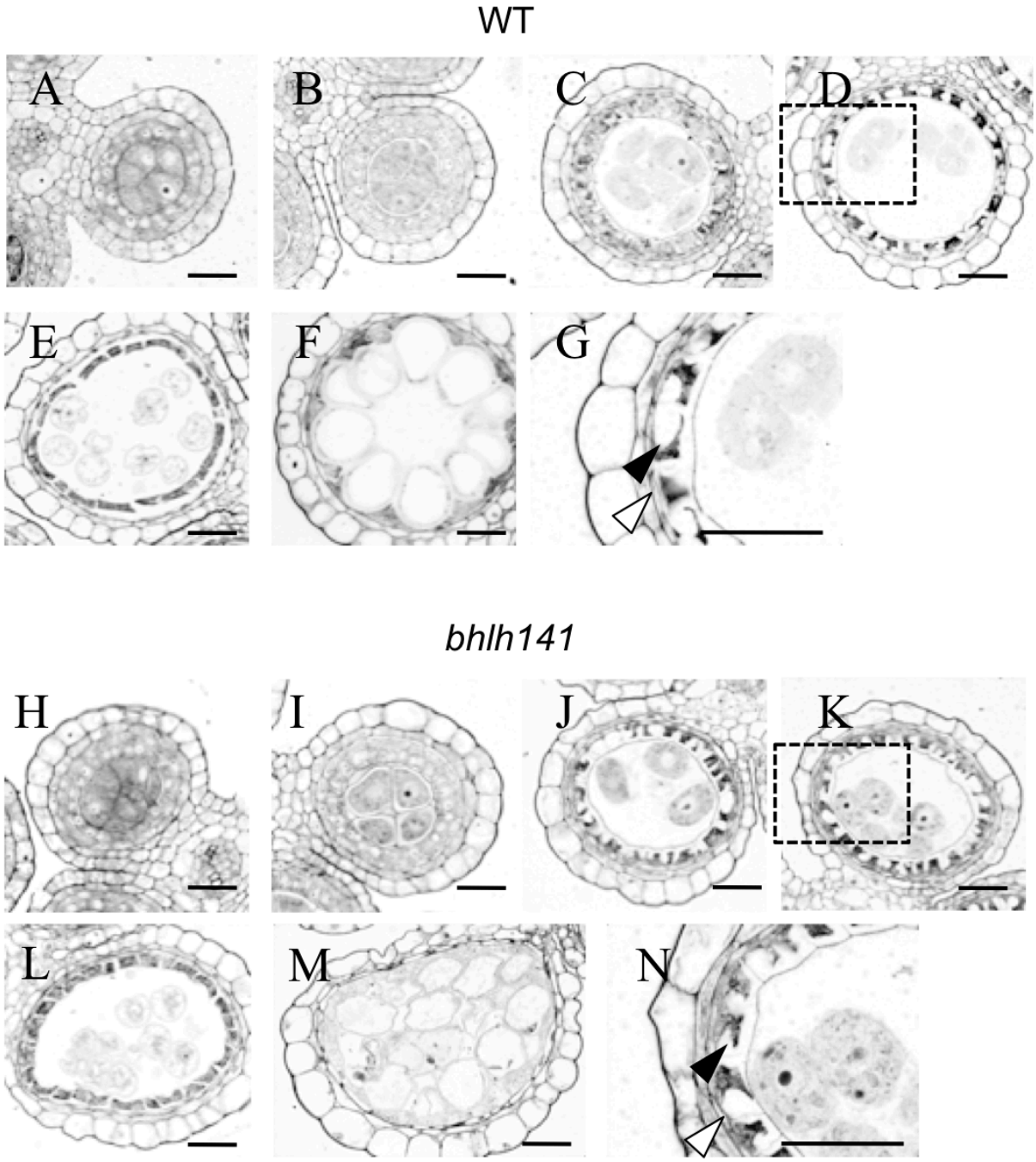

Fig. 7. Anther morphology of *bhlh141*.

(A-G) Cross-sections of anthers from WT homozygous plants. **(H-N)** Cross-sections of anthers from *bhlh141* homozygous plants. **(A and H)** Pre-meiotic stage. **(B and I)** Early-meiotic stage. **(C and J)** Middle-meiotic stage. **(D and K)** Late-meiotic stage. **(E and L)** Microspore stage. **(F and M)** Pollen developmental stage. **(G and N)** Magnified view of enclosed region of dotted lines in D and K, respectively. Solid arrowheads indicate tapetum(-like) cells. Empty arrowheads indicate middle layer(-like) cells.

Bars, 20μm

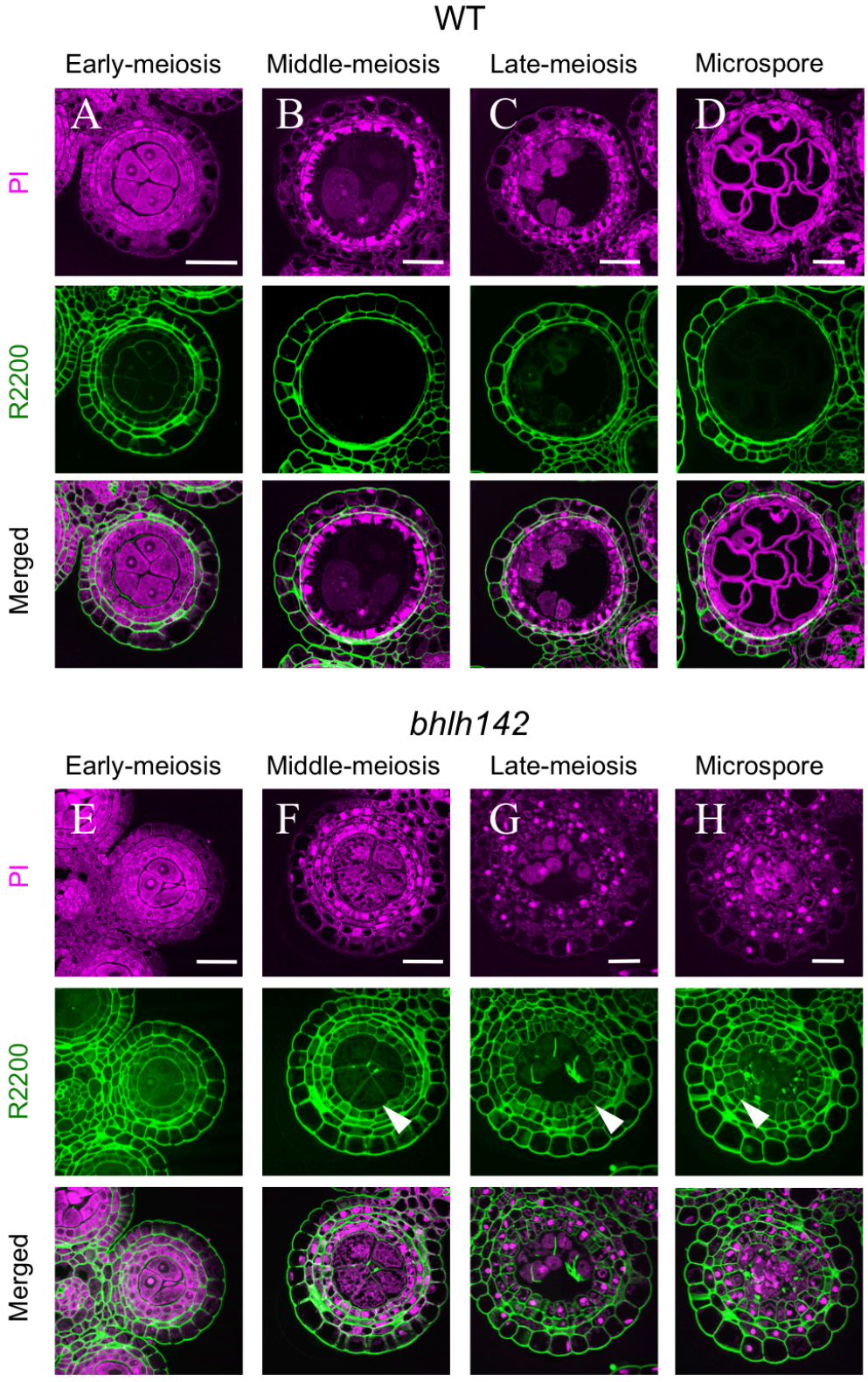

Fig. 8. Cellulosic cell wall signals in WT and *bhlh142* anthers.

(A-D) WT anther sections stained with PI and Runaissence2200 (R2200). **(E-H)** *bhlh142* anther sections. **(A and E)** Early-meiotic stage. **(B and F)** Middle-meiotic stage. **(C and G)** Late-meiotic stage. **(D and H)** Microspore stage. Arrowheads indicate remains of cellulosic cell walls in *bhlh142* mutant. Bars, 20μm.

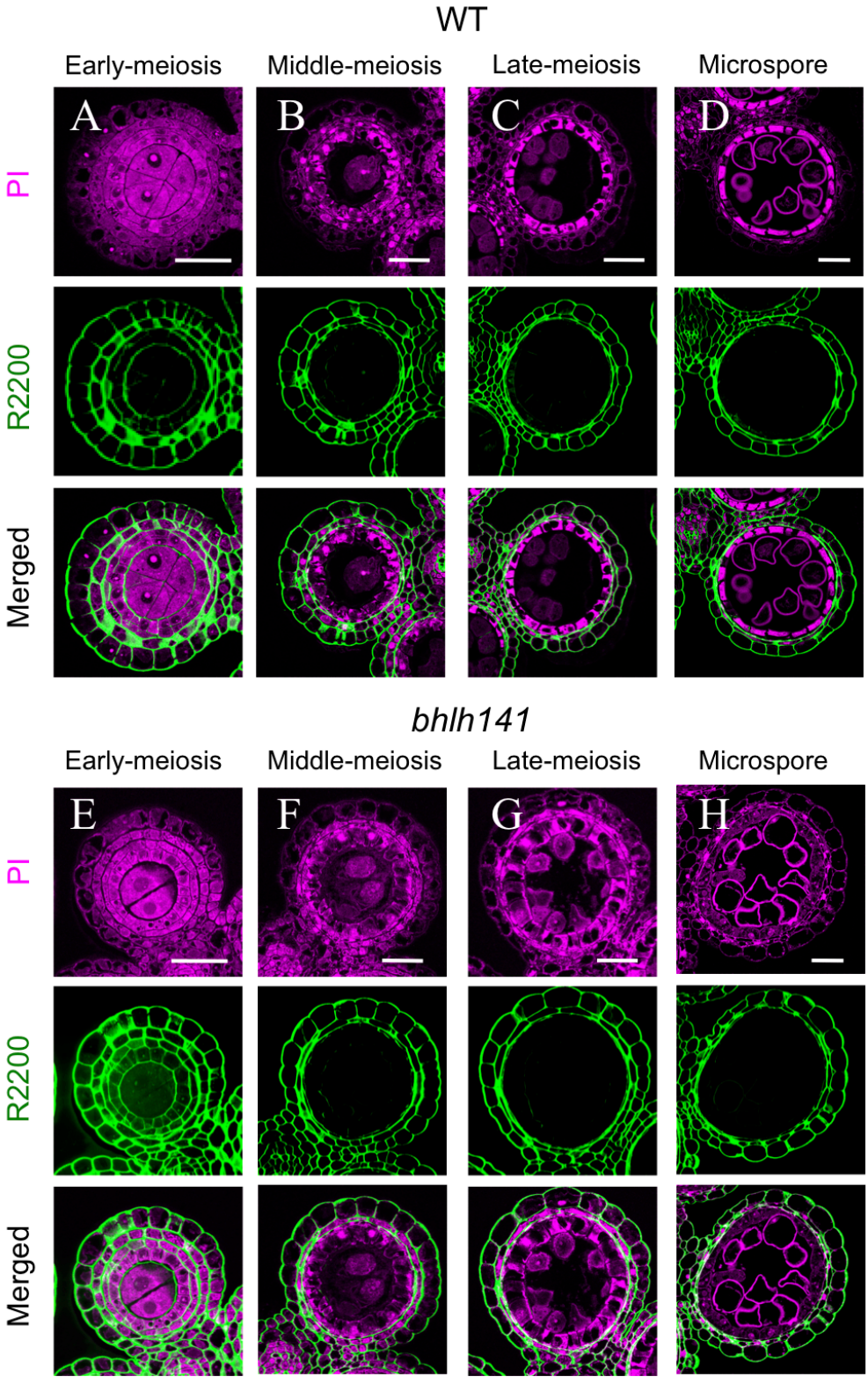

Fig. 9. Cellulosic cell wall signals in WT and *bhlh141* anthers.

(A-D) WT anther sections stained with PI and Runaissence2200 (R2200). **(E-H)** *bhlh141* anther sections. **(A and E)** early-meiotic stage. **(B and F)** Middle-meiotic stage. **(C and G)** Late-meiotic stage. **(D and H)** microspore stage. *bhlh141* anthers also exhibit degradation of cellulosic cell wall signals after early meiotic stages as well as WT anthers.

Bars, 20μm.

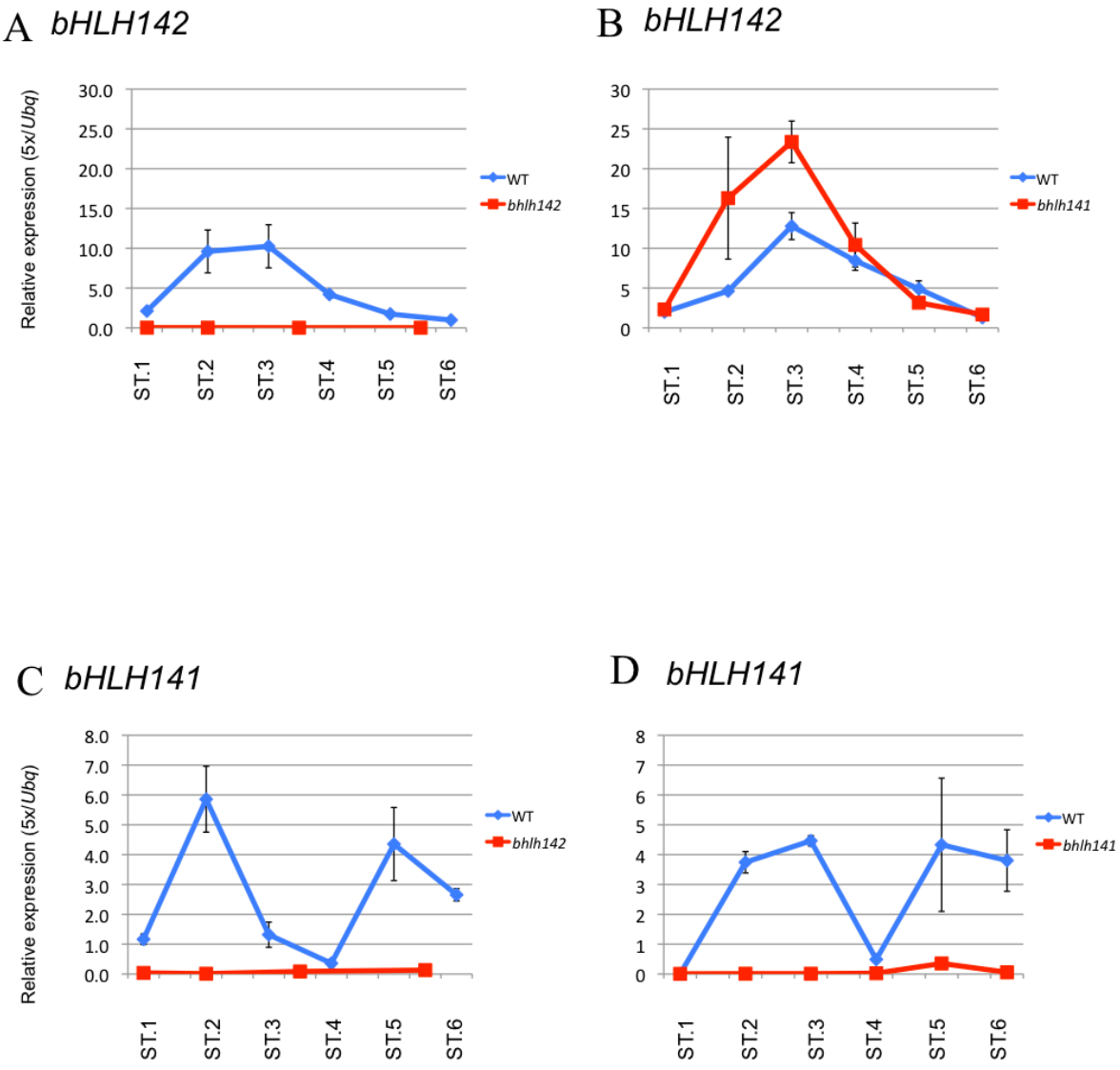

Fig. 10. Temporal expression profiles of *bHLH142* and *bHLH141*.
(A) *bHLH142* expression in *bhlh142* mutant and WT anthers. **(B)** *bHLH142* expression in *bhlh141* mutant and WT anthers. **(C)** *bHLH141* expression in *bhlh142* mutant WT anthers. **(D)** *bHLH141* expression in *bhlh141* mutant and WT anthers. Error bars indicate standard errors of three replications in each experiment.

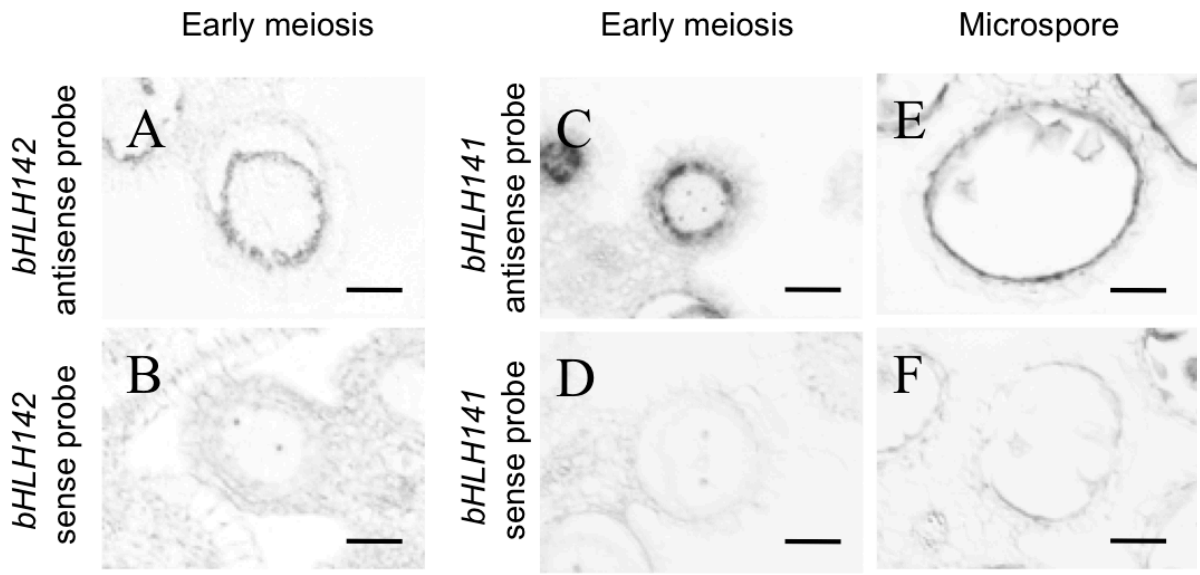

Fig. 11. RNA *in situ* hybridization of *bHLH142* and *bHLH141* in meiotic anthers.
(A) Early-meiotic anther hybridized with *bHLH142* antisense probe. **(B)** Early-meiotic anther hybridized with *bHLH142* sense probe. **(C)** Early-meiotic anther hybridized with *bHLH141* antisense probe. **(D)** Early-meiotic anther hybridized with *bHLH141* sense probe. **(E)** Microspore stage anther hybridized with *bHLH141* antisense probe. **(F)** Microspore stage anther hybridized with *bHLH141* sense probe.
Bars 20µm

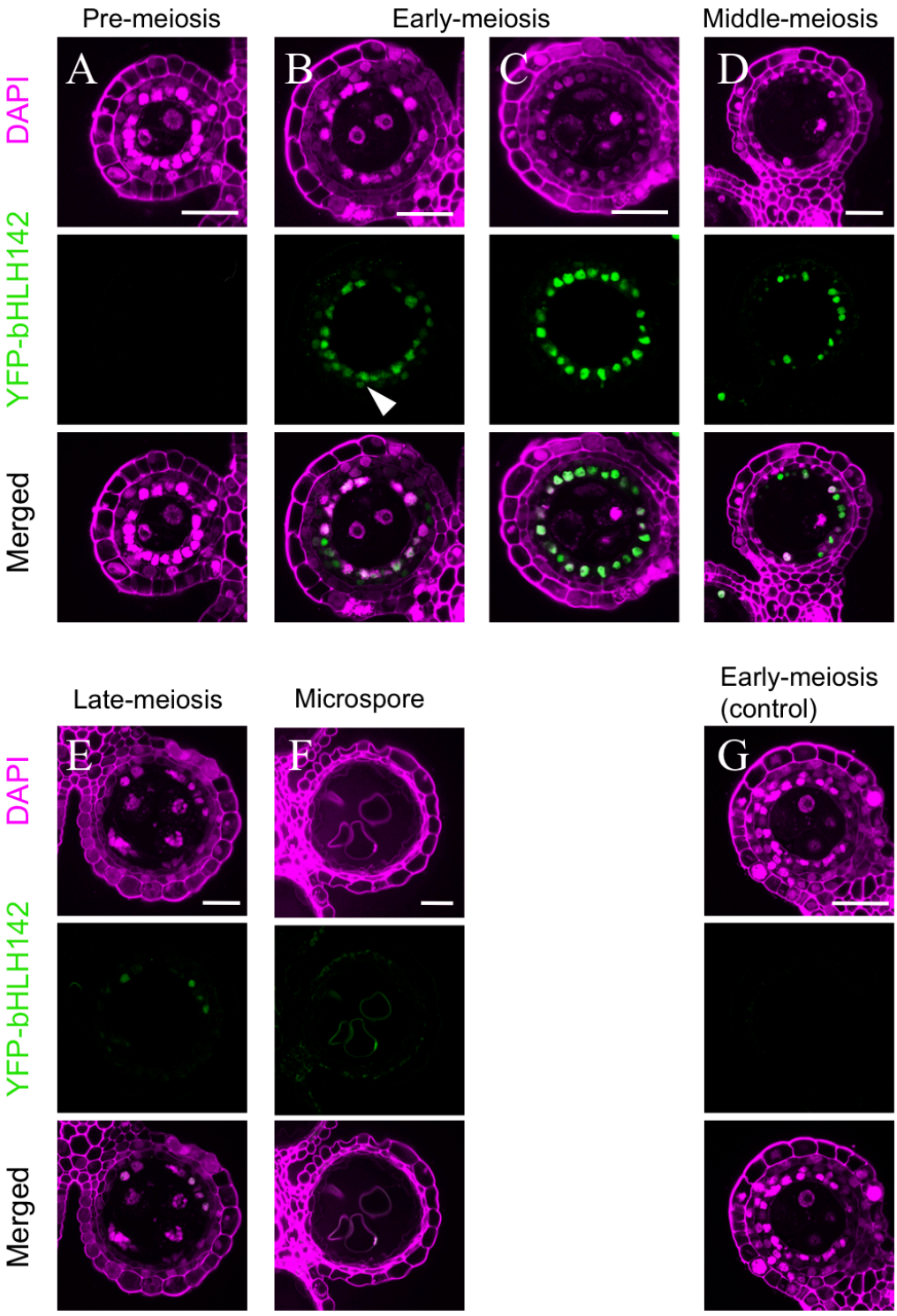

Fig. 12. Fluorescence signals of YFP-tagged bHLH142 in the anthers of transgenic lines.
(A-F) Anther sections of T_0 transgenic lines having p*bHLH142::YFP-bHLH142* with DAPI counter staining. **(A)** Pre-meiosis **(B and C)** Early-meiotic stage. **(D)** Middle-meiotic stage. **(E)** Late-meiotic stage. **(F)** Microspore stage. **(G)** Early-meiotic anther sections of a control T_0 transgenic line having vector sequence only. Arrowhead indicates YFP signals in middle layer cell.
Bars, 20μm.

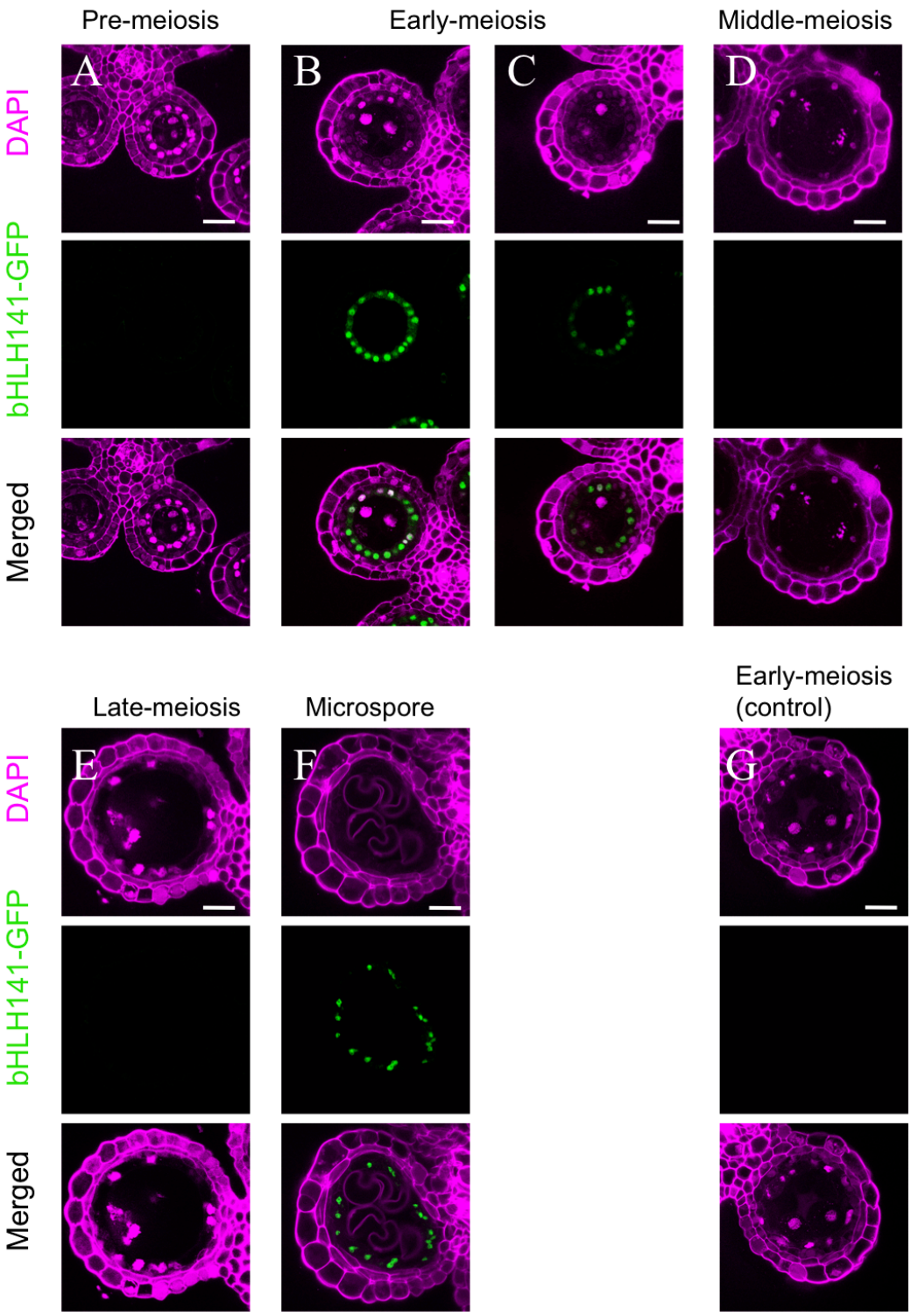

Fig. 13. Fluorescence signals of GFP-tagged bHLH141 in the anthers of transgenic lines.
(A-F) Anther sections of T_1 transgenic lines having p*bHLH141::bHLH141-GFP* with DAPI counter staining. **(A)** Premeiotic three-layered stage. **(B and C)** Early-meiotic stage. **(D)** Middle-meiotic stage. **(E)** Late-meiotic stage. **(F)** Microspore stage. **(G)** Early-meiotic anther sections of a control T_1 transgenic line having vector sequence only.
Bars, 20μm.

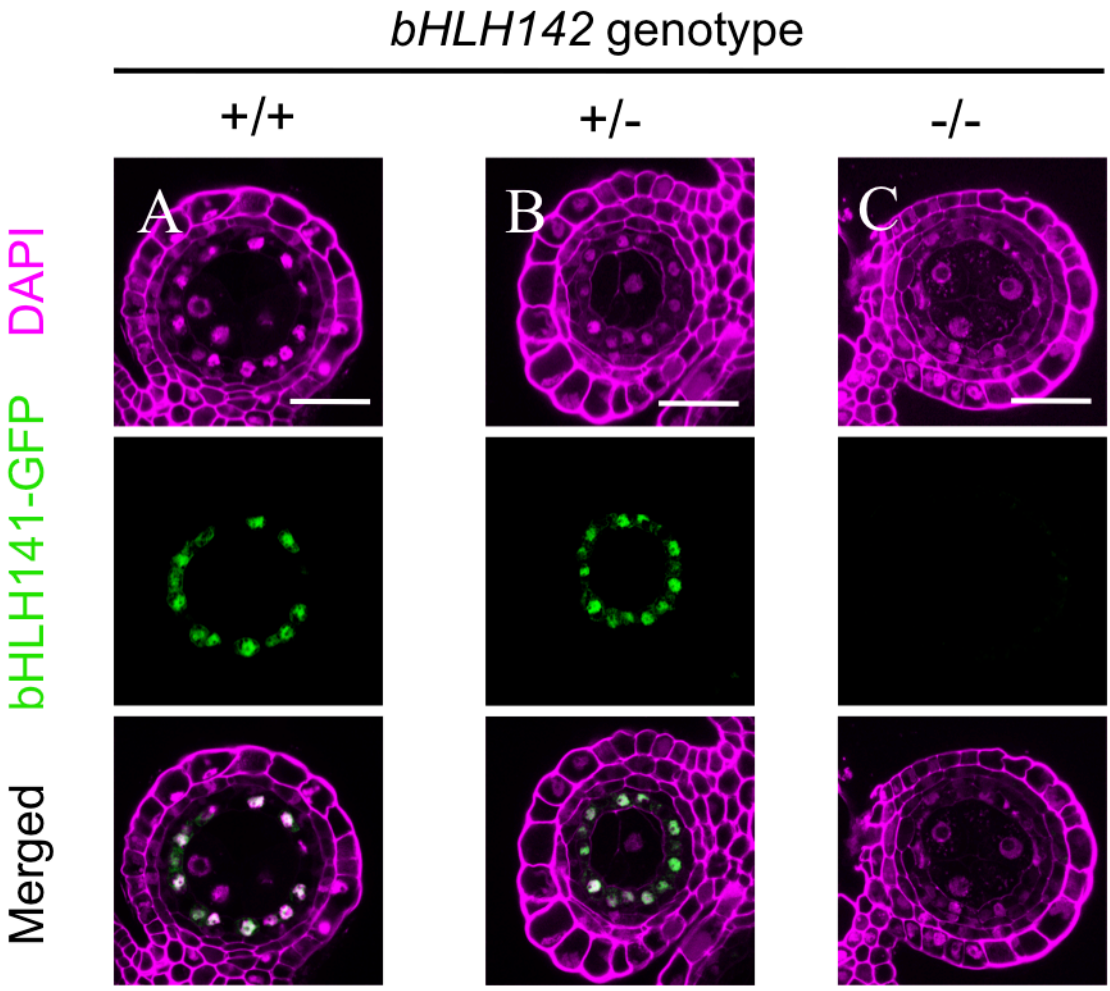

Fig. 14. Fluorescence signals of GFP-tagged bHLH141 in the background of *bhlh142*.
(A-C) Anther sections of *bhlh142* mutant lines carrying p*bHLH141::bHLH141-GFP* with DAPI counter staining. **(A)** WT homozygous (+/+), **(B)** WT/*bhlh142* heterozygous (+/-) and **(C)** *bhlh142* homozygous (-/-) lines.
Bars, 20µm.

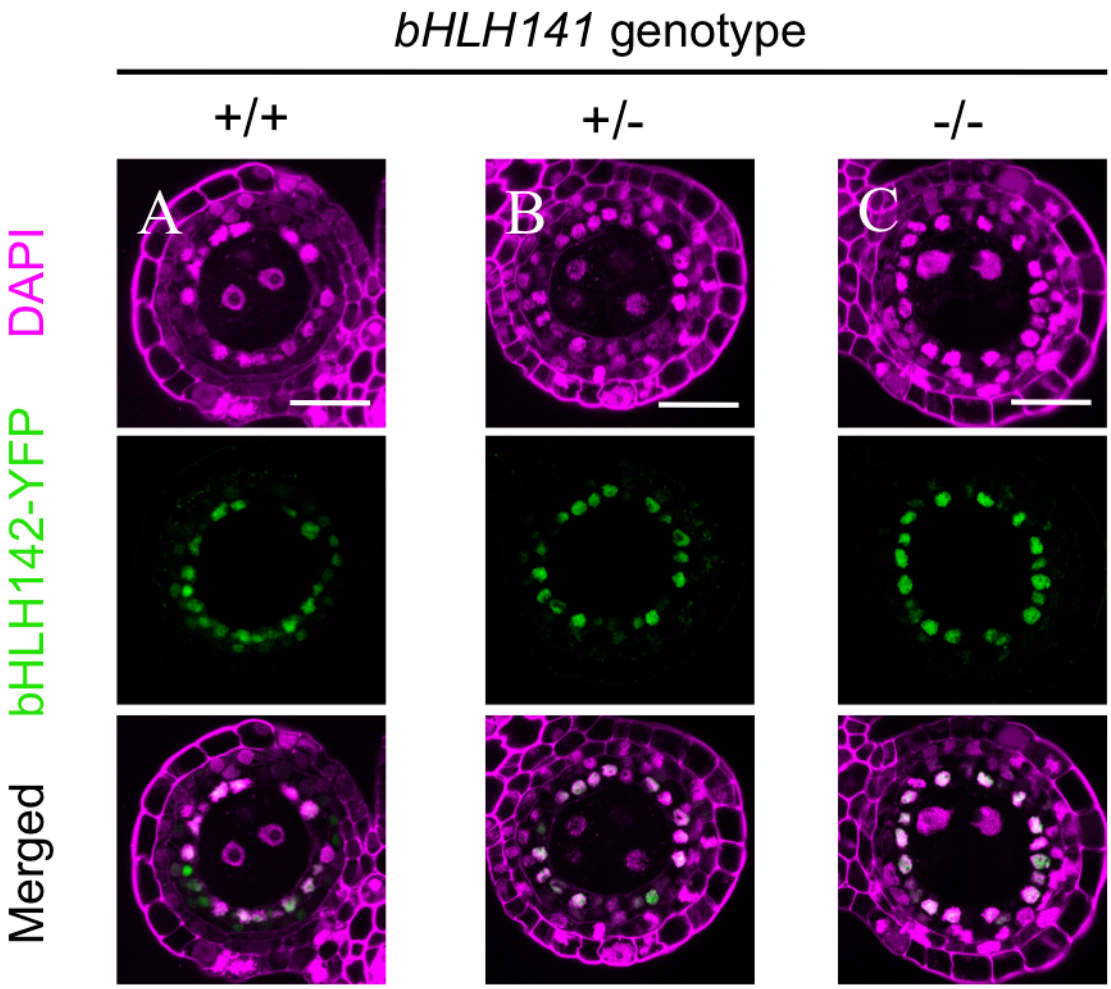

Fig. 15. Fluorescence signals of YFP-tagged bHLH142 in the background of *bhlh141*.
(A-C) Anther sections of *bhlh141* mutant lines carrying p*bHLH142::bHLH142-YFP* with DAPI counter staining. **(A)** WT homozygous (+/+) line, identical to Fig. 12B. **(B and D)** WT/*bhlh141* heterozygous (+/-) and **(C, E and F)** *bhlh141* homozygous (-/-) lines.
Bars, 20µm.

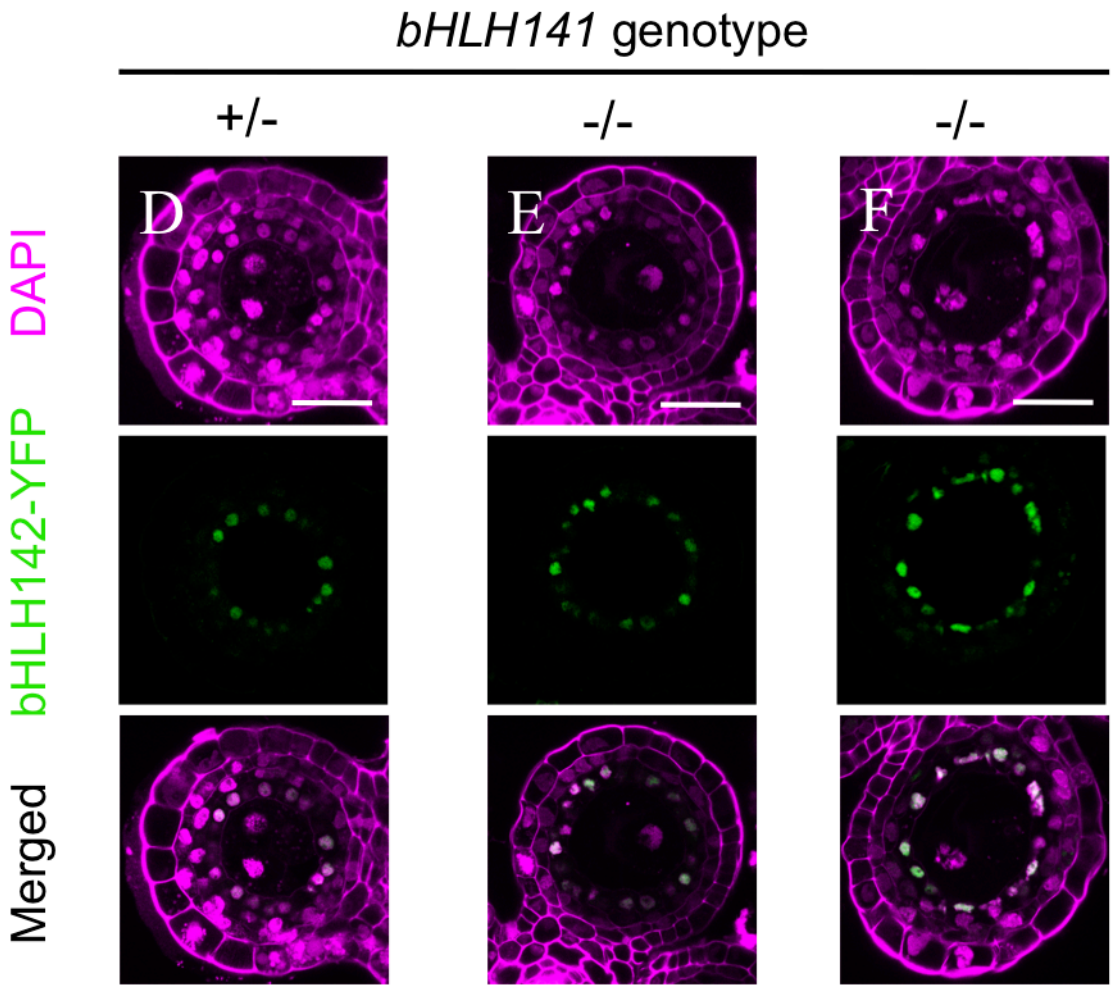

Fig. 15. Continued.

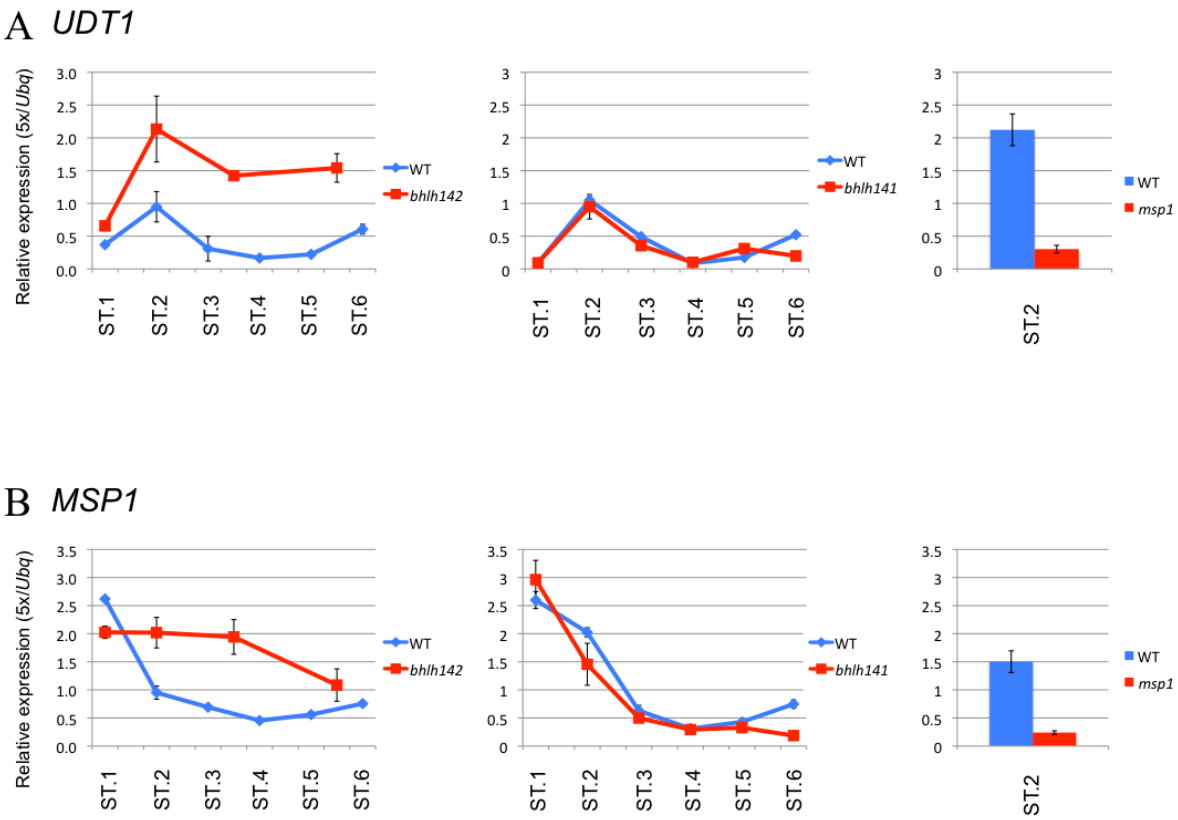

Fig. 16. Gene expression profiles in *bhlh142*, *bhlh141* and *msp1* anthers.
1. Genes known to function in early or global anther development.
(A) *UDT1*, **(B)** *MSP1*, **(C)** *GAMYB* **and (D)** *DTM1*.
In each panel, the left and mid line graphs show their expression profiles in *bhlh142* and *bhlh141* mutant anthers, respectively. The rightmost bar graph shows expression levels in early-meiotic *msp1* anther. Error bars represent standard errors of three replications.

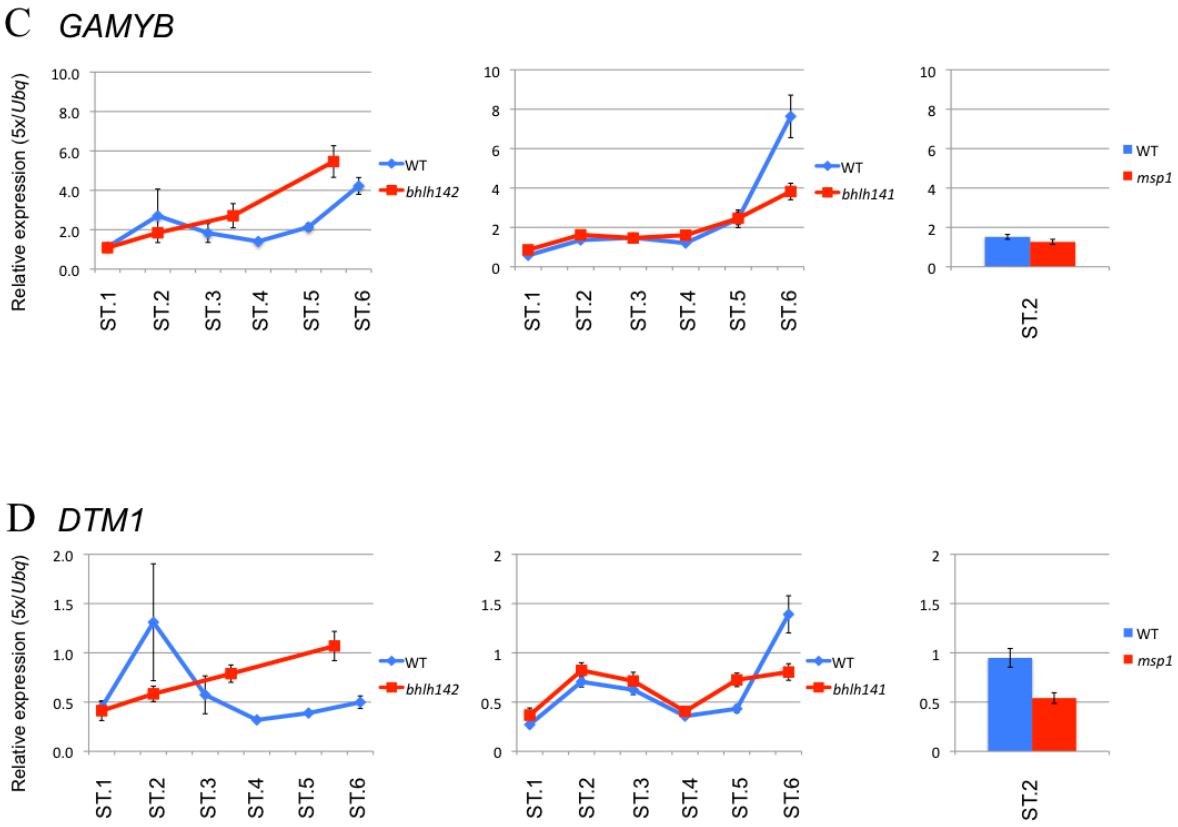

Fig. 16. Continued.

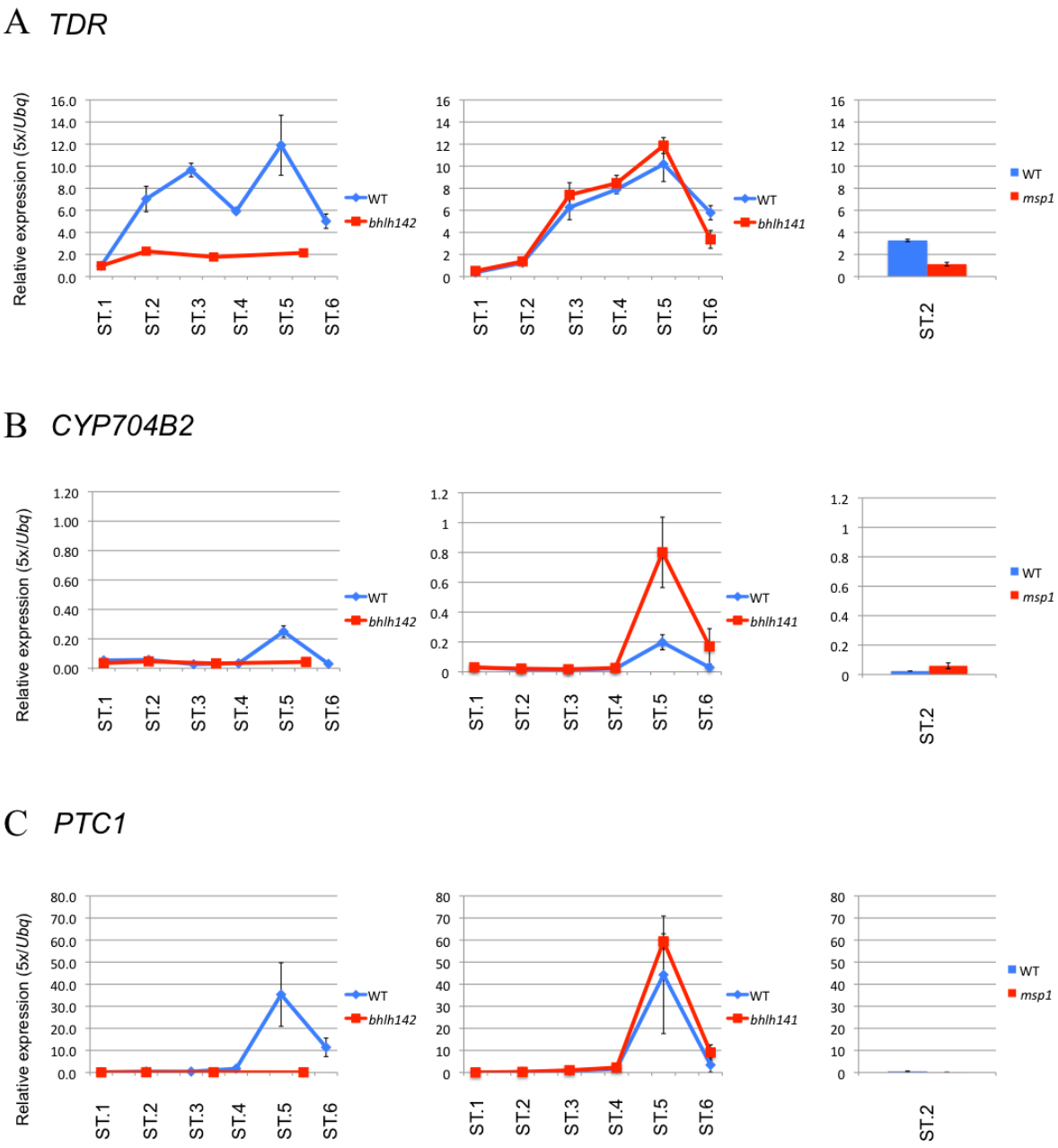

Fig. 17. Gene expression profiles in *bhlh142*, *bhlh141* and *msp1* anthers.
2. Genes known to function in post-meiotic tapetum PCD or nutrient supply for microspore.
(A) *TDR*, **(B)** *CYP704B2*, **(C)** *PTC1*, **(D)** *AP25* **and (E)** *AP37*.
In each panel, the left and mid line graphs show their expression profiles in *bhlh142* and *bhlh141* mutant anthers, respectively. The rightmost bar graph shows expression levels in early-meiotic *msp1* anther. Error bars represent standard errors of three replications.

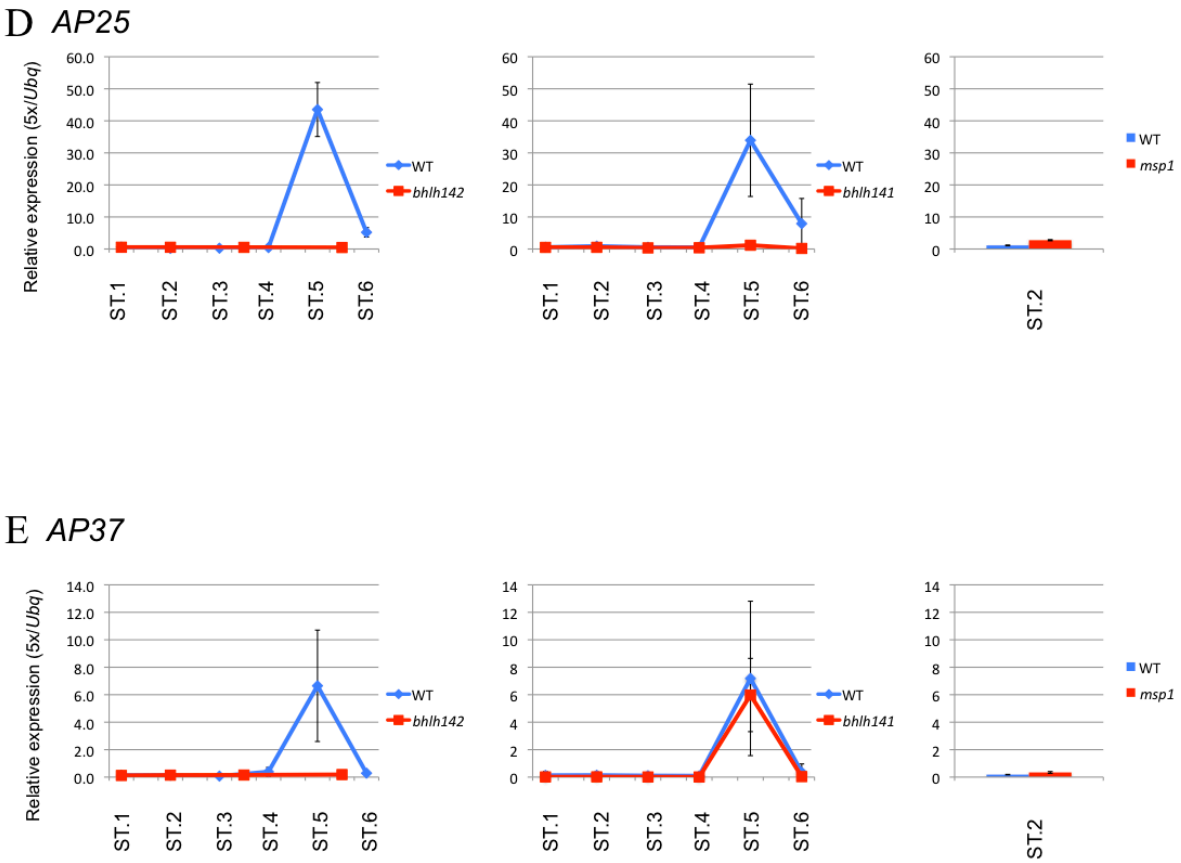

Fig. 17. Continued.

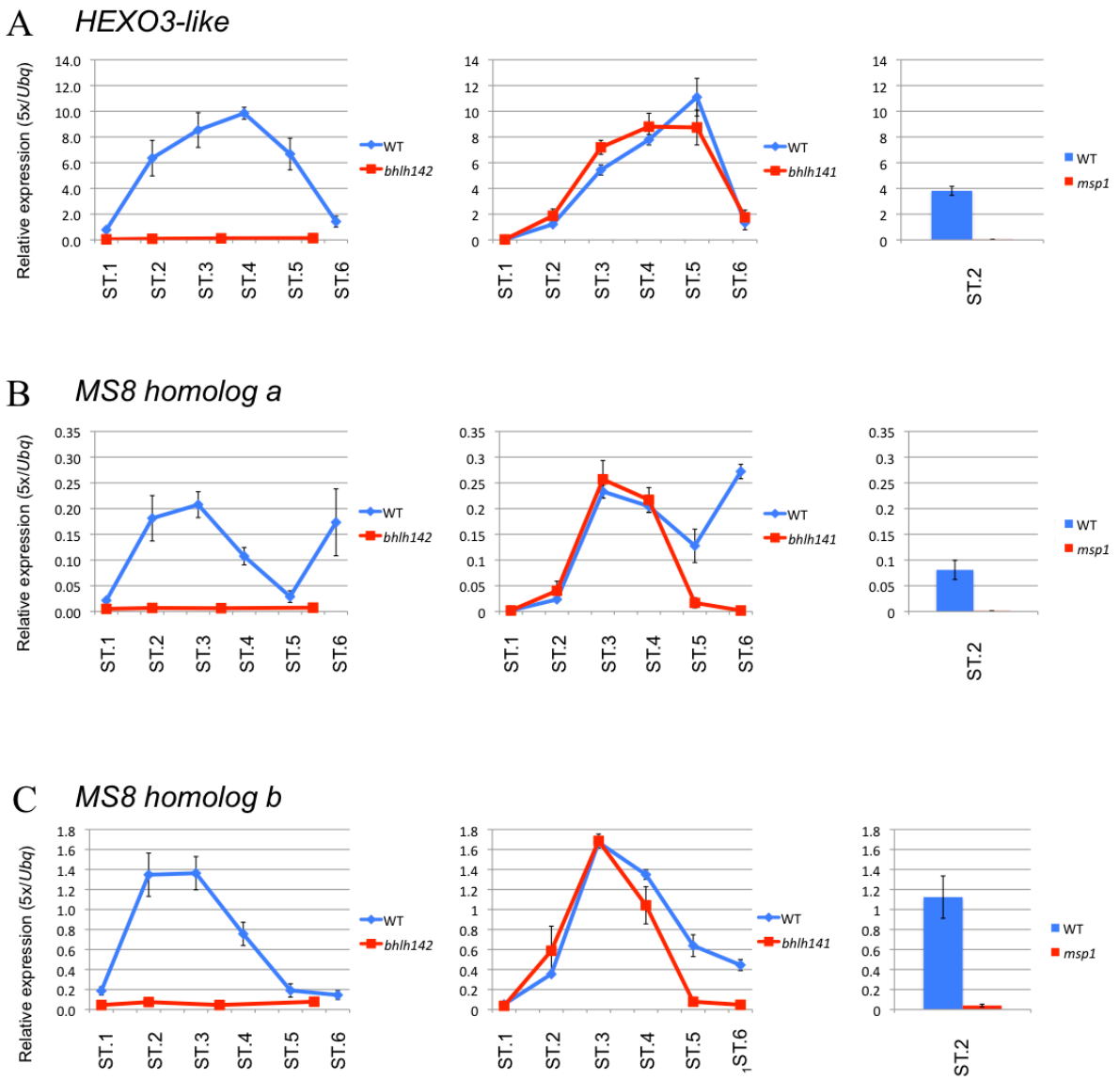

Fig. 18. Gene expression profiles in *bhlh142*, *bhlh141* and *msp1* anthers.

3. Functionaly-unknown genes.

(A) *Hexo-3 like,* **(B)** *MS8 homolog a*, **(C)** *MS8 homolog b,* **(D)** *NDST-a*, **(E)** *XTH19* and **(F)** *MYB35-like*.

In each panel, the left and mid line graphs show their expression profiles in *bhlh142* and *bhlh141* mutant anthers, respectively. The rightmost bar graph shows expression levels in early-meiotic *msp1* anther. Error bars represent standard errors of three replications.

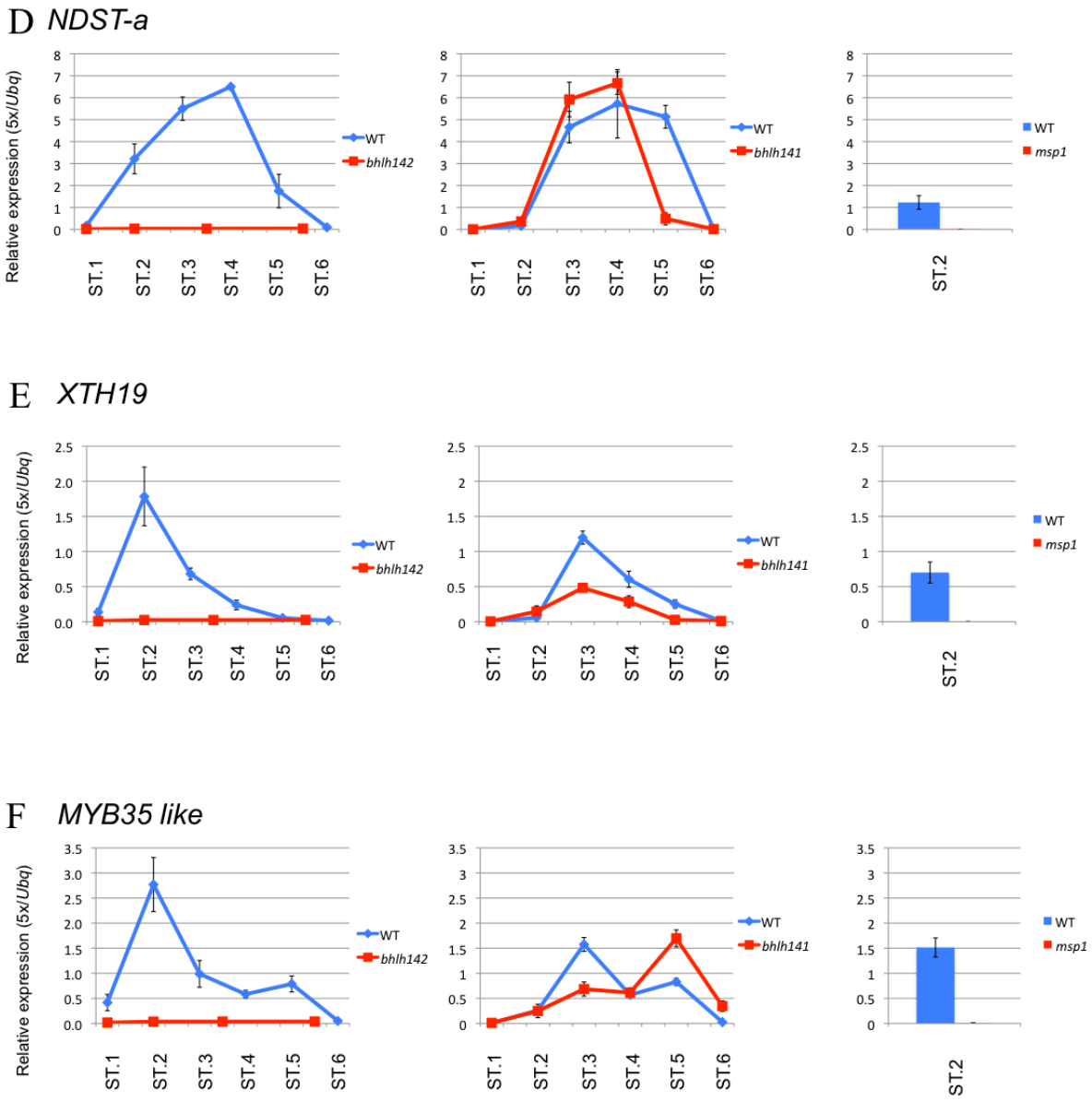

Fig. 18. Continued.

A

Locus (RAD-DB)	Probe set	Normalized signal intensity		Fold change		Gene symbol
		WT	*msp1*	*msp1*/WT	WT/*msp1*	
Os10g0485600	OsAffx.8007.1.S1_at	2.19	0.437	0.200	5.00	*DCL3b*

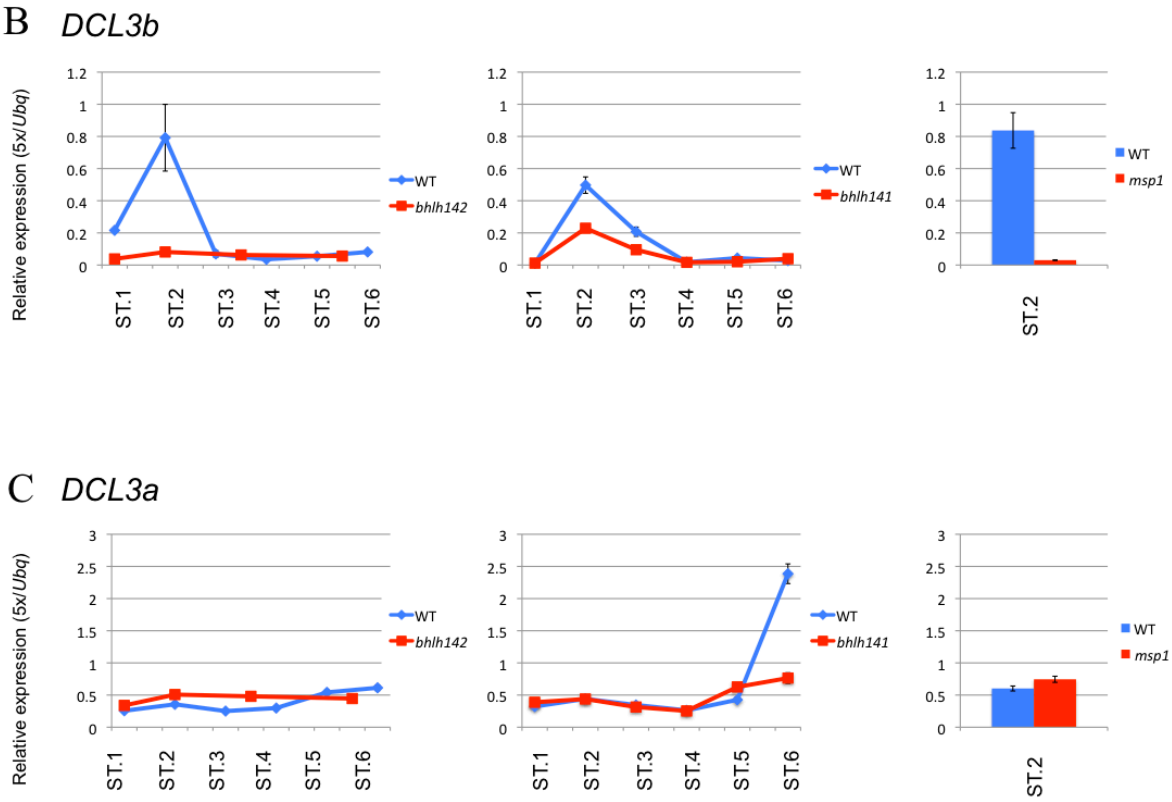

Fig. 19. Gene expression profiles in *bhlh142*, *bhlh141* and *msp1* anthers.
3. Dicer-like ribonuclease family genes.
(A) Expression levels of *DCL3b* in early-meiotic *msp1* mutant anthers revealed by microarray experiment. **(B)** *DCL3b*, **(C)** *DCL3a*, **(D)** *DCL4* and **(E)** *DCL1*. In each panel, the left and mid line graphs show their expression profiles in *bhlh142* and *bhlh141* mutant anthers, respectively. The rightmost bar graph shows expression levels in early-meiotic *msp1* anther. Error bars represent standard errors of three replications.

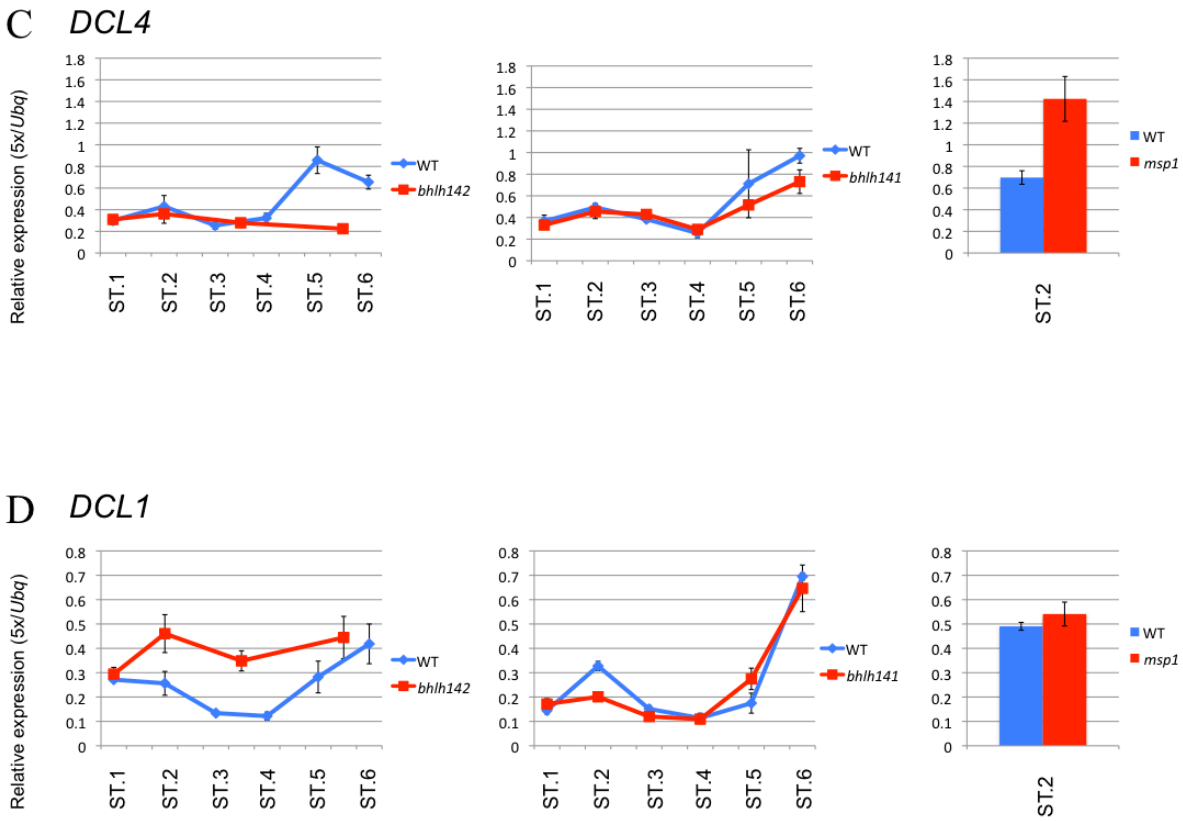

Fig. 19. Continued.

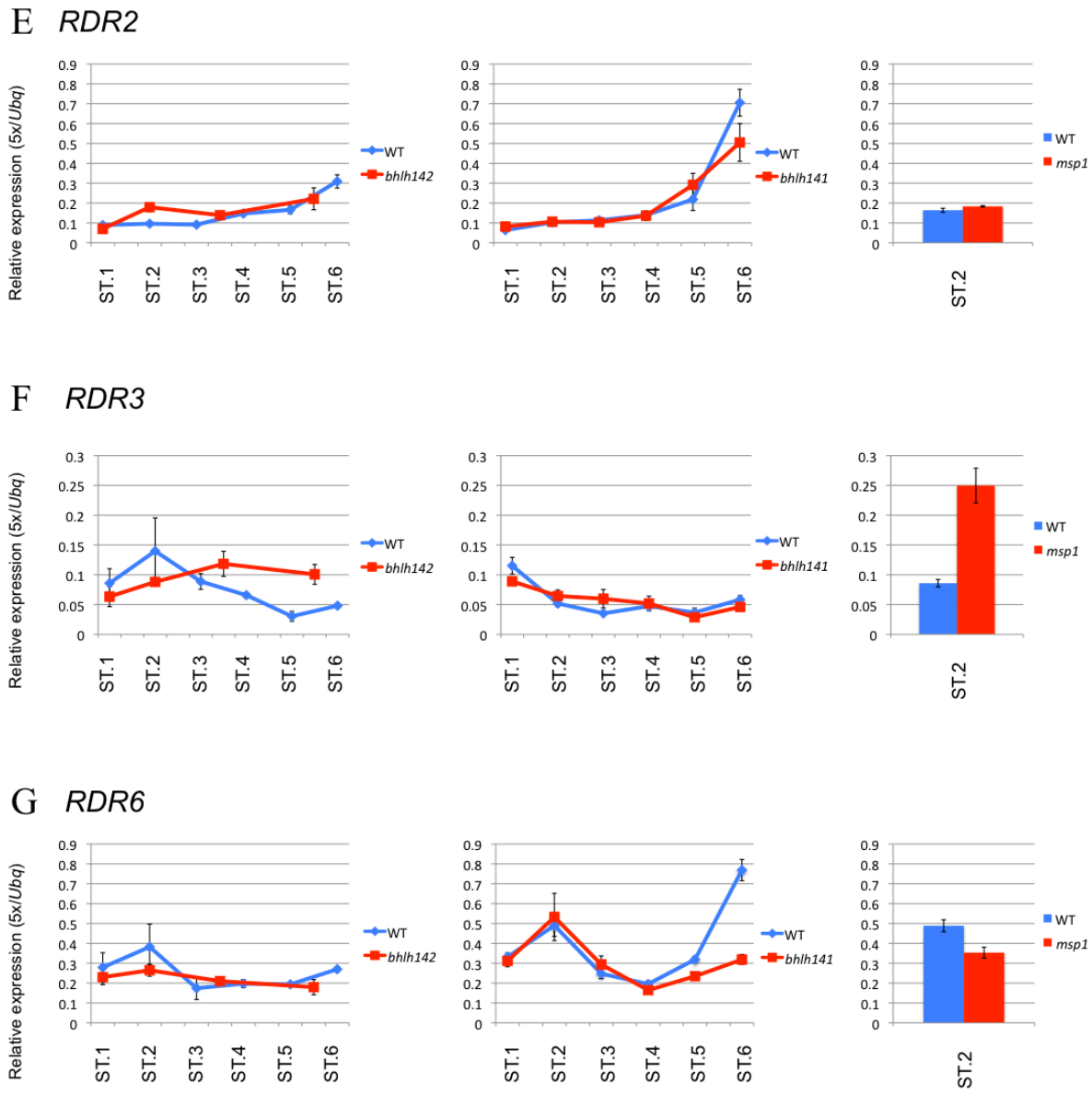

Fig. 20. Gene expression profiles in *bhlh142*, *bhlh141* and *msp1* anthers.

4. RNA-dependent RNA polymerase family genes.

(A) *RDR2*, **(B)** *RDR3* and **(C)** *RDR6.*

In each panel, the left and mid line graphs show their expression profiles in *bhlh142* and *bhlh141* mutant anthers, respectively. The rightmost bar graph shows expression levels in early-meiotic *msp1* anthers. Error bars represent standard errors of three replications.

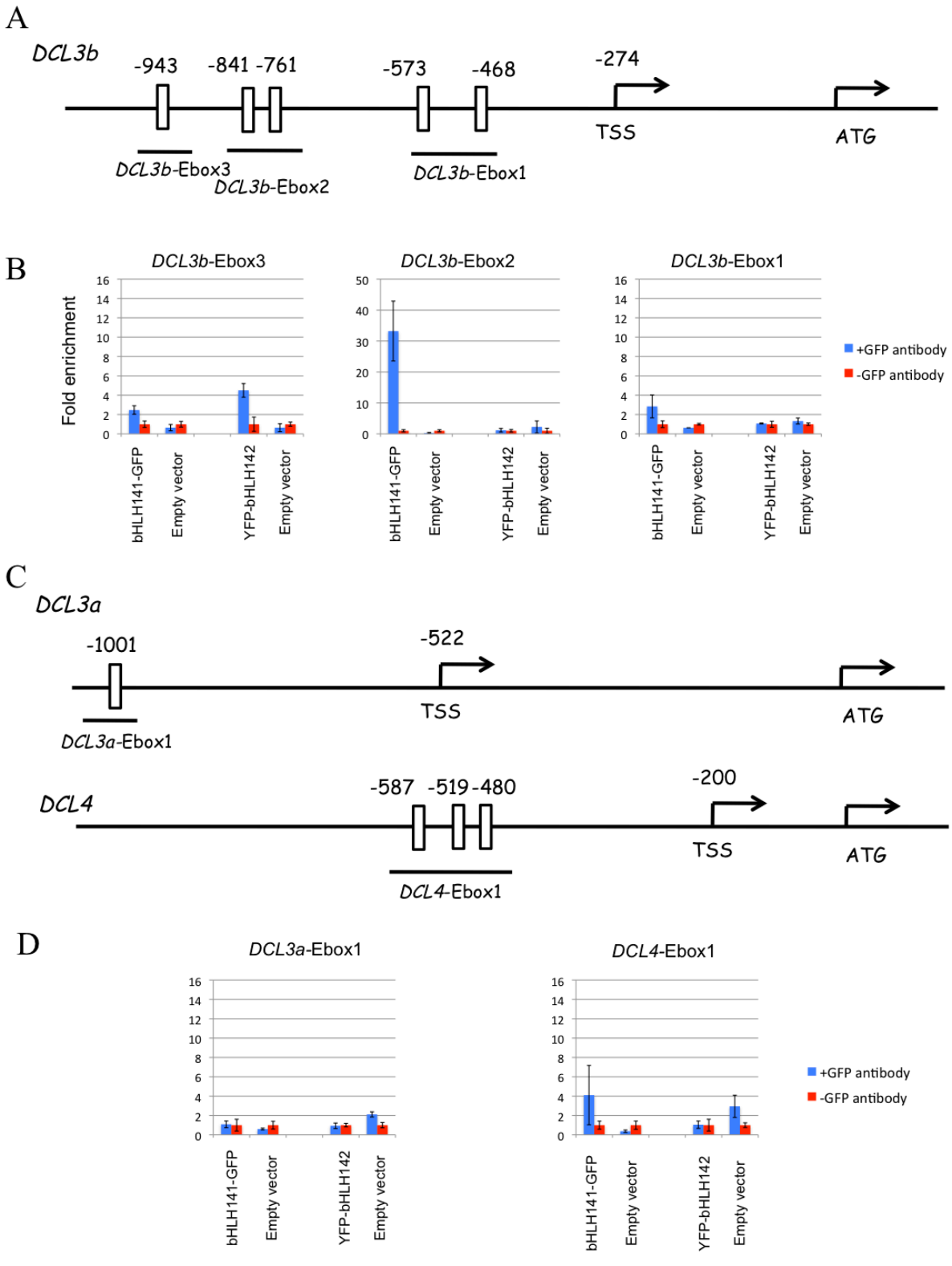

Fig. 21. qChIP-PCR target to promoter region of *DCL* family genes.

(A and C) Schematics of promoter region of *DCL3b, DCL3a* and *DCL4*. White boxes indicate positions of consensus E-box motives. Underlined regions were examined for ChIP-PCR analyses. **(B and D)** Fold enrichment values of underlined regions in (A) and (C). In each ChIP experiment, enrichment values were normalized with antibody-negative samples. Error bars represent standard error of three replications. TSS: transcription start site. ATG: translation initiation site.

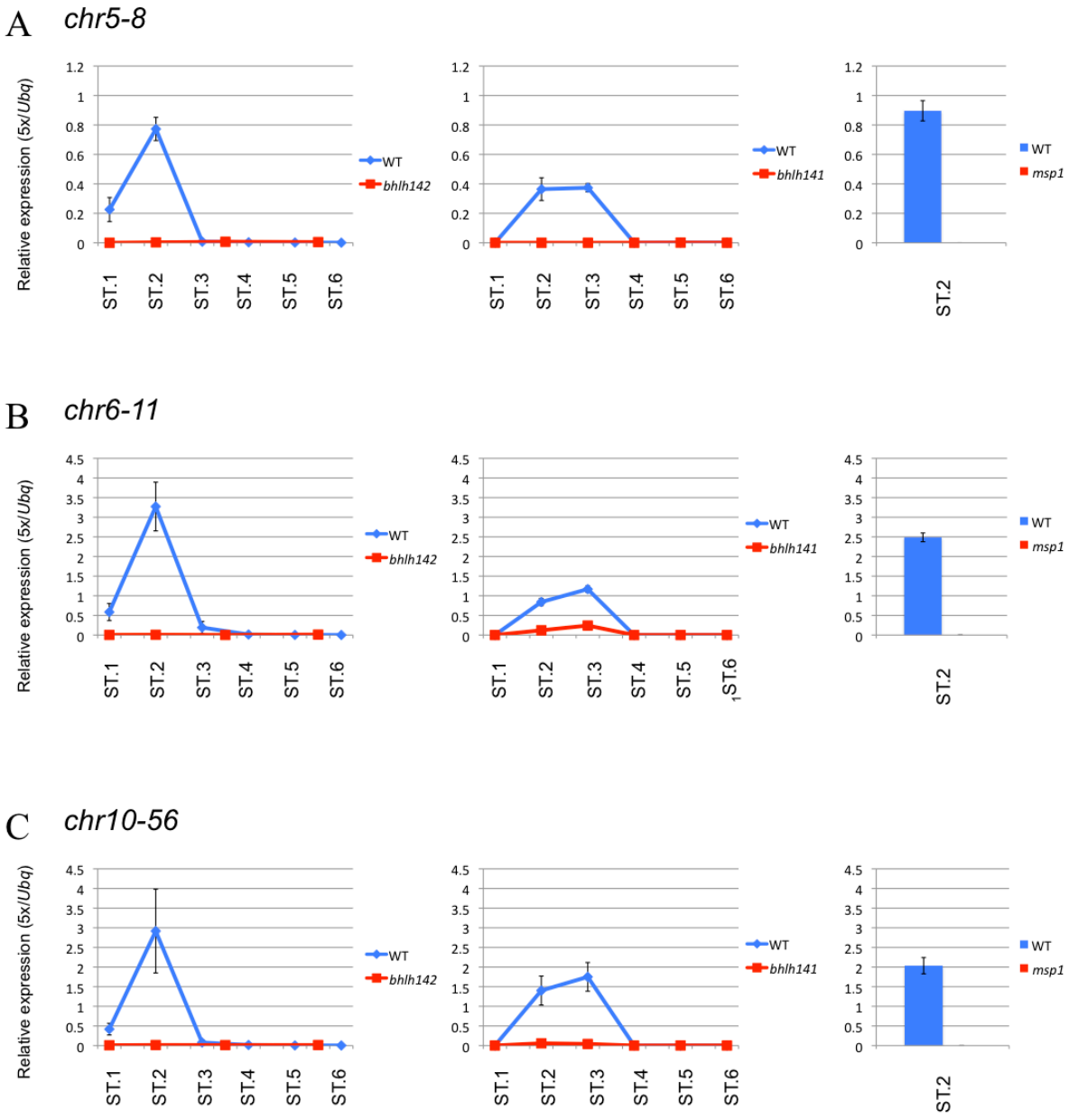

Fig. 22. Expression profiles in *bhlh142*, *bhlh141* and *msp1* anthers.
5. *DCL3b*-associated phasiRNA precursor transcripts,
(A) *chr5-8*, **(B)** *chr6-11,* **(C)** *chr10-56,* **(D)** *chr10-57* and **(E)** c*hr12-29.*
In each panel, the left and mid line graphs show their expression profiles in *bhlh142* and *bhlh141* mutant anthers, respectively. The rightmost bar graph shows expression levels in early-meiotic *msp1* anthers. Error bars represent standard errors of three replications.

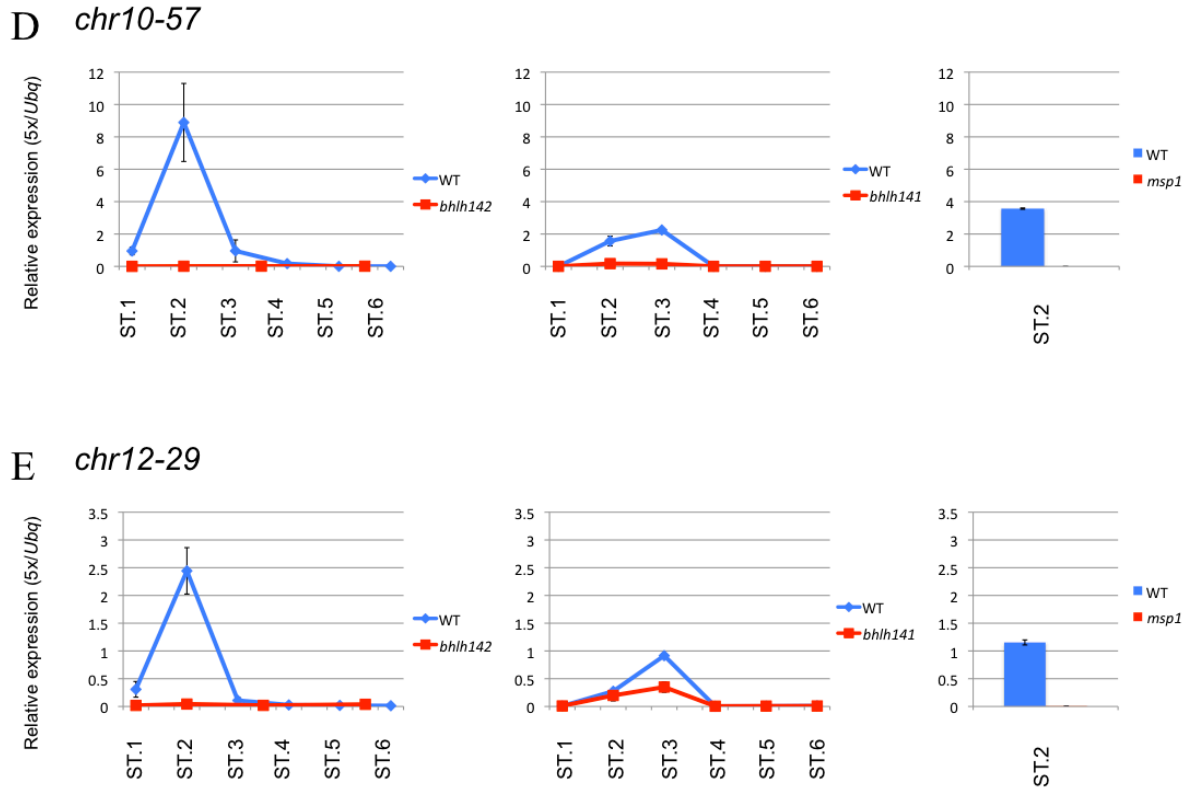

Fig. 22. Continued.

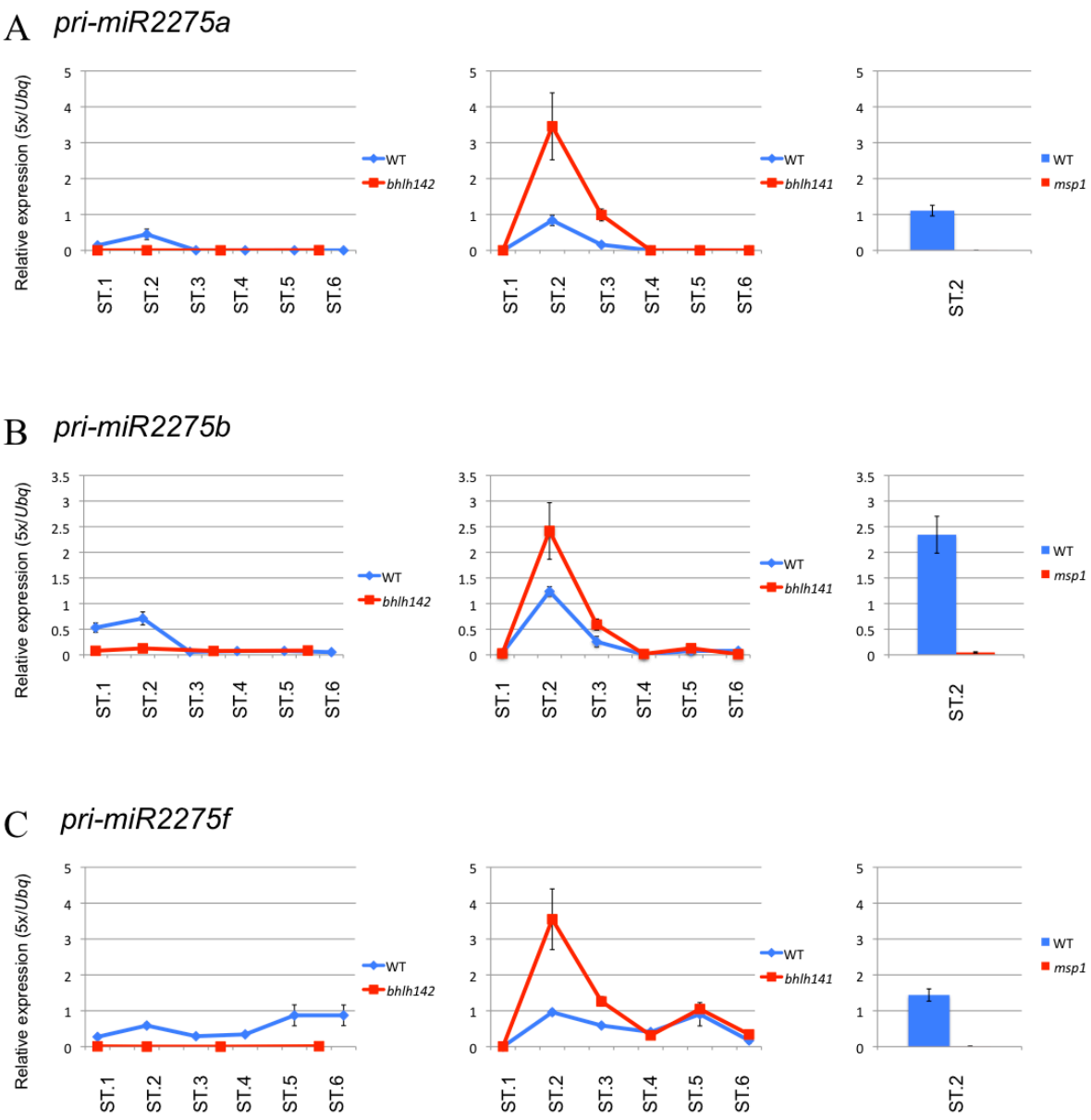

Fig. 23. Expression profiles in *bhlh142*, *bhlh141* and *msp1* anthers.
5. *miR2275* precursor transcripts,
(A) *pri-miR2275a*, **(B)** *pri-miR2275b* and **(C)** *pri-miR2275f.*
In each panel, the left and mid line graphs show their expression profiles in *bhlh142* and *bhlh141* mutant anthers, respectively. The rightmost bar graph shows expression levels in early-meiotic *msp1* anthers. Error bars represent standard errors of three replications.

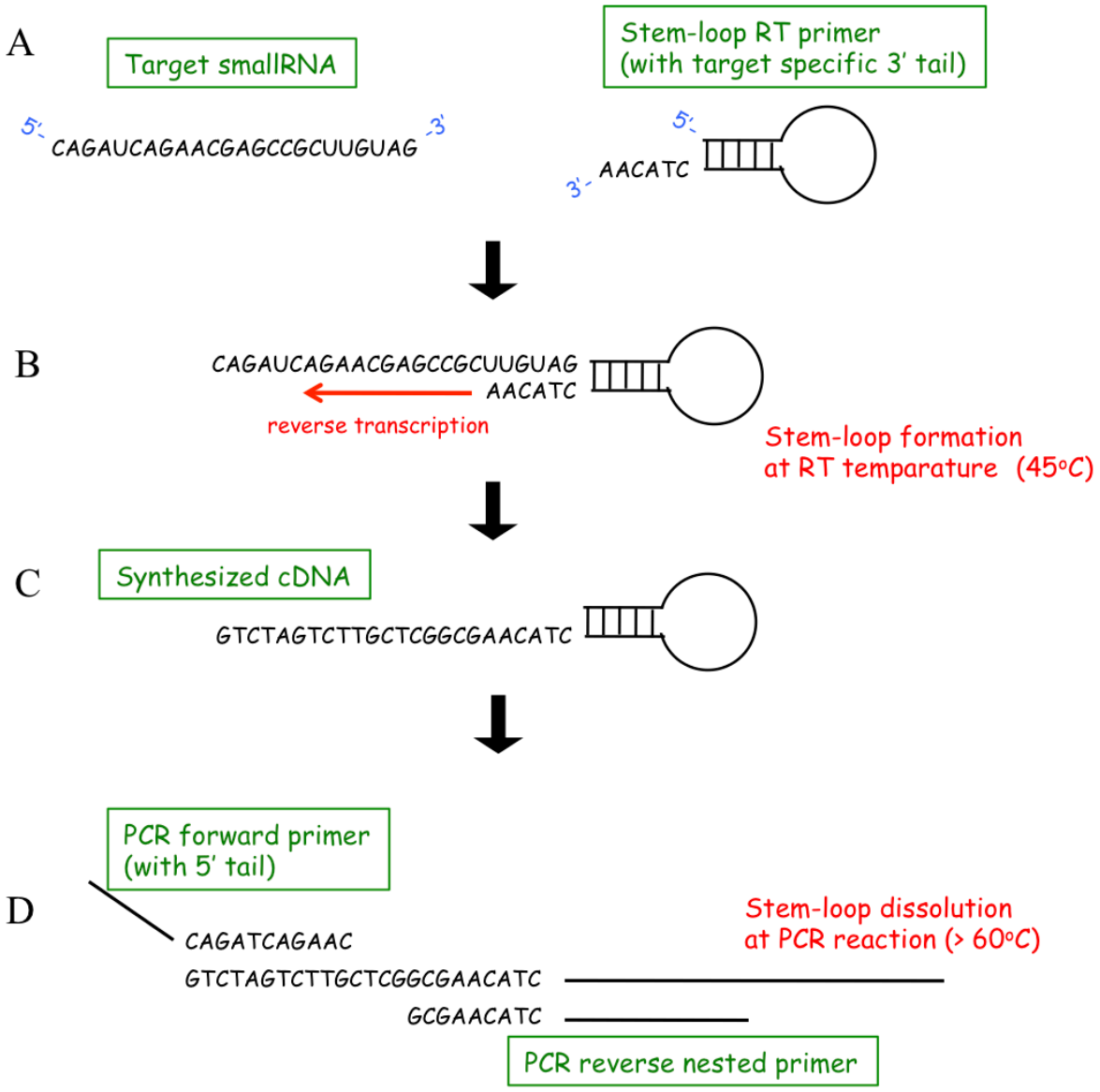

Fig. 24. Schematic representations of principles of PCR-based small RNA quantification described in Wan et al., (2010)

(A) Stem-loop RT primers were designed to having 3' sequences complimentary to 3' end of target small RNA. **(B)** RT primer oligo retained their stem-loop structures at the temperature of reverse transcription reaction (45^{o}C) and hence, prevent non-specific primer binding another RNA molecoles. **(C)** Resultant synthesized cDNA having compliment sequence of target siRNA on their 3' end and sequence of stem-loop primers on their 5' region. **(D)** At the temperature of PCR (more than 60^{o}C), stem-loop structure of RT primers was dissolved and allowed PCR amplification and subsequent detection. Forward and reverse PCR primers were designed as partially overlapped to 5' and 3' sequence target siRNA, respectively. Reverse primer also having identical sequence to stem-loop RT primers allowing specific amplification of successfully reverse transcribed cDNA.

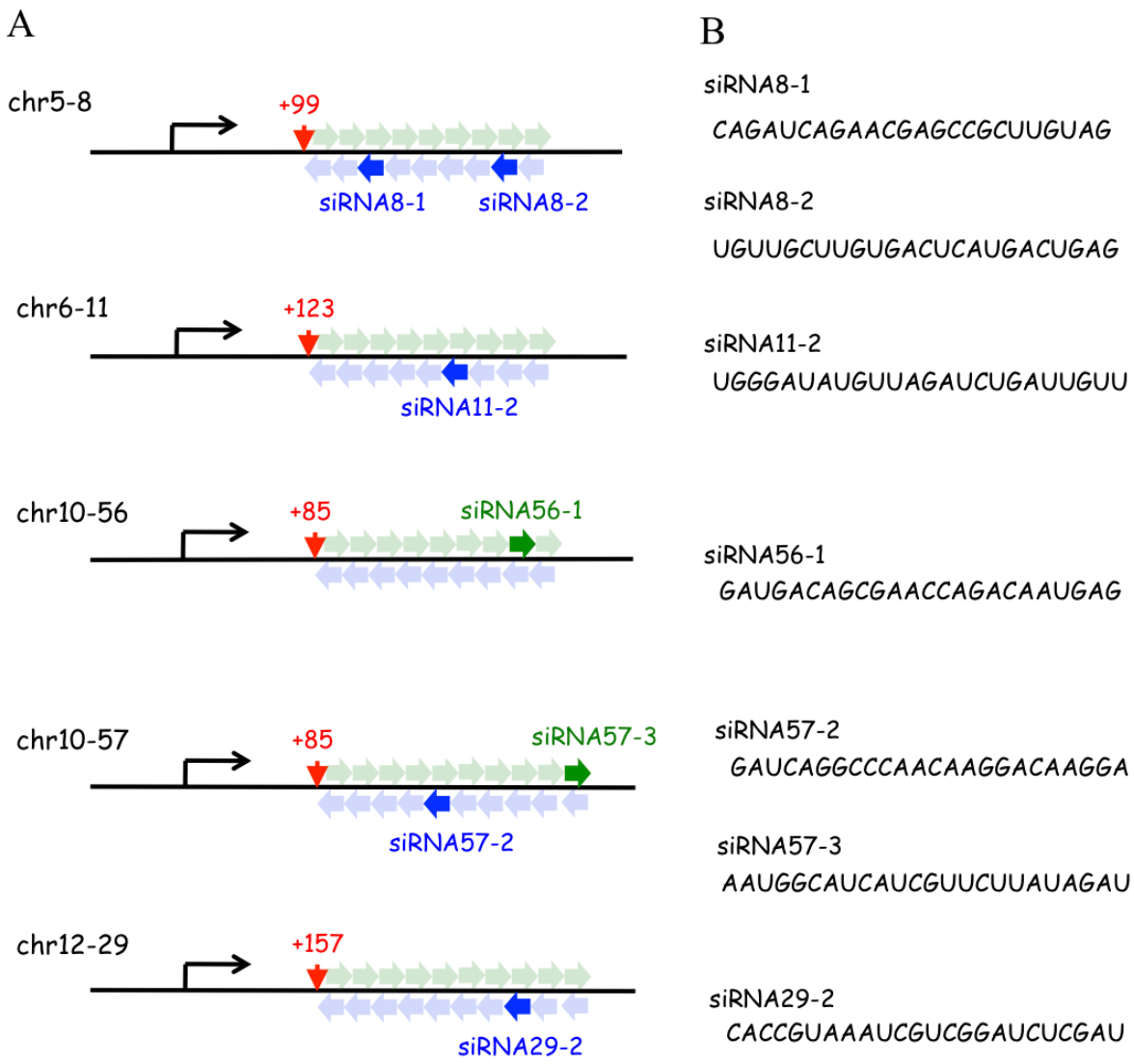

Fig. 25. Schematic representations of exploited siRNAs assayed for quantification.
(A) Genomic positions of exploited siRNAs. Black arrows indicate transcription start site (TSS) revealed by 5' RACE in this study. Red arrows indicate miR2275 cleavage site proposed in Song et al., (2012). Numbered green and blue arrows indicate the positions of exploited siRNAs in this study, having 24nt phased intervals, represented pale green and blue arrows, from miR2275 cleavage site. **(B)** Sequence of each siRNA.

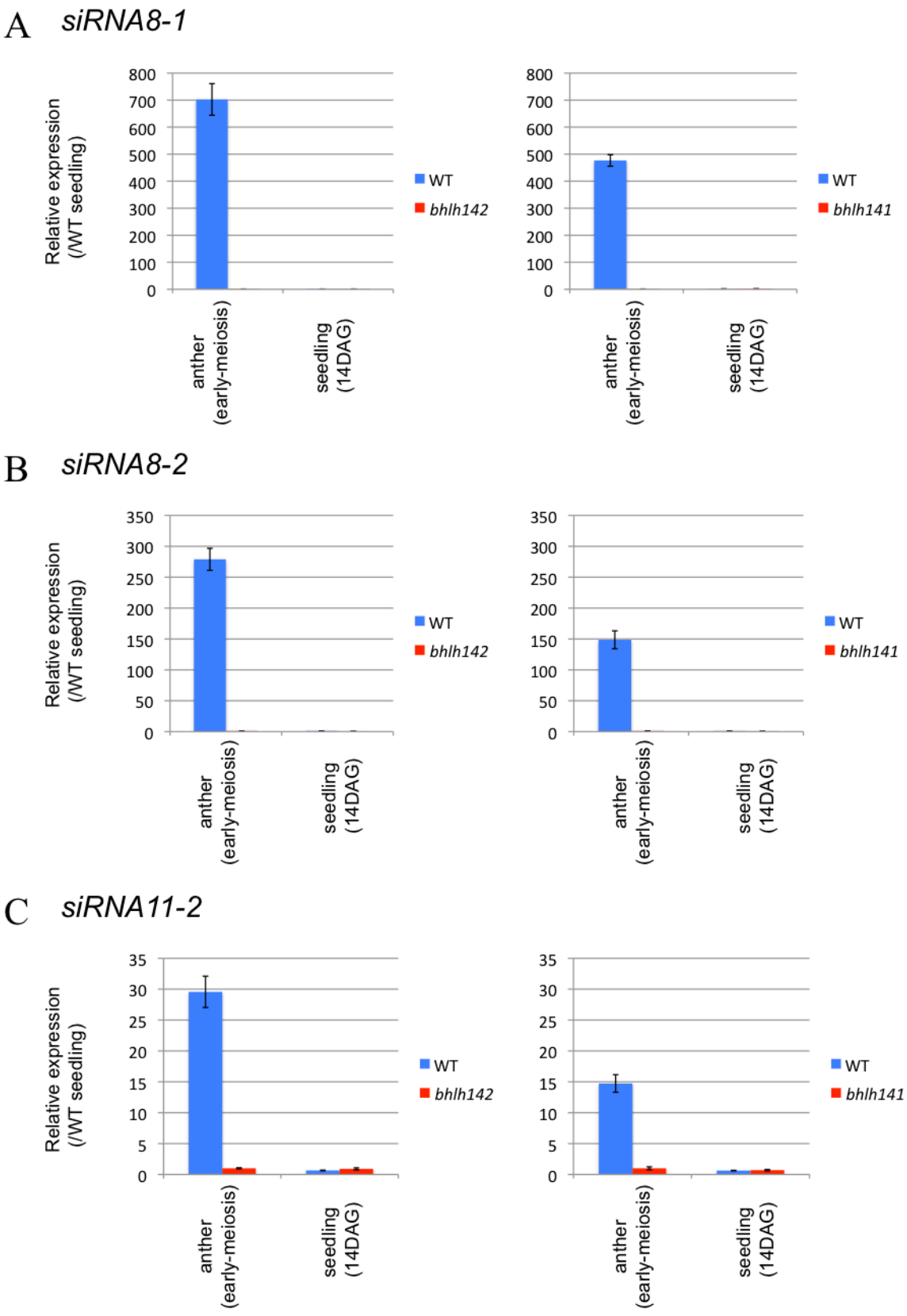

Fig. 26. Quantification of siRNAs in *bhlh142* and *bhlh141* anthers and seedlings.
(A) *siRNA8-1*, **(B)** *siRNA8-2*, **(C)** *siRNA11-2*, **(D)** *siRNA56-1*, **(E)** *siRNA57-2*, **(F)** *siRNA57-3* and **(G)** *siRNA29-2*. The expression values were normalized with the values of WT seedling samples. Error bars represent standard errors of three replications.

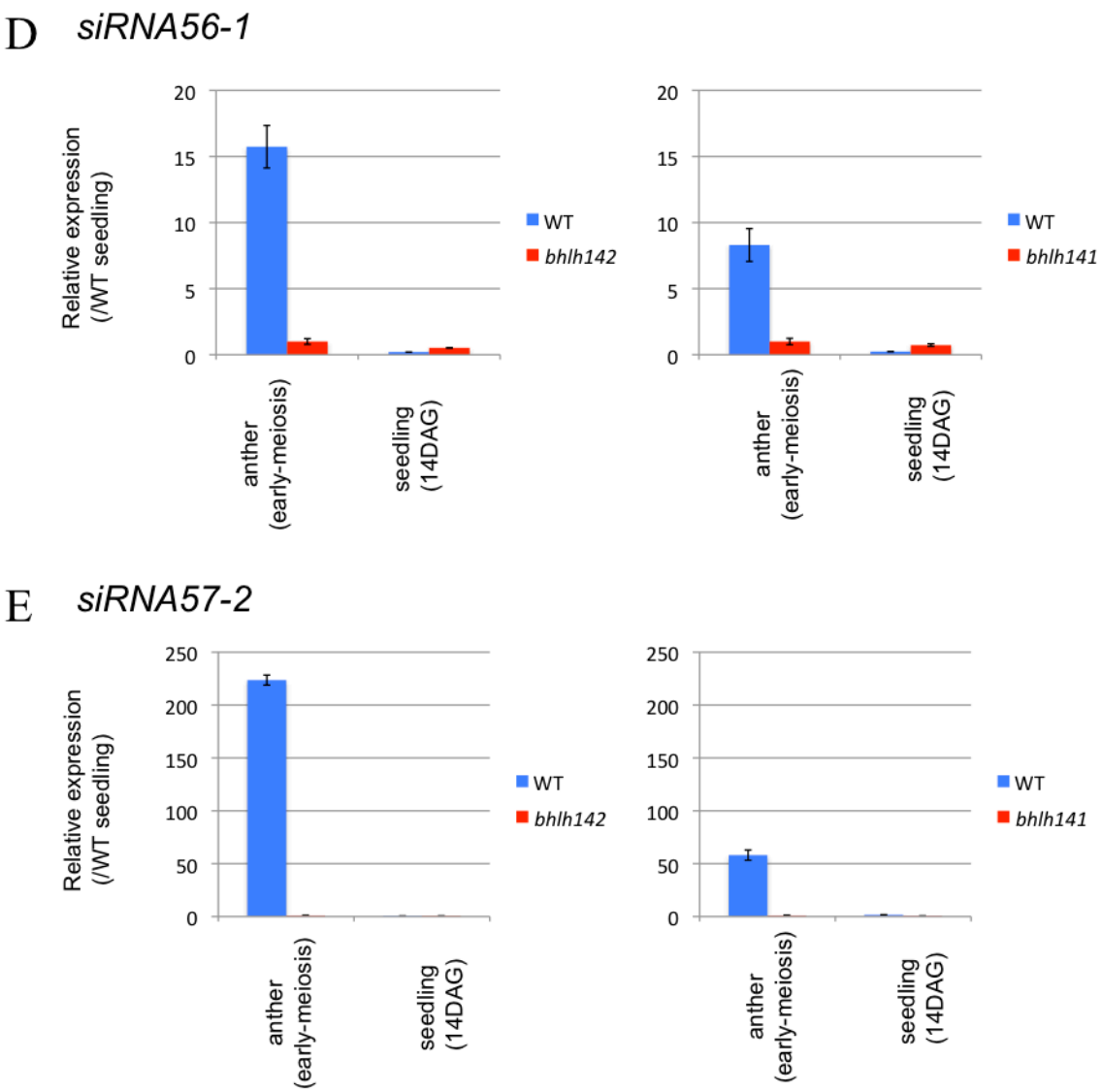

Fig. 26. Continued.

F *siRNA57-3*

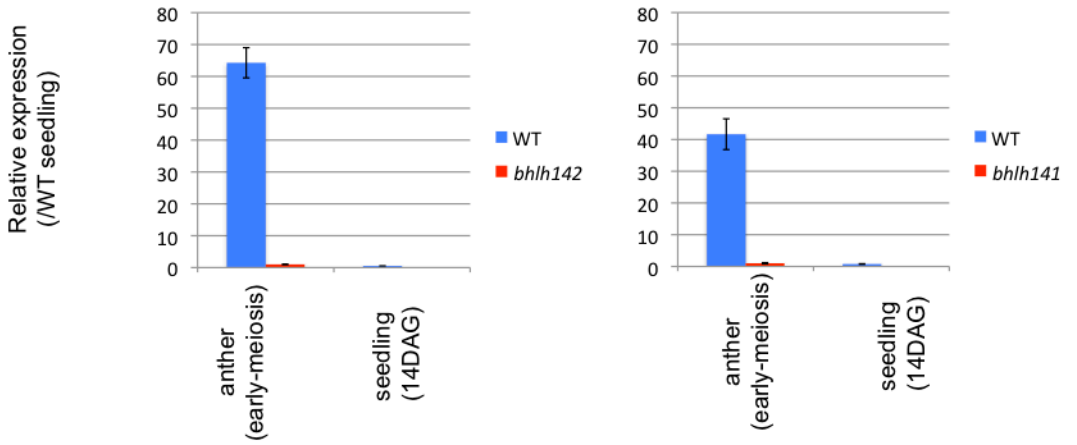

G *siRNA29-2*

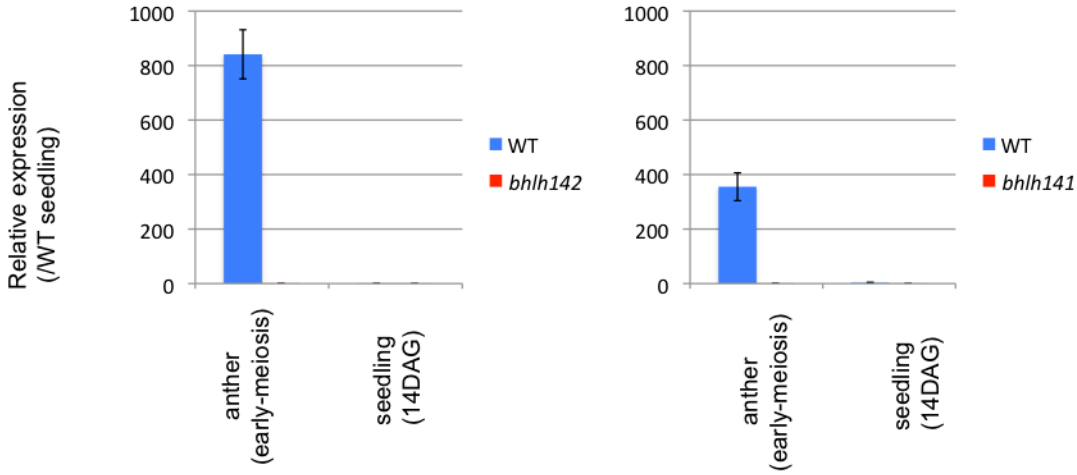

Fig. 26. Continued.

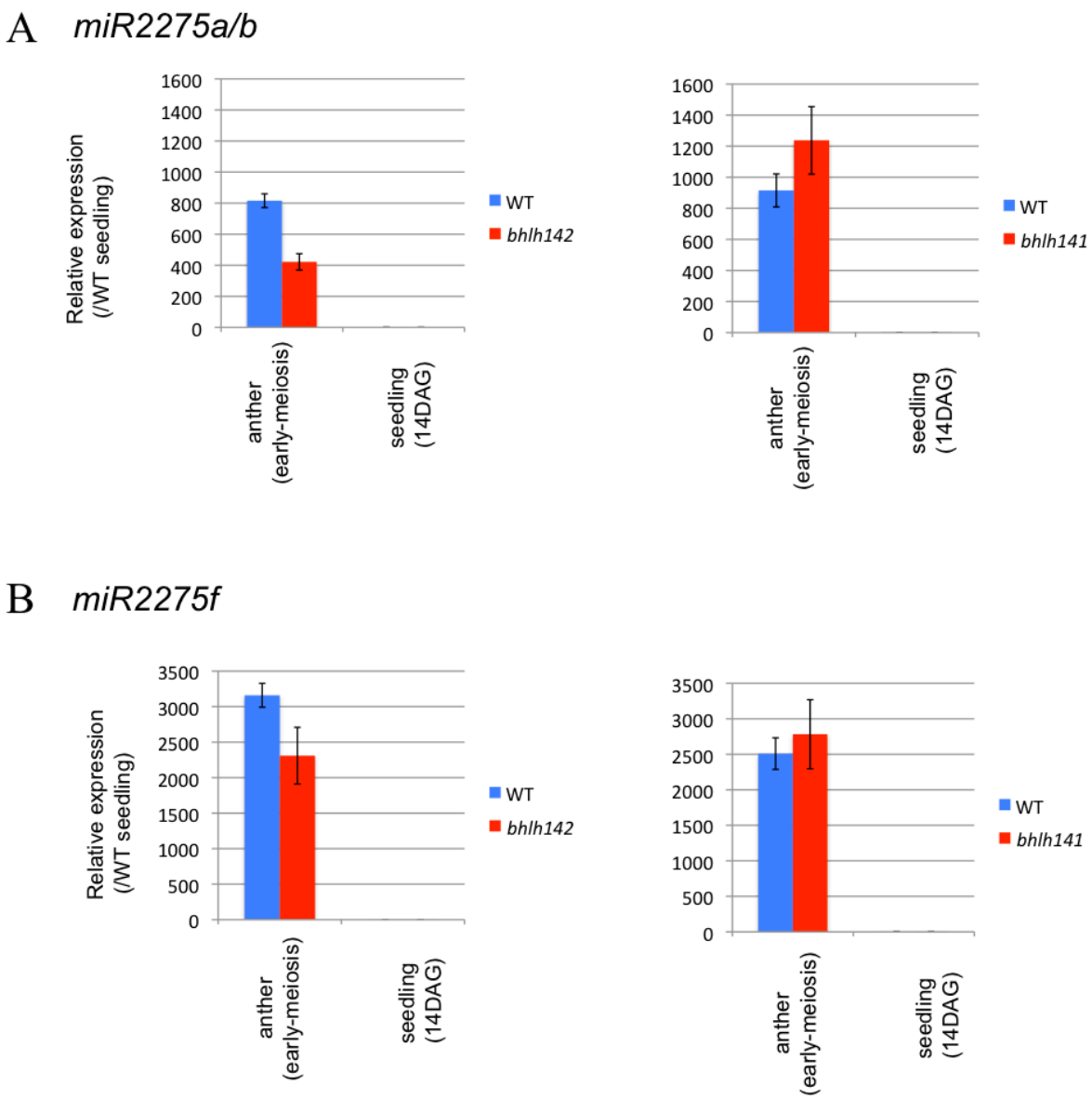

Fig. 27. Quantification of miR2275s in *bhlh142* and *bhlh141* anthers and seedlings.
(A) *miR2275a/b* and **(B)** *miR2275f*. The expression values were normalized with the values of WT seedling samples. Error bars represent standard errors of three replications.

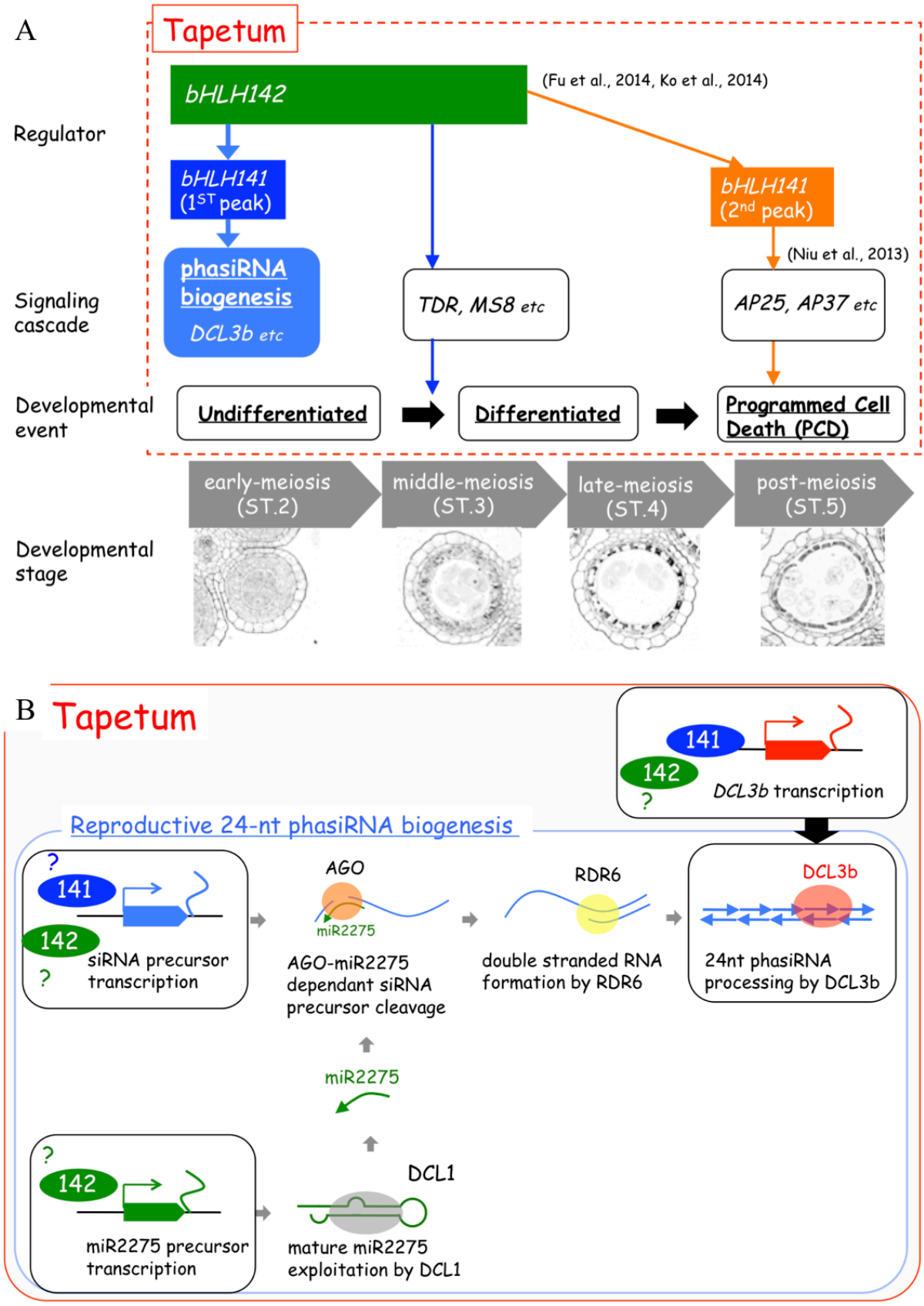

Fig. 28. Models for regulatory networks of bHLH142 and bHLH141 in rice anther wall cells. **(A)** An overview of proposed regulatory networks of bHLH142 and bHLH141 from early-meiosis to post-meiosis stages. **(B)** A detailed view of proposed reproductive 24nt siRNA biogenesis pathway. In tapetum cells.

Table1. Stages of anther samples used in this study.

A; *bhlh142* mutants and its WT siblings

Stages	Corresponding meiotic stage (WT)	Corresponding anther wall stage (WT)	Anther length (WT)	Anther length (*bhlh142*)
ST.1	Pre-meiosis, Meiosis entry	Four-layered anther wall formation	0.4mm	0.4mm
ST.2	Leptotene Zygotene		0.5mm	0.5mm
ST.3	Late zygotene Pachytene	Tapetum becomes to be di-nuculeated	0.6mm	0.6mm-0.7mm
ST.4	Around Metaphase I	Well differentiated tapetum and middle layer	0.7-0.8mm	
ST.5	2nd meiosis, tetrad, microspore release	PCD initiation in tapetum cells	0.9-1.0mm	0.8mm-0.9mm
ST.6	Pollen development	Tapetum degeneration	>1.0mm (yellow)	

B; *bhlh141* mutants and its WT siblings

Stages	Corresponding meiotic stage (WT)	Corresponding anther wall stage (WT)	Anther length (WT)	Anther length (*bhlh141*)
ST.1	Pre-meiosis, Meiosis entry	Four-layered anther wall formation	0.3-0.4mm	0.3-0.4mm
ST.2	Leptotene Zygotene		0.4-0.5mm	0.4-0.5mm
ST.3	Late zygotene	Tapetum becomes to be di-nuculeated	0.6-0.7mm	0.6mm-0.7mm
ST.4	Pachytene Metaphase I	Well differentiated tapetum and middle layer	0.8-0.9mm	0.8-0.9mm
ST.5	2nd meiosis, tetrad, microspore release	PCD initiation in tapetum cells	1.0-1.5mm	1.0mm-1.2mm
ST.6	Pollen development	Tapetum degeneration	>1.5mm (yellow)	> 1.2mm